Loss of CLPP Ameliorates Consequences of DARS2 Depletion in Neurons

Inaugural-Dissertation

zur

Erlangung des Doktorgrades

der Mathematisch-Naturwissenschaftlichen Fakultät

der Universität zu Köln

vorgelegt von

Anastasia Rumyantseva

aus Leningrad (St.Petersburg), Russland

Köln, 2021

Berichterstatter: Prof. Dr. Aleksandra Trifunovic

Dr. David Vilchez

Tag der mündlichen Prüfung: 19. Februar 2021

Time is the moments and events we so readily try to measure. [….] in every moment, in every instant, in every event, is hidden the past, the present and the future. Eternity is hidden in every moment. [….] Everything is simultaneously a beginning and an end.

Andrzej Sapkowski, *The Lady of the Lake*

To my dearest mother and father

Table of Contents

List of Figures

List of Tables

Abbreviations

%	Per cent
µ	Micro
1C	One-carbon
A	Ampere
AAVs	Adeno-associated viral vectors
AB	Antibody
ACADs	Acyl-CoA dehydrogenase family
acetyl-CoA	Acetyl coenzyme A
AD	Alzheimer's disease
ALDH1L2	Mitochondrial 10-formyltetrahydrofolate dehydrogenase
AMP	Adenosine monophosphate
ANOVA	Analysis of variance
ApoE4	Apolipoprotein E4 variant
APS	Ammonium persulfate
ARSs	Aminoacyl-tRNA synthetases
A-T	Ataxia-telangiectasia
ATF4	Activating transcription factor 4
ATP	Adenosine-5'-triphosphate
ATPB	ATP synthase subunit beta
Aβ	Amyloid β-peptide
BN-PAGE	Blue native polyacrylamide gel electrophoresis
BSA	Bovine-serum albumin
CA1	Corni ammonis 1
Ca2+	Calcium ion
CamKIIα	Calcium/calmodulin-dependent kinase II alpha

Cas9	CRISPR associated protein 9
CB_1R	Cannabinoid receptor 1
CI	Complex I
CLPP	Caseinolytic mitochondrial matrix peptidase proteolytic subunit
Clpp_KO^{WB}	*Clpp* whole-body knockout mouse model
CMT	Charcot-Marie-Tooth disease
CNS	Central nervous system
CO2	Carbon dioxide
COX	Cytochrome c oxidase
COX15	Cytochrome c oxidase assembly homolog
Cre	Bacteriophage P1 derived site-specific recombinase
CRISPR	Clusters of regularly interspaced short palindromic repeats
CTRL	Control
DAB	Diaminobenzidine tetrahydrochloride
DAMPs	Damage-associated molecular patterns
DAPI	4′,6-diamidino-2-phenylindole
DARS	Aspartyl-tRNA synthetase
DARS2	Mitochondrial aspartyl-tRNA synthetase
Dars2_Hz^{PC}	Purkinje cell-specific *Dars2* haploinsufficient
Dars2_KO^{FbNe}	Forebrain neuron-specific *Dars2* knock-out
Dars2_KO^{PC}	Purkinje cell-specific *Dars2* knock-out mice
ddH_2O	Double distilled water
DDM	n-dodecyl-β-d-maltoside
DG	Dentate gyrus
DKO	Double knock-out
DKO^{FbNe}	Forebrain-neuron specific Dars2/Clpp double knockout
DKO^{PC}	Purkinje cell-specific Dars2/Clpp double knock-out
DNA	Deoxyribonucleic acid

DNs	Dopaminergic neurons
dNTP	Desoxyribonucleoside triphosphate
dpi	Dots per inch
DRP1	Dynamin-related protein 1
E	Embryonic day
EB	Equilibration buffer
ECL	Enhanced chemiluminescent
EDTA	Ethylenediaminetetraacetic acid
ERRγ	Oestrogen-related receptor gamma
ETC	Electron transport chain
FACS	Fluorescence-activated cell sorting
FDA	U.S Food and Drug Administration
FELASA	Federation of European Laboratory Animals Associations
g	Gram
G6P	Glucose-6-phosphate
GABA	γ-aminobutyric acid
gDNA	Genomic DNA
GFAP	Glial fibrillary protein
GLUT3	Glucose transporter 3
GS	Glycogen synthetase
GSH	Reduced state glutathione
GSK3	Glycogen synthetase kinase 3
GTP	Guanosine-5'-triphosphate
h	Hour
H&E	Haematoxylin and Eosin
H2O2	Hydrogen peroxide
HCl	Hydrogen chloride
HEPES	4-(2-hydroxyethyl)-1-piperazineethanesulfonic acid
HK	Hexokinase

HRP	Horseradish-peroxidase
HSP25	Heat shock protein 25
IBA-1	Ionised calcium-binding adaptor protein-1
IBA-1^{+}	IBA-1 positive microglia
IF	Immunofluorescent
IHC	Immunohistochemical
KCl	Potassium chloride
KD	Ketogenic diet
kDa	Kilo Dalton
KH_2PO_4	Potassium phosphate monobasic
KO	Knock-out
L	Litre
LANUV	Landesamt für Natur, Umwelt, Verbraucherschutz
LBSL	Leukoencephalopathy with brain stem and Spinal cord involvement and lactate elevation disease
LDH1	Lactate dehydrogenase 1
LHON	Leber's hereditary optic neuropathy
loxP	Locus of X-over P1
LS	Leigh syndrome
LTP	Long-term potentiation
M	Molar
m	Meter
m	Milli-
MAP2	Microtubule-associated protein 2
MELAS	Mitochondrial encephalopathy, lactic acidosis, and stroke-like episodes
MFN1-2	Mitofusin-1-2
$MgCl_2$	Magnesium chloride
min	Minute

Miro	Mitochondrial Rho GTPase
MRI	Magnetic-resonance images
MRT	Mitochondrial replacement therapy
mtDNA	Mitochondrial DNA
mTORC1	Mammalian target of rapamycin complex 1
mtZFNs	Mitochondrially targeted zinc-finger nucleases
NaCl	Sodium chloride
NAD^+	Oxidised nicotinamide adenine dinucleotide
NADH	Reduced nicotinamide adenine dinucleotide
NADPH	Reduced nicotinamide adenine dinucleotide phosphate
ND1-ND6	NADH-ubiquinone oxidoreductase chain 1-6
nDNA	Nuclear DNA
NDUFS4	NADH dehydrogenase iron-sulfur protein 4
NeuN	Neuronal nuclear protein
NMDA	N-methyl-D-aspartate
NPC	Niemann-Pick type C1
NPCs	Neuronal progenitor cells
NSCs	Neuronal stem cells
O_2	Molecular oxygen
^oC	Degree Celsius
OXPHOS	Oxidative phosphorylation
PARK2	Ubiquitin E3 ligase Parkin gene
PBS	Phosphate buffered saline
PBST	Phosphate buffered saline supplemented with Tween®-20
PC	Purkinje cell
PCR	Polymerase chain reaction
PD	Parkinson’s disease
PDK4	Pyruvate dehydrogenase kinase 4
PFA	Paraformaldehyde

PGC1α	Peroxisome proliferator-activated receptor-gamma co-activator 1-alpha
pH	Potential of hydrogen
PINK1	Mitochondrial serine/threonine PTEN-induced kinase 1
PKC	Protein kinase C
PPP	Pentose phosphate pathway
PVDF	Polyvinylidene difluoride
RC	Respiratory chain
RGCs	Retinal ganglion cells
RNA	Ribonucleic acid
ROI	Region of interest
ROS	Reactive oxygen species
rpm	Revolutions per minute
RSC	Retrosplenial cortex
RT	Room temperature
S.E.M	Standard error of the mean
SD	Standard deviation
SDH	Succinate dehydrogenase
SDS	Sodium dodecyl sulfate
SDS-PAGE	Sodium dodecyl sulfate-polyacrylamide gel electrophoresis
SHMT2	Mitochondrial serine hydroxymethyltransferase
SNCA	A-synuclein gene
SOD1	Superoxide dismutase 1
SV	Synaptic vesicles
TALENs	Transcription activator-like effector nucleases
TBS	Tris-buffered saline
TBST	Tris-buffered saline supplemented with Tween®-20
TCA	Tricarboxylic acid

TEM	Transmission electron microscopy
TEMED	N,N,N′,N′-Tetramethylethane-1,2-diamine
THF	Tetrahydrofolate
TRAK	Trafficking protein, kinesin binding
Tris	Tris(hydroxymethyl)aminomethane
tRNA	Transport-RNA
TUNEL	Terminal deoxynucleotidyl transferase dUTP nick end labelling
UPRmt	Mitochondrial unfolded protein response
V	Volt
v:v	Volume per volume
VHL	Von Hippel-Landau
w	Week
w:v	Weight per volume
WB	Western blot
WES	Whole-exome sequencing
WT	Wild-type
x *g*	Times gravity

Abstract

Mitochondria are epicentres of neuronal metabolic and signalling pathways. Unsurprisingly, mitochondrial dysfunction, commonly presented as a reduction in OXPHOS, is a feature accompanying almost all neurodegenerative diseases. Mitochondrial diseases are a group of clinically, genetically, and biochemically heterogeneous disorders, arising from the dysfunctional respiratory chain. In most cases, mitochondrial diseases deteriorate life quality severely and are associated with high mortality. The tremendous progress made in the understanding of the genetic basis of mitochondrial diseases, however, is not matched by a breakthrough in therapeutic strategies. Disappointingly, conventional therapy for mitochondrial diseases offers only a modest curative effect. Patients are often treated with vitamin cocktails, intended to merely curb symptoms, or subjected to palliative care, emphasising the demand of novel therapeutic approaches.

Intriguingly, we have previously discovered that devastating cardiomyopathy symptoms caused by the mitochondrial aspartyl-t-RNA synthetase (DARS2) deficiency can be ameliorated by the concomitant loss of mitochondrial matrix CLP protease proteolytic subunit (CLPP).

In this study, we aimed to explore a possibility of CLPP targeting to alleviate neurodegeneration in two distinct models of mitochondrial encephalopathy. To this end, we employed newly generated Purkinje-cell specific DARS2-deficient mice and previously described forebrain-neurons specific DARS2 knockout mice. To tackle the potential bias of targeting only one neuronal population, we generated double KOs for both models.

Here, we showed that the loss of CLPP is beneficial in both models of mitochondrial encephalopathy, driven by *Dars2*-deficiency. Importantly, we demonstrated that CLPP ablation delays neurodegeneration in several brain regions, including Purkinje cell layer, retrosplenial cortex and hippocampus. The reduced neuroinflammation and neurodegeneration significantly improved motor performance of mice highlighting the therapeutic potential of the CLPP targeting.

1 Introduction

1.1 Neuronal mitochondria: Pleiotropy of functions

The evolutionary advantage of the mammalian brain, namely the development of highly elaborated and enlarged neocortex came at the price of its metabolic costs. Even though *Homo sapiens* brain makes up just 2 % of total body weight, it is classically viewed to be one of the most energy-consuming organs, accounting for 20 % of the total individual's energy expenditure (Camandola and Mattson, 2017; Isler and van Schaik, 2006; Mink et al., 1981; Rangaraju et al., 2019). As the brain comprises two major cell types – neurons and glial cells (astrocytes, oligodendrocytes, microglia), the brain's metabolic homeostasis is tightly regulated and depends on intricated functioning of both cell types. Neurons, by far, are the most energy-consuming cells of the brain, estimated to expend 70-80 % of the total energy (Camandola and Mattson, 2017; Hyder et al.,

2013). A growing number of gene expression and metabolomic studies in mammals, including primates, shows a uniform upregulation of genes and metabolites involved in oxidative metabolism underlying the essential role of mitochondria for neuronal survival and function (Camandola and Mattson, 2017; Cáceres et al., 2003; Grossman et al., 2001; Jöbsis and Rosenthal, 1978; Uddin et al., 2004). Classically viewed as cells' "powerhouses" for generating adenosine-5'-triphosphate (ATP) via the oxidative phosphorylation (OXPHOS) reaction at electron transport chain (ETC), mitochondria reside in the epicentre of numerous fundamental metabolic and signalling pathways. Lipid biogenesis, Ca^{2+} homeostasis, redox signalling, regulation of apoptosis, emphasise pleiotropic roles for mitochondria (Spinelli and Haigis, 2018).

1.1.1 Mitochondria as neuronal "powerhouses"

Neuronal bioenergetics relies foremost on the OXPHOS (Jang et al., 2016; Rangaraju et al., 2019). Although the utilisation of ketone bodies during brain development and prolonged fasting periods was reported, neurons in the adult brain rely predominantly on glucose as an energy source (Camandola and Mattson, 2017; Nehlig and Pereira de Vasconcelos, 1993; Owen et al., 1967). The reliance of neurons on glucose is further confirmed by the expression of a specialised, insulin-independent "neuronal" glucose transporter 3 (GLUT3). GLUT3 was shown to exhibit higher glucose affinity and transport capacity, ensuring uninterrupted supply of glucose even when interstitial levels of glucose are low (Camandola and Mattson, 2017; Nagamatsu et al., 1992). The fate of glucose (Fig.1.1), entering a neuron via GLUT3 is a defined by the set of oxidising biochemical reactions via glycolysis, the pentose phosphate pathway (PPP), the tricarboxylic acid (TCA) cycle and the OXPHOS, which culminates in the production of carbon dioxide, water and, can yield maximum 38 molecules of ATP (Camandola & Mattson, 2017) altogether.

Notably, after the irreversible phosphorylation of glucose by hexokinase (HK) to glucose-6-phosphate (G6P), neurons preferentially utilise PPP to convert G6P into 5-carbon sugars used for the generation of reduced nicotinamide adenine dinucleotide phosphate (NADPH). Intriguingly, the neuronal reliance on PPP, a low rate of glycolysis in neurons, and their limited ability to upregulate glycolysis even under the stress conditions are tightly coupled to the NADPH generation (Camandola and Mattson, 2017; Herrero-Mendez et al., 2009). NADPH production is highly relevant for neurons, for the maintenance of redox homeostasis. Quantitatively, the most NADPH-consuming process is replenishing of the reduced state of the antioxidant glutathione (GSH), which is highly important for the detoxification of peroxides and free radicals (Dringen, 2000). The presence in neurons of the low-pyruvate-affinity isoform of lactate dehydrogenase 1 (LDH1) facilitates pyruvate entrance into the TCA cycle while preventing its conversion to lactate (Camandola and Mattson, 2017). Remarkably, the metabolic bias towards TCA in neurons is emphasised further by low expression levels of pyruvate dehydrogenase kinase 4 (PDK4), which generally localised to mitochondrial matrix inhibiting the decarboxylation of pyruvate to acetyl coenzyme A (acetyl-CoA) (Halim et al., 2010). The largest energy reserve in the brain is comprised of glycogen; however, its amount in the brain is negligible compared to the liver and skeletal muscles (Camandola and Mattson, 2017). Although neurons are capable of mobilising glycogen and utilise it to match increased energy requirements, glycogen is synthesised and stored almost exclusively in astrocytes (Swanson et al., 1992). Interestingly, neurons express the key enzyme for glycogen synthesis, glycogen synthetase (GS); however, its activity is shut down. Constitutive hyperphosphorylation of GS by GS kinase 3 (GSK3), and subsequent proteasomal degradation, mediated by malin-laforin complex maintain

GS in the inactive state, thus preventing the glycogen accumulation in neurons that otherwise might be damaging (Vilchez et al., 2007).

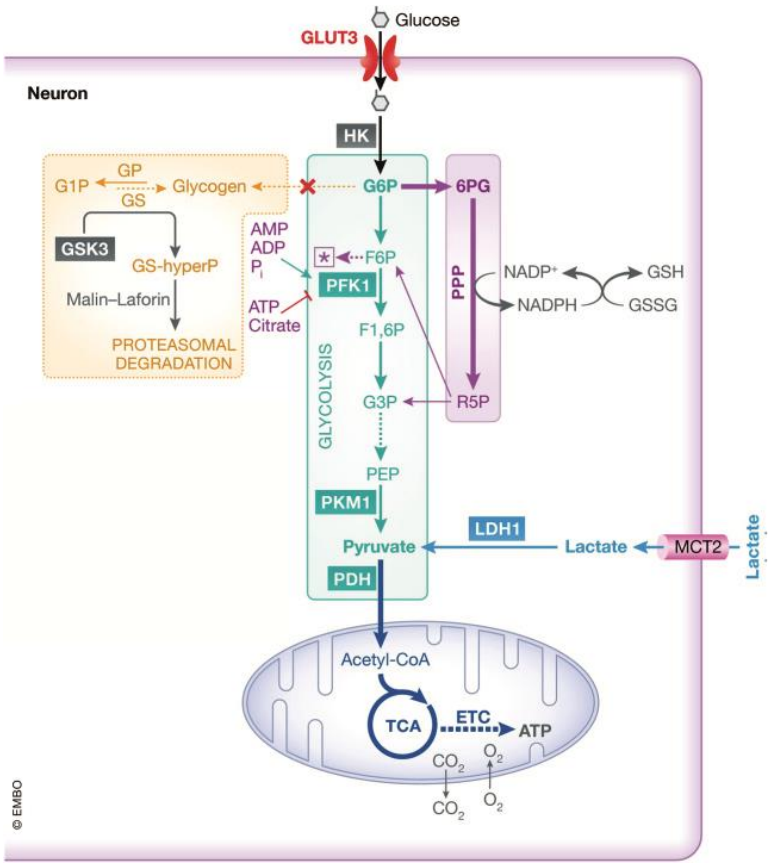

Figure.1.1: Metabolic pathways of neuronal glucose utilisation. Glucose enters neurons via glucose transporter 3 (GLUT3) and is phosphorylated by hexokinase (HK) to glucose-6-phosphate (G6P), which is subsequently rerouted predominantly to the pentose phosphate pathway (PPP). In the PPP, G6P is converted to 6-phosphogluconate (6PG) that is transformed in ribulose-5-phosphate (R5P), with the concomitant production of reduced nicotinamide adenine dinucleotide phosphate (NADPH). NADPH used to regenerate oxidised antioxidants such as glutathione (GSH) and thioredoxin. The end product of glycolysis is pyruvate that enters the mitochondria where it is metabolised through the tricarboxylic acid (TCA) cycle and oxidative phosphorylation in the electron transport chain (ETC), generating adenosine-5′-triphosphate (ATP) and carbon dioxide (CO2) while consuming oxygen (O_2). Neurons do not synthesise glycogen due to constitutive degradation of glycogen synthase (GS) via glycogen synthase kinase 3 (GSK3) phosphorylation, and subsequent ubiquitin-dependent proteasomal digestion mediated by the malin–laforin complex *modified from (Camandola and Mattson, 2017).*

In addition to supplying neurons with copious amounts of ATP, the bioenergetic function of neuronal mitochondria is tightly interconnected with the generation of TCA intermediates that are used to synthesise acetylcholine, γ-aminobutyric acid (GABA) and glutamate neurotransmitters (Guo et al., 2017; Sibson et al., 1998; Waagepetersen et al., 2001). Moreover, mitochondria are major players in the synthesis of haem – the key component of cytochromes and haemoglobin, which regulate signalling processes in the brain (Devine and Kittler, 2018). Haem deficiency was demonstrated to result in neurite degeneration, caused by the inhibition of N-methyl-D-aspartate (NMDA) receptor (Chernova et al., 2007).

Hence, mitochondrial dysfunction may compromise not only ATP levels per se, but also alter neurotransmitter levels, rendering neurons, and therefore, brain uniquely vulnerable to impairment of the oxidative metabolism (Nunnari and Suomalainen, 2012).

1.1.2 Mitochondria as neuronal signalling hubs

The large amounts of ATP produced by neurons are required to perform a wide range of functions. Maintenance of resting membrane potential, control over synaptic vesicles (SV), restoration of ion balance after the depolarisation underscore the high energy demanding functions of neuronal activity (Harris et al., 2012; Pathak et al., 2015; Seager et al., 2020). Ca^{2+} predominantly mediates the intracellular signalling underlying diverse functions. During an action potential, a neurotransmitter release occurs after the opening of voltage-gated Ca^{2+} channels that allow the Ca^{2+} influx into the presynaptic terminal (Fig.1.2). The proton pumping activity of the ETC generates the mitochondrial membrane potential that favours cations, including Ca^{2+} sequestration

within the matrix (Billups and Forsythe, 2002; Levy et al., 2003). However, mitochondria are far from being just passive players, operating as Ca^{2+} dump sink. In fact, they are actively recruited to the presynaptic compartment and can tune the synaptic activity over time (Devine and Kittler, 2018; Vaccaro et al., 2017). In vitro studies in primary neuronal cultures have shown that the increase in Ca^{2+} sequestration within the mitochondrial matrix activates TCA cycle and OXPHOS enzymes, leading ultimately to an increase in ATP production (Duchen, 1992; Llorente-Folch et al., 2015).

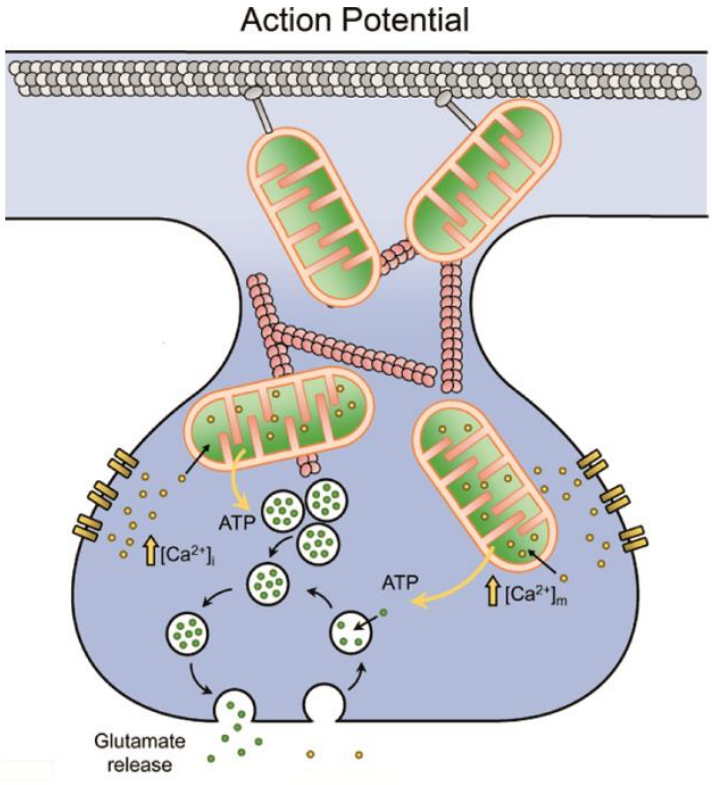

Figure.1.2: Roles of mitochondria ATP production and calcium Ca^{2+} sequestration during action potential. An influx of Ca^{2+} rapidly enters mitochondria, stimulating OXPHOS activity and increased ATP generation. The enhanced ATP generation powers energy-demanding processes such as SV recycling and neurotransmitter release. Local mitochondria stop trafficking and are stabilised by the action of syntaphilin (anchoring protein) and rearrangements of the Miro-TRAK complex *modified from (Seager et al., 2020)*

Thereby, neuronal synaptic activity is controlled by the powerful homeostatic mechanism: enduring prolonged synaptic activity is linked to appropriate energy supply; however, the Ca2+ buffering tempers the excess of the activity (Devine and Kittler, 2018). Mitochondria are also able to integrate and respond to other signals, potentially impacting presynaptic function. To date, it is largely recognised that mitochondria-derived reactive oxygen species (ROS) are not mere inducers of the oxidative damage. In fact, the conventional view of "damaging" ROS has been broadened to encompass their versatility as signalling molecules to govern physiological processes of hypoxia adaptation, immune response, longevity, and autophagy (Devine and Kittler, 2018; Sena and Chandel, 2012). In line with this, it has been shown that ROS activate hippocampal long-term potentiation (LTP). Generally, LTP is a long-lasting increase in the synaptic activity, guiding important processes of mammalian memory and learning (Klann et al., 1998). The activation of protein kinase C (PKC) is one of the crucial steps for the LTP induction, as its selective inhibition abolishes the LTP induction (Malinow et al., 1989). Importantly, superoxide has been shown to increase PKC activity (Klann et al., 1998; Knapp and Klann, 2002), and the overexpression of a ROS-scavenger superoxide dismutase 1 (SOD1) dramatically impairs mouse spatial learning and memory (Levin et al., 1998).

Furthermore, a recent study has provided evidence that mitochondria-derived ROS regulate the strength of GABA type A receptors at inhibitory synapses of cerebellar stellate cells (Accardi et al., 2014). Another evidence of the central role of mitochondria in neuronal intracellular signalling comes from studies of the cannabinoid receptor 1 (CB1R). The direct stimulation of CB1R has been demonstrated to reduce presynaptic mitochondria respiration, contributing to the hippocampal short-term synaptic plasticity, and underlying the memory impairment effect

produced by cannabinoids (Bénard et al., 2012; Devine and Kittler, 2018; Hebert-Chatelain et al., 2016). Although many molecular mechanisms remain elusive, bioenergetics of mitochondria is tightly coupled with the crucial role they play in integrating cellular signalling. Thus, mitochondrial functioning and homeostasis are critical for neuronal survival, synaptic activity, and integrity of neuronal circuits.

1.1.3 Mitochondria as determinants of neuronal differentiation

Neurons are highly polarised cells, possessing unique cytoarchitecture (Cáceres et al., 1986; Dotti et al., 1988). This unique cytoarchitecture is acquired during neurogenesis and subsequent morphogenetic processes and accompanied by profound metabolic remodelling (Rangaraju et al., 2019). Given their central place in cellular metabolism, it is unsurprising that mitochondria play a pivotal role in neurogenesis and neuronal differentiation (Fig 1.3). A metabolic switch from glycolysis and fatty acid oxidation pathways to OXPHOS is crucial for the commitment of neuronal stem cells (NSCs) to neuronal progenitor cells (NPCs) and finally to neuronal lineage (Beckervordersandforth et al., 2017; Khacho et al., 2019; Llorens-Bobadilla et al., 2015; Maffezzini et al., 2020). Notably, the OXPHOS metabolic switch is accompanied by dynamic changes in mitochondrial content and morphology (Mattson et al., 2008). First, the number of mitochondria per cell rises rapidly during neurogenesis. This is accompanied by the increase in mitochondrial DNA (mtDNA) levels, and activity, governed by the increase of mitochondrial gene expression (Chen et al., 2010; Erecinska et al., 2004; Maffezzini et al., 2020; O'Brien et al., 2015). Moreover, the increase in the mitochondrial content is preceded by the upregulation of the peroxisome proliferator-activated receptor gamma co-activator 1-alpha (PGC1α) and the oestrogen-related receptor gamma (ERRγ), confirming further the role of mitochondrial biogenesis in the neuronal fate determination (O'Brien et al., 2015; Zheng et al., 2016).

Second, mitochondria have been reported to change their morphology during neurogenesis. The commitment of NSCs coincides with the morphological changes of mitochondria from rounded and small to becoming steadily more elongated. The precise regulatory mechanism is remained to be elucidated, but several studies suggest that the reactive oxygen species (ROS)-signalling plays a major role (Bhaskar et al., 2020; Khacho et al., 2016; La Rosa et al., 2019).

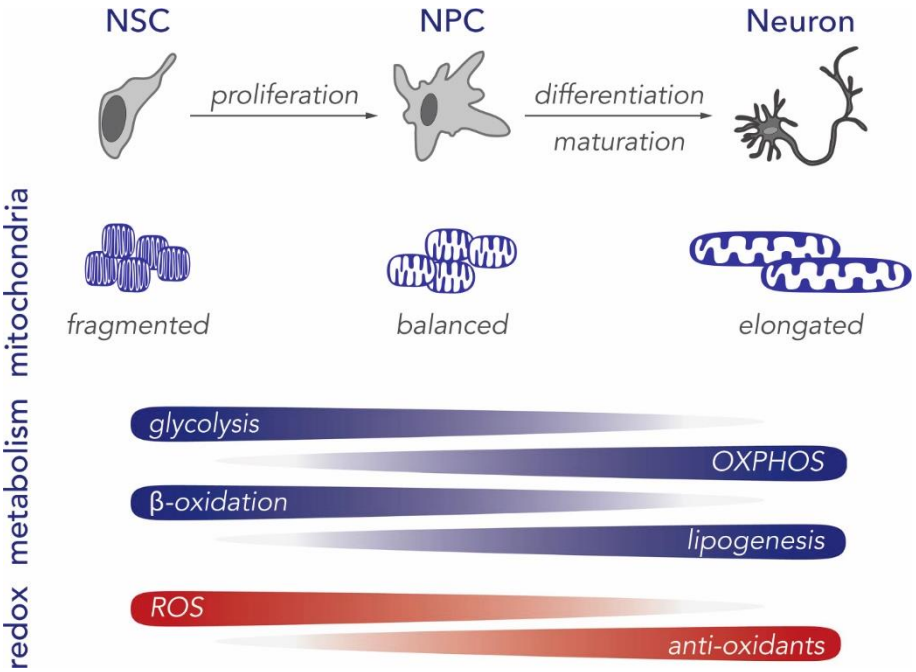

Figure 1.3: Neurogenesis, metabolic switch. During neuronal differentiation, neuronal stem cells (NSCs) proliferate into neuronal progenitor cells (NPCs) and subsequently to neurons this progression is accompanied by several shifts, including the proliferation and morphological changes of mitochondria, a transition from glycolysis to OXPHOS for ATP synthesis. Additionally, fatty acid metabolism shifts to *de novo* lipogenesis. The increased metabolic activity of the cells is accompanied by ROS, which is countered by the activation of oxidative stress response genes to reduce overall ROS levels *unmodified from (Maffezzini et al., 2020).*

Once neurons are differentiated from NSCs, several radial neurites extend, one of which starts growing fast, acquiring morphological, molecular, and functional characteristics of an axon, while other neurites become dendrites. Interestingly, mitochondria are critical determinants

of axogenesis (Mattson et al., 2008). Mitochondria concentrate at the base of the dendrite that eventually becomes the axon and show increased entry into the axon during its development. Conversely, the mitochondria abundance in dendrites decreases (Ruthel and Hollenbeck, 2003). Furthermore, the treatment of primary hippocampal neurons with ethidium bromide to deplete mtDNA impairs axogenesis, while not affecting dendrites outgrowth (Mattson and Partin, 1999).

1.2 Neurodegenerative diseases: Implications of mitochondrial dysfunction

Mitochondria are sites that integrate numerous neuronal signalling and metabolic pathways. Given that fact, it is unsurprising that mitochondrial dysfunction, commonly addressed as a reduction in OXPHOS, has been reported for virtually all neurodegenerative diseases. Classically, mitochondrial diseases are divided into primary and secondary (Murphy and Hartley, 2018). The former group includes diseases caused by mutations in mtDNA or nuclear DNA (nDNA) that directly affect OXPHOS complexes assembly and function. The latter group includes diseases exhibiting "mitochondrial" clinical manifestation and phenotype, without attributable pathogenic mutations in mtDNA or nDNA that would impair OXPHOS machinery (Niyazov et al., 2016).

1.2.1 Alzheimer's disease

Alzheimer's disease (AD, OMIM 104300) is the most prevalent neurodegenerative disorder, and clinically characterised by the progressive synaptic dysfunction, neuronal loss in brain regions crucial for memory processing and learning — predominantly in neocortex and hippocampus (Goedert and Spillantini, 2006; Mattson et al., 2008). The histopathological findings reveal the accumulation of extracellular plaques, consisting of amyloid β-peptide (Aβ) and intracellular aggregated neurofibrillary tangles composed of the microtubule-associated protein tau (Mattson et al., 2008; TERRY et al., 1964). Even though it is still debatable, whether primary mitochondrial dysfunctions on their own cause AD, the neurodegeneration downstream of Aβ involves impaired energy metabolism, alterations in Ca^{2+} homeostasis, excessive oxidative stress and potentially apoptosis, suggesting roles for mitochondrial impairment in the AD progress (Mattson et al., 2008). The

reduced cytochrome C oxidase activity was documented in platelets isolated from AD patients (Parker et al., 1990). Furthermore, *in vitro* cellular models have reduced activities of OXPHOS enzymes in the presence of Aβ, and cells eventually commit to death, if they are exposed to Aβ for prolonged time (Pereira et al., 1998). Intriguingly, ρ0 cells depleted of mtDNA are resistant to cytotoxic effects of Aβ (Cardoso et al., 2001). Remarkably, not only RC enzymes were demonstrated to have their activity reduced in brains of AD patients, but also enzymes of TCA cycle, for instance, pyruvate dehydrogenase complex, mitochondrial isocitrate dehydrogenase and α-ketoglutarate dehydrogenase were found to be decreased, further emphasising bioenergetic deficiency in AD brains (Cenini and Voos, 2019). Perturbed Ca^{2+} homeostasis is another pathological hallmark of Aβ aggregation (Supnet and Bezprozvanny, 2010). Aβ interaction with mitochondrial membrane and mutations in ApoE4 (cause of familial AD) shown to result in elevated cytoplasmic Ca^{2+} concentrations rendering neurons susceptible to excitotoxicity (Corder et al., 1993; Mattson et al., 1992; Tolar et al., 1999).

1.2.2 Parkinson's disease

Parkinson's disease (PD, OMIM 168600) is the second most common neurodegenerative disease after AD (Nussbaum and Ellis, 2003). The clinical picture features a loss of midbrain dopaminergic neurons (DNs), leading to the classical triad of symptoms: bradykinesia, tremor and rigidity (Devine and Kittler, 2018). Mitochondrial dysfunction was first implicated in PD aetiology when a severe reduction in CI activity was observed in the post-mortem examination of PD patients' substantia nigra (Schapira et al., 1989). Interestingly, CI deficiency is not confined to substantia nigra, but in fact, was also observed in the frontal cortex (Parker et al., 2008). Intriguingly, numerous epidemiological studies have strengthened further the link between PD and CI deficiency. Agricultural

workers and farmers were found to be at higher risk of developing sporadic PD (Hancock et al., 2008; Pouchieu et al., 2018; Van Maele-Fabry et al., 2012). Inhibitors of CI, paraquat and rotenone which have a long history of application in agriculture as a herbicide and an insecticide, respectively, are potent neurotoxic agents, causing DNs loss in vivo and in vitro (Höglinger et al., 2003; Sherer et al., 2003; Smeyne et al., 2016). Cohort studies in farmers and agricultural workers, conducted in different countries showed a positive correlation between occupational exposure to CI inhibitors and emerging PD cases (Pouchieu et al., 2018).

The genetic cause of PD has remained elusive for long time, and PD has been thought to be predominantly sporadic, until mutations in SNCA gene, encoding α-synuclein were discovered in families with PD (Polymeropoulos et al., 1997). Although, α-synuclein is a principal component of the pathological hallmark of PD – Lewy's bodies, the precise mechanism underlying adverse effects of aggregated α-synuclein remains poorly understood (Devine and Kittler, 2018; Nussbaum and Ellis, 2003). Indirect clues imply that α-synuclein aggregation leads to presynaptic mitochondrial dysfunction. Studies in transgenic mice, overexpressing human mutant α-synuclein show progressive neurodegeneration, with axonal swelling with altered mitochondrial morphology and defects in mitochondrial trafficking (Devine and Kittler, 2018; Martin et al., 2006). Furthermore, the overexpression of mutant α-synuclein was demonstrated to impair neurotransmitter release (Devine and Kittler, 2018; Nemani et al., 2010).

The discovery of mutations in PARK2, which encodes ubiquitin E3 ligase Parkin (Kitada et al., 1998) and the follow-up identification of mutations in PINK1 (Valente et al., 2004), which encodes mitochondrial serine/threonine protein kinase PINK1 provided the most compelling

evidence for the mitochondria involvement in PD pathogenesis (Mouton-Liger et al., 2017).

1.2.3 Leber's Hereditary Optic Neuropathy

The first patient having Leber's Hereditary Optic Neuropathy (LHON, OMIM 535000) was described in the middle of the nineteenth century; however, it took about 20 years until the disease was recognised as a distinct clinical entity by the German ophthalmologist Theodor Leber. The early studies of LHON highlighted the characteristic pattern of bilateral visual loss, associated with the almost exclusive involvement of the optic nerve and its preponderance in young males, which made physicians consider it to be X-linked for the long time (Kirches, 2011; Yu-Wai-Man et al., 2002). The genetic transmission had remained puzzling for more than hundred years, until 1988 when Douglas C. Wallace and colleagues reported the first LHON-associated mutation in mtDNA ND4 gene, encoding a subunit of CI of the RC (Wallace et al., 1988). By now several points mutations exclusively in mtDNA CI genes ND1, ND4 and ND6 were discovered and are accounted to be responsible for 90-95% LHON cases (Hudson et al., 2007; Yu-Wai-Man et al., 2002). LHON typically has an onset in early adulthood, starting with dyschromatopsia. Unlike most other optic neuropathies and glaucoma that progress slowly, the dyschromatopsia is very rapidly followed by the acute loss of vision in one eye with symptoms developing within months in another eye (Hudson et al., 2007; Huoponen, 2001; Wallace et al., 1988; Yu et al., 2018). On the cellular level, LHON manifests as a rapid non-inflammatory death of retinal ganglion cells (RGCs). The mechanism underlying selective vulnerability of RGCs is not well understood, but several studies indicate that disturbed OXPHOS and increased formation of ROS are implicated in the rapid decline of RGCs (Jun et al., 1996; Kirches, 2011; Lin et al., 2012).

1.2.4 Leigh Syndrome

Unlike LHON that arises from mutations exclusively in mtDNA encoded CI subunits, mutations in more than 75 genes in mtDNA and nDNA were identified in the connection to Leigh syndrome (LS, OMIM 256000) (Gorman et al., 2016; Gorman et al., 2015). First described by Dennis Leigh in 1951 as "infantile subacute necrotising encephalomyelopathy" (LEIGH, 1951), LS nowadays is considered to be the most common pediatric mitochondrial disorder affecting 1 in 40,000 live births (Rahman et al., 1996). LS is a highly debilitating progressive neurodegenerative disorder that leads to a premature death within the first years from the perinatal onset. The clinical symptoms are diverse and multisystemic (Quintana et al., 2012). They often include not only neurological manifestations, such as developmental retardation, ataxia, dystonia, deafness, and acute respiratory failure, but also non-neurological manifestations, like lactacidosis, endocrine abnormalities and cardiomyopathy (Chol et al., 2003; Finsterer, 2008). The most common characteristic is the presence of necrotic bilateral symmetric hyperintense lesions in T_2 magnetic-resonance images (MRI) that might affect various brain regions (Finsterer, 2008; Greenberg et al., 1990). Genetically, mutations in CI subunits are the most frequent cause of LS and account for almost 30% of LS cases (Nesbitt et al., 2012; Ng et al., 2019). However, the genetic spectrum is not limited to CI genes. In fact, mutations affecting subunits of every complex of RC, or complexes assembly factors, or genes that are involved in additional steps of energy metabolism, such as pyruvate dehydrogenase complex or coenzyme Q10 might cause LS (DiMauro and Schon, 2008; Finsterer, 2008). Certain success in the understanding pathophysiological mechanism of LS was achieved with the generation of NDUFS4 whole-body knock-out (NDUFS4 KO) mice. These mice resemble human LS: develop fatal encephalopathy with characteristic T_2 lesions, growth

deficiency, ataxia and respiratory abnormalities (Kruse et al., 2008). Following experiments using pan-neuron specific recombination strategy and targeted ablation of *Ndufs4* in certain neuronal populations confirmed the predominant role of the central nervous system (CNS) in LS disease progression and raised questions of differential susceptibility of various neuronal populations to CI deficiency (Bolea et al., 2019; Quintana et al., 2010).

1.2.4 Aminoacyl-tRNA synthetases-associated diseases

Aminoacyl-tRNA synthetases (ARSs) are crucial components of protein synthesis. Their canonical, evolutionary conserved function is to catalyse the first step of protein translation, which is often called charging or aminoacylation. It involves a specific attachment of an amino acid (AA) to its cognate tRNA. All ARSs comprise a catalytic and an anticodon binding domains (Diodato et al., 2014a; Schimmel, 1987). The aminoacylation of tRNA is a two-step reaction (Fig. 1.4). First, an AA and an ATP molecule bind an ARS via its anticodon binding domain to form an aminoacyl-adenylate (AA-AMP) intermediate, releasing a pyrophosphate molecule (PPi). In the second step, the cognate tRNA molecule attaches to the ARS at the anticodon binding site, and the AA is transferred to the tRNA, releasing AMP (Antonellis and Green, 2008; Nie et al., 2019). Additionally, some ARSs have also developed an editing domain to maintain translational fidelity. Those ARSs hydrolyse and deacylate mischarged amino acids during protein synthesis (Schimmel, 2008; Yao and Fox, 2013). Based on their site of action, all ARS can be divided into three groups: 1) cytoplasmic ARS 2) mitochondrial ARS (ARS2), encoded by the distinct set of nuclear genes. 3) two bifunctional, which charge tRNA molecules in both locations (KARS and GARS). According to the standard nomenclature for ARS genes and proteins, the cytoplasmic forms are abbreviated as the single-letter amino acid code followed by ‘ARS’ (e.g.

DARS —aspartyl-tRNA synthetase). For mitochondrial ARS genes, a '2' is appended (e.g. DARS2 — mitochondrial aspartyl-tRNA synthetase).

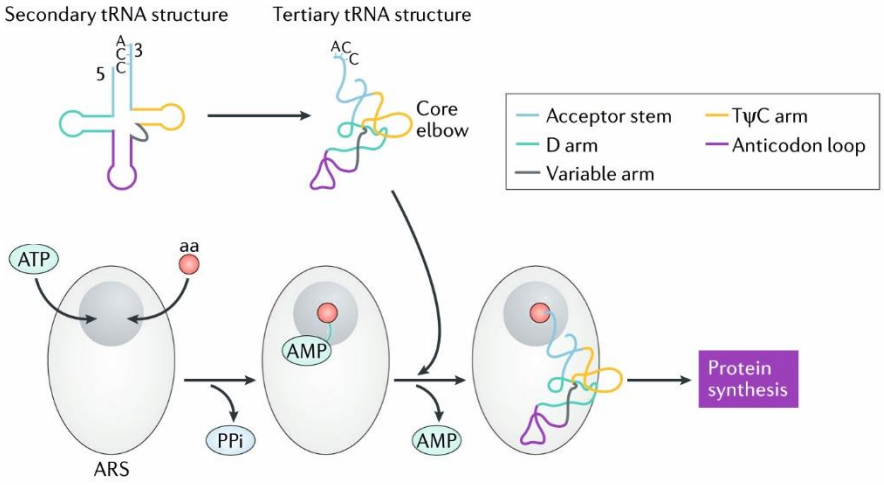

Figure 1.4: Aminoacylation of a tRNA. Two-step catalytic reaction of aminoacyl-tRNA synthetases (ARSs). ARSs use an amino acid (aa), ATP and tRNA as substrates to produce aa-tRNA (lower part). The upper part shows the secondary (left) and tertiary (right) structures of tRNA. The secondary tRNA structure consists of an anticodon loop, D and TψC arms, a variable arm and an acceptor stem to which the aa is ligated *modified from (Kwon et al., 2019).*

ARS2 gained an interest of researchers in the last decade, due to rapidly emerging new mutations and associated with them disease phenotypes (Fine et al., 2019). To date, pathological mutations in each of 19 ARS2 genes were reported (Sissler et al., 2017). The onset of the disease is predominantly right after birth or within the first months of life (Table 1.1).

The prognosis is usually worse for individuals with the perinatal onset: lack of developmental progress, psychomotor delay, and aberrant metabolism frequently result in premature death within first months (Diodato et al., 2014a).

Although ARS2 diseases are phenotypically different and can be multisystemic, DARS2-associated disease seems to be an exception (Rumyantseva et al., 2020). Interestingly, all reported DARS2 patients,

following the first described case (Scheper et al., 2007), were diagnosed with leukoencephalopathy with brain stem and spinal cord involvement and lactate elevation disease (LBSL, OMIM 611105). A distinctive MRI pattern, showing differences from the other defined leukoencephalopathies, gives a diagnostic tool for the disease. LBSL is a postnatal or juvenile-onset disorder, clinically characterised by cerebellar ataxia and spasticity (van Berge et al., 2014; van Berge et al., 2013). Progressive decline of motor skills usually commences in childhood or adolescence and is accompanied by dysarthria. Occasional findings include epilepsy; learning problems; cognitive decline and neurologic deterioration (van Berge et al., 2013).

Table 1.1: Pathologies associated with ARS2 genes

modified from Rumyantseva A. Master Thesis (unpublished)

Gene	Clinical manifestation	Age of onset
AARS2	• Hypertrophic cardiomyopathy (Götz et al., 2011) • Leukoencephalopathy, ovarian failure (Dallabona et al., 2014)	Infancy Infancy-adulthood
CARS2	• Myoclonic epilepsy and progressive cognitive decline (Hallmann et al., 2014) • Epileptic encephalopathy (Coughlin et al., 2015)	Childhood Infancy
DARS2	Leukoencephalopathy with brainstem and spinal cord involvement and lactate elevation (LBSL) (Scheper et al., 2007)	Infancy-adulthood
EARS2	Leukoencephalopathy with thalamus and brainstem involvement, and high lactate (LTBL) (Steenweg et al., 2012)	Perinatal
FARS2	• Encephalopathy and hepatic failure (Alpers-Huttenlocher syndrome) (Elo et al., 2012) • Myoclonic epilepsy without cerebral atrophy (Almalki et al., 2014) • Hereditary spastic paraplegia (HSP) (Yang et al., 2016)	Perinatal Infancy Infancy-adulthood
HARS2	Ovarian failure and progressive hearing loss (Pierce et al., 2011) (Perrault syndrome)	Childhood-adulthood
IARS2	Cataracts, growth hormone deficiency, sensory neuropathy, sensorineural hearing loss, and skeletal dysplasia (CAGSSS) (Schwartzentruber et al., 2014)	Infancy
MARS2	• Autosomal recessive spastic ataxia with leukoencephalopathy (ARSAL) (Bayat et al., 2012) • Growth failure, sensorineural hearing loss, developmental delay, pectus carinatum (Webb et al., 2015)	Infancy-adulthood Perinatal
LARS2	• Ovarian failure and progressive hearing loss (Perrault syndrome) (Pierce et al., 2013) • Lactic acidosis and sideroblastic anemia (Riley et al., 2015)	Adolescence-adulthood Infancy
NARS2	• Epilepsy, myopathy (Vanlander et al., 2015) • Nonsyndromic hearing loss and Leigh syndrome (Simon et al., 2015) • Diffuse degeneration of grey matter, renal dysfunction (Sofou et al., 2015)	Childhood Infancy Infancy
PARS2	Progressive cerebral cortical atrophy, hypertrophic cardiomyopathy (Sofou et al., 2015)	Infancy
RARS2	• Pontocerebellar hypoplasia type 6 (PCH6) (Edvardson et al., 2007) • Epileptic encephalopathy without PCH (Nishri et al., 2016)	Perinatal Infancy
SARS2	• Hyperuricemia, pulmonary hypertension, renal failure, and alkalosis (HUPRA) (Belostotsky et al., 2011) • Spastic paresis (Linnankivi et al., 2016)	Perinatal Infancy
TARS2	Axial hypotonia, severe psychomotor delay (Diodato et al., 2014b)	Perinatal-infancy
VARS2	Microcephaly and epilepsy (Diodato et al., 2014b)	Infancy
WARS2	Leukoencephalopathy (Theisen et al., 2017) Parkinsonism (Burke et al., 2018)	Infancy Infancy
YARS2	Myopathy, lactic acidosis, and sideroblastic anemia (MLASA) (Riley et al., 2010)	Infancy-childhood
GARS	Charcot-Marie-Tooth disease (CMT) dominant (Antonellis et al., 2003)	Childhood-adulthood
KARS	Charcot-Marie-Tooth disease (CMT), recessive and dominant (McLaughlin et al., 2010)	Childhood-adulthood

1.3 Mitochondrial diseases: Search for a cure

The heterogeneity in clinical manifestations of mitochondrial diseases underlies difficulties in diagnostic and therapeutic approaches. The situation for patients is even more complicated, as mitochondrial diseases are associated with high morbidity and mortality and deteriorate severely the life quality (McFarland et al., 2010). To date, the most common therapeutic strategies are aimed to curb symptoms to prevent organ-specific complications, to reduce mortality, or simply limited to palliative care (Gorman et al., 2016). Contrasting an astounding breakthrough, achieved with the whole-exome sequencing (WES) in understanding genetical bases of mitochondrial disease, we are still constrained in our ability to treat them. Mitochondrial diseases are extraordinary heterogeneous on genetic, biochemical, and clinical levels, impeding establishing homogeneous patients' cohorts to analyse the efficacy of a treatment.

1.3.1 Conventional therapeutic strategies

The common therapeutic approaches to treat mitochondrial diseases are the nutritional supplementation with various vitamins, cofactors, antioxidants, and lifestyle changes, including diet and exercises (Gorman et al., 2016).

The limited effectiveness of diet-supplements frequently used to treat mitochondrial diseases is illustrated by the administration of coenzyme Q10 (CoQ10, ubiquinone) and riboflavin (vitamin B2), which are two most widely used medications in a so-called "mitochondrial treatment cocktail" (Parikh et al., 2009). For example, the clinical presentation of CoQ10 primary deficiency varies from isolated myopathy, encephalomyopathy, nephrotic syndrome, severe infantile multisystemic disease, and cerebellar ataxia (López et al., 2014; Ogasahara et al., 1989;

Viscomi et al., 2015). As the CoQ10 is ultimately diagnosed by the detection of its lowered levels in muscle biopsies, the compelling approach for the CoQ10 deficiency treatment would be a diet supplementation with CoQ10 (Yubero et al., 2018). However, for unknown reasons, only a small number of patients have responded to CoQ10 deficiency (Viscomi et al., 2015). Similarly, the diet-supplementation with flavoprotein precursor riboflavin, which is a critical component of some subunits of complexes I and II and a catalytic cofactor of mitochondrial acyl-CoA dehydrogenase family (ACADs), has been only modestly beneficial (Ghezzi et al., 2012; Nouws et al., 2014; Viscomi et al., 2015).

More promising results come from studies of aerobic endurance exercise training and a ketogenic diet (Gorman et al., 2016; Gorman et al., 2015). The exercise training was shown to be beneficial and safe for patients with mtDNA mutations. In particular, the endurance training has led to an increase of mitochondrial mass, achieved by the stimulation of mitochondrial biogenesis, and an upregulation of mitochondrial enzyme activities (Hirano et al., 2018; Taivassalo et al., 2001). Notably, patients with mtDNA mutations who had participated in trials reported improved quality of life, beneficial physiological adaptations, and an increase in the exercise capacity (Gorman et al., 2015; Taivassalo et al., 2006). The ketogenic diet (KD) consisting of high fat, low protein and low carbohydrates regimen has been in used as a treatment for refractory epilepsy for a century (Bough and Rho, 2007). Intriguingly, the KD has demonstrated beneficial effects in mitochondrial diseases patient, who have epilepsy as a symptomatic manifestation like MELAS and LS (Lee, 2012; Steriade et al., 2014; Wijburg et al., 1992). Moreover, the promising results come from a study that combined endurance exercise training with the KD, hinting at the beneficial synergic effect (Miller et al., 2020). However, further work is still needed to explore mitochondrial disease

spectrum responding to the KD and whether the benefits of the KD are preserved on a long-term run.

1.3.2 Innovative therapeutic approaches

The modest curative effect of conventional therapy for the mitochondrial diseases emphasises the need for novel therapeutic approaches. Fortunately, innovative methods and strategies are being developed and showing promising results in pre-clinical studies.

Following the pioneering work of Johnson et al. in 2013, which described the ameliorating effect of rapamycin administration in NDUFS4_KO mice, a model of LS (Johnson et al., 2013), mTORC1 inhibition has emerged as a potential therapeutic strategy. On the one hand, the rapamycin treatment showed a beneficial effect in several mouse models. The improvement in a disease progression was ascertained in mitochondrial myopathy models, caused by COX15 deficiency (Civiletto et al., 2018) and “deletor” mice that carry a mutation in mitochondrial helicase Twinkle (Khan et al., 2017). On the other hand, the rapamycin administration was reported to exacerbate the disease progression in mice with CoQ10 deficiency (Barriocanal-Casado et al., 2019) and in mice, mimicking neuropathology of Alpers syndrome (Ignatenko et al., 2020). Although rapamycin clinical trials have been started in patients with LS, the clinical transferability is debatable. The precise mechanism underlying the beneficial effect of rapamycin remains to be resolved and evaluated in each specific model (Barriocanal-Casado et al., 2019). Additional concerns arise from the rapamycin administration in mice at supramaximal doses that potentially cause adverse side-effects, especially in paediatric use (Felici et al., 2017).

Another unanticipated, but potentially propitious therapeutic approach has emerged from a high-throughput CRISPR-Cas9-mediated whole-genome KO screen (Jain et al., 2016). The screen substantiated that the

inhibition of the Von Hippel-Landau (VHL) factor leading to the constitutively activated hypoxia response pathway, is a genetically effective strategy to ameliorate mitochondrial RC defects (Gorman et al., 2016; Gorman et al., 2015; Jain et al., 2016). Notably, the subsequent animal trials demonstrated the efficacy of this approach in NDUFS4_KO mice. Placing NDUFS4_KO mice in the mildly hypoxic environment of 11 % O_2 significantly increased lifespan, prevented the appearance of bilateral T2 brain lesions, and dramatically improved locomotor function (Ferrari et al., 2017; Jain et al., 2016). Future studies should aim to validate whether hypoxia approach can be used to ameliorate mitochondrial diseases in human patients. Again, clinical transferability remains uncertain as chronic hypoxia was shown to be detrimental and have widespread adverse effects, impairing kidney and pulmonary function that can culminate in heart failure (Brusselmans et al., 2003; Fine and Norman, 2008).

The gene therapy field is developing rapidly, offering exciting therapeutic opportunities to previously incurable diseases. Unsurprisingly, several approaches of the gene therapy for mitochondrial diseases are currently under investigation. The introduction of adeno-associated viral vectors (AAV) has created novel opportunities for the safe delivery and expression of missing/mutated gene. AAVs possesses key features that are of high importance for the clinical application. Firstly, they remain episomal in host cells for prolonged time, not integrating into the genome and thus reducing the risk of the insertional mutagenesis (Duan et al., 1998; Gorman et al., 2016; Gorman et al., 2015). Secondly, they are not associated with human or animal disease (Flotte and Berns, 2005). Lastly, several serotypes of AAVs were selected, enabling tissue/organ specificity (Gao et al., 2005; Gorman et al., 2016; Gorman et al., 2015). The major constraint of AAV application is their limited ability to cross blood-brain

barrier (BBB), which makes AAV-targeting of brain challenging (Silva-Pinheiro et al., 2020). To date, the partial amelioration of deleterious phenotype in a mouse model was reported for AAV-mediated delivery of *Ndufs4* (Di Meo et al., 2017). Recently, the promising data has been obtained using a novel derivative of AAV9 serotype – AAV-PHP.B that shows an enhanced capacity to cross BBB and raises great expectations for the gene therapy for neurodegenerative diseases (Reynaud-Dulaurier et al., 2020; Silva-Pinheiro et al., 2020).

Mitochondrial diseases caused by mutations in mtDNA classically present an additional challenge, as a result of co-existence of mutated DNA and wild-type (WT) mtDNA. The favourable way to prevent the severity of the clinical phenotype would be the reduction of the mutational load of mtDNA below the disease threshold level (Hashimoto et al., 2015). To date, two studies have demonstrated in vivo the effectiveness of mitochondrial-targeted DNA editing enzymes. The selective elimination of mutant mtDNA with either mitochondrially targeted zinc-finger nucleases (mtZFNs) or transcription activator-like effector nucleases (mito-TALENs) in a mouse model with a heteroplasmic pathogenic mtDNA have rescued the phenotype without apparent toxicity. (Bacman et al., 2018; Gammage et al., 2018). Perhaps, even more promising, and effective way to prevent mitochondrial diseases arising from mtDNA mutations is mitochondrial replacement therapy (MRT). In this approach, a mother's nuclear material is isolated and transferred into enucleated donor's oocytes, excluding the transmission of mutated mtDNA to offspring (Zhang et al., 2017).

1.3 Objectives

Neurodegeneration is a typical feature of mitochondrial diseases. Currently, no specific treatment has been developed to prevent it, and patient care is palliative and focused on symptoms management. Our laboratory has previously demonstrated that by removing mitochondrial matrix protease proteolytic subunit (CLPP), we could alleviate symptoms of mitochondrial cardiomyopathy, caused by DARS2 deficiency (Seiferling et al., 2016). The concomitant loss of CLPP in DARS2-deficient heart-specific background ameliorates COX-deficiency, decreases cardiomyopathy markers levels, leading to partial rescue of the lifespan of mice (Seiferling et al., 2016). The open question now is whether effects observed in heart reflect tissue specificity.

Therefore, the overarching goal of this study was to ascertain the therapeutic potential of CLPP ablation in mouse models of mitochondrial encephalopathy driven by DARS2 deficiency. To this end, we employed two different conditional knock-out (KO) models: forebrain-neuron-specific Dars2 KO (*Dars2_KO*^{FbNe}) (Aradjanski et al., 2017) and newly developed Purkinje cell-specific Dars2 KO (*Dars2_KO*^{PC}) mice. Generation of double KOs (DKOs) for both models allowed us to avoid the bias of targeting only one specific neuronal population. Moreover, it enabled simultaneous analysis of the effect exerted by the CLPP loss in two distinct models of mitochondrial encephalopathy.

2 Materials and Methods

2.1 Animal care and experiments

2.1.1 Mouse models, housing, and care

Dars2$^{loxP/loxP}$ mice, described previously (Dogan et al., 2014) were crossed to L7-Cre mice (Barski et al., 2000). The resulting double heterozygous animals were crossed to *Dars2*$^{loxP/loxP}$ mice to generate Purkinje cell-specific knock-outs (*Dars2_KO*^{PC}). Forebrain-specific *Dars2_KO* was mediated by CamkIIα promoter and has been described previously (Aradjanski et al., 2017) Double knock-out animals under control of L7 and CamkIIα promoters were generated by mating with double floxed animals *Dars2*$^{loxP/loxP}$ *Clpp*$^{loxP/loxP}$, described previously (Seiferling et al., 2016). All mice used in experiments were of C57BL/6N genetic background.

All mice were kept in individually ventilated cages, with an enriched environment at ambient room temperature of 22-24 °C in the CECAD *in vivo* research facility. All mice had *ad libitum* access to food (normal chow diet for breeding and standard keeping ssniff cat. number V1154-7331 and V1554-7331) and water and were maintained in a specific pathogen-free facility with 12 h:12 h light:dark cycle. Mating of mice was performed once they reached eight weeks of age and one male was simultaneously housed with maximum two females. Upon weaning, mice of the same sex were housed 2-5 animals per cage. If *Dars2_KO*^{FbNe} and *DKO*^{FbNe} mice started to scratch themselves, they were placed alone in a cage. Mouse housing, breeding and all experiments were approved by the Landesamt für Natur, Umwelt, Verbraucherschutz (LANUV), Nordrhein-Westfalen, Germany. All procedures were conducted in accordance with university,

national, European recommendations and followed the guidelines of the Federation of European Laboratory Animals Associations (FELASA).

2.1.2 Isolation of genomic DNA and genotyping

Isolation of crude genomic DNA (gDNA) for genotyping purposes was done from mouse ear biopsies. The ear biopsies were lysed in 500 µL lysis buffer (100 mM Tris-HCl, 200 mM NaCl, 5 mM EDTA, 0.2 % w:v SDS, 0.2 mg/mL Proteinase K) at 55 °C under shaking for minimum 4 h. Afterwards, the precipitation of gDNA was achieved with 500 µL of 2-propanol at 20,000 x *g* for 20 min at RT. The precipitated gDNA was washed once with 70 % (v:v) ethanol at 20,000 x *g* for 20 min at RT. gDNA pellet was dried at RT and dissolved in 90 µL ddH_2O and stored at 4 °C until use. The correct genotype of animals was determined by genotyping PCR, followed by electrophoresis in 2 % agarose gel with ethidium bromide, allowing to resolve wild-type (WT) alleles and alleles possessing loxP sites and presence of Cre transgene. Primer sequences are given in the table 2.1

<u>*Dars2* PCR mix:</u>

1 µL	gDNA template
0.8 µL	Each primer (10 µM)
2 µL	DreamTaq™ buffer (10x)
1 µL	dNTP mix (1.25 mM each)
0.1 µL	DreamTaq™ polymerase (5 u/µL)
14.3 µL	ddH_2O

Clpp PCR mix:

1 µL	gDNA template
0.8 µL	Each primer (10 µM)
4 µL	GoTaq® buffer (5x)
2 µL	MgCl2 (25 mM)
1 µL	dNTP mix (1.25 mM each)
0.05 µL	GoTaq® polymerase (5 u/µL)
10.35 µL	ddH_2O

Cre PCR mix:

1 µL	gDNA template
0.6 µL	Each primer (10 µM)
4 µL	GoTaq® buffer (5x)
2 µL	$MgCl_2$ (25 mM)
3.2 µL	dNTP mix (1.25 mM each)
0.1 µL	GoTaq® polymerase (5 u/µL)
8.5 µL	ddH_2O

PCR cycling conditions for *Dars2* and *Clpp*:

Initiation	5 min	95 °C	
Denaturation	30 sec	95 °C	30 cycles
Annealing	30 sec	60 °C	
Extension	45 sec (*Dars2*) 1 min (*Clpp*)	72 °C	
Final extension	7 min (*Dars2*) 10 min (*Clpp*)	72 °C	

PCR cycling conditions for *Cre:*

Initiation	5 min	95 °C	
Denaturation	30 sec	95 °C	35 cycles
Annealing	30 sec	53 °C	
Extension	30 sec	72 °C	
Final extension	7 min	72 °C	

Table 2.1: Primer sequences for genotyping PCRs

PCR	Primer Fw [5'-3']	Primer Rv [5'-3']
Dars2	ATGAATTCTAGGCCAGCCAC	TGGCAATCTCTTAGGACTAAG
Clpp	GTGGATGATGGTCAGTAGAATCC	CCCAGACATGATTCCTAGCAC
Cre	CACGACCAAGTGACAGCAAT	AGAGACGGAAATCCATCGCT

2.1.3 Simple Composite Phenotype Scoring

The simple composite phenotype scoring system, described previously (Guyenet et al., 2010) consisting of separate tests: Ledge Test, Hind Limb Test, Gait Test and Kyphosis Test was used to evaluate mice behaviour. Each test utilised a scale of 0-3, with 0 corresponding to "unimpaired performance" and 3 — "severely impaired". Below, a brief description of each test is given, each test was repeated three times.

Ledge Test: a mouse was placed on the ledge of the cage. 0 = a mouse was walking along the ledge, not losing balance and was able to descent smoothly back into the cage. 1 = a mouse was losing balance, slipping occasionally. 2 = a mouse was not effectively using its hind limbs and was not landing gracefully on its paws when descending. 3 = a mouse was not able to walk and stay on the ledge, falling from it.

Hind Limb Test: a mouse was griped and lifted by its tail for 10 sec. 0 = hind limbs were spread wide and away from its abdomen. 1 = one hind limb was retracted to the abdomen and stayed there for more than 5 sec. 2 = a mouse repeatedly pulled both hind limbs towards the abdomen. 3 = both hind limbs were retracted to the abdomen and stayed there for more than 5 sec.

Gait Test in open field: a mouse was placed on a flat surface facing away from the researcher. 0 = a mouse was walking normally, no limping, abdomen was not touching the surface. 1 = a mouse appeared to limp or

have tremor during walking. 2 = a mouse was limping or tremoring severely, exhibited lowered pelvis, or feet was pointing away from the body. 3 = a mouse had severe difficulties in moving, dragged its abdomen along the surface, and, in case of *Dars2_KO*^{PC}, exhibited difficulties of keeping balance on the surface.

Kyphosis Test: a mouse was placed on a flat surface, and its dorsal curvature was monitored. 0 = a mouse was able to straighten its spine while walking. 1 = a mild kyphosis was present, but it was not persistent. 2 = a persistent mild kyphosis was present, and a mouse was not able to completely straighten its spine. 3 = a pronounce, persistent kyphosis was observed, as a mouse was walking or sitting.

2.1.4 Euthanasia

For tissue harvest intended for protein lysis, mitochondria isolation and cryosectioning mice (male and female) were sacrificed by cervical dislocation.

For immunohistochemistry (IHC), mice (male and female) were anaesthetized intraperitoneally with ketamine (100 mg/kg body weight) and xylazine (20 mg/kg body weight) and perfused transcardially with 0.01 M PBS followed by 4 % paraformaldehyde (PFA) in 0.01 M PBS. Cerebella or forebrains were dissected, post-fixed overnight at 4 °C in 4 % PFA in 0.01 M PBS and stored until use at 4 °C in 0.01 M PBS.

2.2 Biochemistry

2.2.1 Isolation of protein from brain

Following the cervical dislocation, cerebella, cortices, hippocampi, or alternatively, the whole forebrain were rapidly dissected, snap-frozen on dry ice, and stored at -80 °C until use. The lysis of tissues was performed in RIPA buffer (50 mM Tris/HCl pH = 7.4, 150 mM NaCl, 5 mM EDTA, 1 % w:v sodium deoxycholate, 1 % v:v Triton-X, 1 % w:v SDS supplemented with protease inhibitor SIGMAFast). First, tissues were homogenised with ceramic bead CK14 (Precellys, Bertin Instruments) in a benchtop tissue homogeniser (Precellys 24, Bertin Instruments) twice at 6000 rpm 20 sec. Subsequently, samples were incubated on ice for 10 min and spun down at 20,000 x *g* for 30 min at 4 °C. Cleared supernatants containing protein fraction were transferred into fresh 1.5 mL microcentrifuge tubes and either stored at -80 °C until use or immediately used for the protein quantification. The protein concentration was determined by the Bradford assay against a series of bovine-serum albumin (BSA) standard, using SpectraMax® Paradigm® (Molecular Devices).

2.2.2 SDS polyacrylamide gel electrophoresis and western blot

Proteins were separated according to their molecular size with sodium dodecyl sulfate-polyacrylamide gel electrophoresis (SDS-PAGE). Gels for SDS-PAGE consist of two parts. The upper part, a ‘stacking gel’ possesses larger pores, thus allowing protein samples to gather uniformly before entering the resolving (separation) part of the gel. The recipes for the resolving and stacking gels are given in the table 2.2. Gels were cast between glass plates and assembled into the Mini-PROTEAN® Tetrasystem (Biorad, Munich, Germany). The chamber was filled with

running buffer (25 mM Tris/HCl pH= 8.3, 250 mM glycine, 0.1 % w:v SDS). 30 µg of protein sample was mixed with Laemmli buffer (50 mM Tris/HCl, pH=6.8, 2 % SDS w:v, 10 % glycerol v:v, 1 % 2-mercaptoethanol v:v , 12.5 mM EDTA, 0.02 % w:v bromophenol blue) boiled at 95 °C for 5 min, centrifuged at 20,000 x *g* (5430R centrifuge) for 1 min and directly loaded onto a gel. After the loading of the protein samples was completed, gels were run at 80 V for 20 min and then at 150 V for 50 min. The molecular weight of proteins was approximated with Prestained Page-ruler™ Plus protein ladder (Thermo Fischer Scientific). After the SDS-PAGE was completed, proteins were immobilised onto a nitrocellulose membrane (Amersham™ Protran™ 0.45 µm NC GE Healthcare) by wet transfer. SDS-PAGE electrophoresis chamber was disassembled, and gels were incubated shortly in a transfer buffer (25 mM Tris, 192 mM glycine, 0.1 % SDS, 20 % methanol). Subsequently, a gel holder wet transfer cassette, in which a gel and nitrocellulose membrane were pressed together between two fibre pads and Whatmann filter paper sheets (GE Healthcare), was placed into a Criterion™ (Biorad) tank filled with the transfer buffer and run at 400 mA, at 4 °C for 2 h, or at 80 mA, overnight, at 4 °C. To check if the transfer was successful, a nitrocellulose membrane was transiently incubated with Ponceau S solution (0.1 % w:v in 5 % acetic acid) to reveal proteins. To eliminate unspecific antibody (AB) binding, WB membranes were incubated, under constant agitation in a blocking solution (5 % w:v dried non-fat milk powder in 0.01 M PBS supplemented with 1 % Tween®-20, PBST) or alternatively in 2 % fish skin gelatine in Tris-buffered saline (TBS: 20 mM Tris, 150 mM NaCl) supplemented with 1 % Tween®-20 (TBST) for 40 min, RT, under constant agitation. Next, the membranes were incubated in primary AB (table 2.3) in 5 % non-fat milk in PBST or 2 % fish skin gelatine in TBST under constant agitation, overnight, at +4 °C. Next day, the membranes were washed three times in PBST or TBST, 5 min

each wash, at RT and subsequently incubated with secondary AB (table 2.4) conjugated to horseradish-peroxidase (HRP) diluted in PBST or TBST. Subsequently, the membranes were washed in PBST or TBST three times and dipped briefly in ddH_2O to eliminate traces of the detergent. Afterwards, the membrane was immersed into the enhanced chemiluminescent substrate (ECL, Detection Reagent Amersham™) for 1 min. Finally, membranes were exposed to Super RX films (Fujifilm) and developed with an automatic film processor (Kodak).

Table 2.2: Composition of polyacrylamide gels for SDS-PAGE

Separating gel	Stacking gel
10-12 % Acrylamide/bis-acrylamide 40(29:1)	4 % Acrylamide/bis-acrylamide 40(29:1)
375 mM Tris/HCl pH=8.8	125 mM Tris/HCl pH=6.8
0.1 % SDS	0.1 % SDS
1.25 % APS	1.25 % APS
0.125 % TEMED	0.125 % TEMED

2.2.3 Isolation of mitochondria from forebrain

Freshly dissected forebrains were washed on ice-cold 0.01 M PBS and cut into small pieces. The pieces were transferred to an isolation buffer (220 mM mannitol, 70.1 mM sucrose, 104 mM HEPES, 0.2 % w:v BSA, pH = 7.7) and homogenised with 10 strokes at 1000 rpm (Potter S, Sartorius). Homogenates were spun down at 1000 x *g* for 10 min at 4 °C, supernatant containing mitochondria fraction was distributed equally into several 1.5 mL microcentrifuge tubes, while pellet was homogenised again with 10 strokes at 1000 rpm (Potter S, Sartorius). The centrifugation step was repeated (1000 x *g* for 10 min at 4 °C) and supernatant was distributed into several 1.5 mL microcentrifuge tubes, as before. All 1.5 mL microcentrifuge tubes were spun down at 8000 x *g,* 10 min at 4 °C to pellet mitochondria fraction. Next, mitochondria containing pellets were washed in a “freezing” buffer (500 mM sucrose, 10 mM HEPES pH = 7.7)

combining fractions corresponding to the same forebrain, spun down at 8000 x *g*, 10 min at 4 °C. Finally, pelleted mitochondria were resuspended in the "freezing" buffer and either used immediately for *in organello* translation or frozen until use at -80 °C for BN-PAGE and *in-gel* activity assay. Isolation of mitochondria was done together with Mr Matthijs Hermeling.

2.2.4 Blue native polyacrylamide gel electrophoresis and in-gel activities of CI and CIV

Blue native polyacrylamide gel electrophoresis (BN-PAGE) was performed in NativePage Novex Bis-Tris Gel System (Life Technologies) according to the manufacturer's instructions. Briefly, 10 µg mitochondria were lysed 4 % digitonin. First, samples were incubated on ice for 15 min and subsequently spun down at 20,000 x *g* for 30 min at 4 °C. Supernatants were then loaded onto 4-16 % pre-cast Bis-Tris minigels (Novex, Invitrogen), run at 150 V for 30 min 4 °C, and at 250 V for 4 h, 4 °C. To reveal *in-gel* activity of CI, a BN-PAGE gel was incubated in NADH-nitrotetrazolium blue solution (0.1 mg/mL NADH, 2.5 mg/mL nitrotetrazolium blue, 5 mM Tris/HCl pH=7.4) for 1 h, at 37 °C under constant agitation. Next, the BN-PAGE gel was destained for 2 h RT in a solution, containing 50 % v:v methanol, 10 % v:v acetic acid and rehydrated for 2 h in ddH_2O. Next, the BN-PAGE gel was incubated overnight at 37 °C, in cytochrome C and 3, 3 diaminobenzidine tetrahydrochloride (DAB) solution (1 mg/mL cytochrome C, 1 mg/mL DAB, 0.4 mg/mL catalase, 50 mM Tris/HCl pH=7.4) to reveal *in-gel* activity of CIV. Following the destaining and rehydration procedures, described above, wet transfer (see 2.2.2) was performed. The blotting of proteins onto a polyvinylidene difluoride (PVDF) membrane (Biorad) took place in western blot transfer buffer without methanol and SDS, the subsequent

blocking and AB detection was performed as described above (see 2.2.2). BN-PAGE and *in-gel* activity assay was done together with Ms. Milica Popovic.

2.2.5 De novo mitochondrial protein synthesis

In organello translation was evaluated in freshly isolated mitochondria by labelling de novo synthetised mitochondrial proteins with 35S-methionine. For that, 1.5 mg of freshly isolated mitochondria were incubated for 1 h, 37 °C, on rotating wheel in 1 mL [^{35}S]-translation buffer (100 mM mannitol, 10 mM sodium-succinate, 80 mM KCl, 5 mM $MgCl_2$, 1 mM KH_2PO_4, 25 mM HEPES pH=7.4, 5 mM ATP, 200 µM GTP, 6 mM creatine phosphate, 60 µg/mL creatine kinase, 60 µg/mL cysteine, 60 µg/mL tyrosine, 60 µg/mL amino acids (Ala, Arg, Asp, Asn, Glu,Gln, Gly, His, Ile, Leu, Lys, Phe, Pro, Ser, Thr, Trp, Val), 7 µL/mL [^{35}S]-methionine). Subsequently, mitochondria were pelleted at 12,000 x *g* for 2 min and resuspended in 1 mL non-radioactive translation buffer containing unlabelled methionine. Half of the sample ('pulse fraction') was pelleted again, resuspended in 100 µL Laemlli buffer, incubated for 30 min at RT and stored before loading onto a SDS-PAGE gel at -20 °C. The “chase fraction” which enables to estimate protein turnover, was incubated for 3 h at 37 °C on a rotating wheel in a presence of unlabelled methionine. Subsequently, the 'chase fraction' was pelleted 12,000 x *g* for 2 min, resuspended in 100 µL Laemlli buffer, incubated for 30 min at RT. SDS-PAGE was performed in a running buffer (composition given in 2.2.2) in SE600X Chroma Deluxe Dual Cooled Vertical Protein Electrophoresis Unit (Hoefer), overnight at 80 V at RT. On the next day, a gel was stained for 30 min in Coomassie solution (1 % w:v Coomassie Brilliant Blue R-250, 50 % v:v methanol, 10 % v:v acetic acid), to reveal separated according size proteins. Afterwards, the gel was destained for approximately 5 h in a solution containing 45 % methanol, 10 % acetic acid, at RT, under

constant agitation. Subsequently, the gel was dried at 80 °C for 2 h in Gel Dryer (Model 583, Biorad). Finally, the gel was exposed following 5 days to a film (Amersham Hyperfilm, GE Healthcare) which was developed with an automatic film processor (Kodak).

2.3 Histology

2.3.1 Tissue Sectioning

Following the transcardial perfusion (see 2.1.4), stored in 0.01 M PBS brains were cut using a vibratome (Leica Microsystems). Generally, cerebella of *Dars2_KO*^{PC} and *DKO*^{PC} were cut in the midsagittal plane, while forebrains of *Dars2_KO*^{FbNe} and *DKO*^{FbNe} in the coronal plane. For immunohistochemical staining sections of 50 µm were used. Free-floating sections were stored in 0.01 M PBS at 4 °C until use. Alternatively, for the long-term storage, free-floating sections were preserved in the cryoprotectant solution (30 % ethylene glycol, 30 % glycerol, 0.01 M PBS) at -20 °C.

Cryosections were obtained with a cryostat (Leica CM1850). Following cervical dislocation (see 2.1.4) brains were immediately isolated and directly fresh-frozen in Tissue-Tek O.C.T (Sakura) embedding medium on dry ice and stored until further use at -80 °C. As for immunohistochemical procedures, cerebella of *Dars2_KO*^{PC} and *DKO*^{PC} were cut in the midsagittal plane, while forebrains of *Dars2_KO*^{FbNe} and *DKO*^{FbNe} in the coronal plane. Sections were obtained at -25 °C and transferred directly at poly-L-Lysine glass slides (VWR) and stored until use at -20 °C. Thickness of cryosections was 10 µm.

2.3.2 COX/SDH staining

Double enzymatic COX/SDH staining was performed on 10 µm cryosections. Briefly, cryosections were first incubated 37 °C with COX solution (0.8 mL of DAB, 0.2 mL of 500 µM cytochrome c, a few grains of catalase) 45 min, at 37 °C. Next, cryosections were washed briefly in ddH_2O, and incubated 90 min at 37 °C with SDH solution (0.8 mL of 1.875 mM nitrotetrazolium blue, 0.1 mL of 1.3 M sodium succinate, 0.1 mL of 2 mM phenazine methosulphate, 0.01 mL of 100 mM sodium azide).

Subsequently, cryosections were shortly washed in ddH_2O, dehydrated through graded alcohols, each immersion 2 min (70 % ethanol, 96 % ethanol, and 100 % ethanol), cleared in xylol and mounted with Entellan®.

2.3.3 Haematoxylin and Eosin staining

10 µm cryosections were incubated in Mayer's haematoxylin solution for 4 min, washed in tepid water for 30 sec, colour was fully developed during 15 min incubation in cold tap water. Afterwards, cryosections were briefly immersed into ddH_2O, and placed into eosin solution (Sigma-Aldrich) for 1 min. Subsequently, cryosections were washed in cold tap running water, dehydrated through graded alcohols, each immersion 2 min (70 % ethanol, 96 % ethanol, and 100 % ethanol), cleared in xylol and mounted with Entellan®

2.3.4 TUNEL assay

10 µm cryosections were used for terminal deoxynucleotidyl transferase dUTP nick end labeling (TUNEL) assay. Apoptag Plus Peroxidase *In Situ* Apoptosis Detection Kit (Millipore) was used according the manufacturer's protocol. Briefly, cryosections were postfixed in 1 % PFA in 0.01 M PBS solution for 10 min at RT. Subsequently, sections were washed twice in 0.01 M PBS, each time 5 min. Permeabilization of the tissues was done in pre-chilled ethanol:acetic acid 2:1 mixture for 5 min at -20 °C. Following the permeabilisation, sections were washed twice in 0.01 M PBS, each time 5 min, and incubated in 3 % H_2O_2 in 0.01 M PBS solution to quench endogenous peroxidase activity. Next, sections were washed twice in 0.01 M PBS and covered with equilibration buffer (EB) for at least 15 sec. Subsequently, EB was gently tapped-off and sections were incubated with the working strength TdT enzyme for 1 h at 37 °C. The reaction was stopped following the immersion of sections into the washing buffer for 10 min at RT and subsequent three washes in 0.01 M

PBS, 1 min each. Next, sections were incubated with anti-digoxigenin peroxidase conjugate for 30 min at RT, washed four times in 0.01 M PBS, 2 min each wash, briefly immersed in ddH_2O and incubated in DAB Peroxidase substrate for 1.5-2 min. The colour development was monitored under the microscope. Next, sections were briefly washed in ddH_2O and counter-stained in 0.5 % (w:v) methyl green. Afterwards, the sections were washed in tap running water and dehydrated through graded alcohols, each immersion 1 min (70 % ethanol, 96 % ethanol, and 100 % ethanol), cleared in xylol and mounted with Entellan®.

2.3.5 Immunohistochemistry procedures

Free-floating midsagittal sections of cerebella and coronal sections of forebrain (50 µm thickness) were first permeabilized with 0.5 % Triton-X in 0.01 M PBS for 15 min at RT. For SHMT2 this step was exchange for heat-induced antigen retrieval in Tris/EDTA pH=9 buffer for 25 min at 80 °C. Next, sections were incubated overnight at 4 °C, under agitation with primary AB in 3 % BSA in 0.01 M PBS. The list of primary AB and their respective dilutions is given in table 2.3. The next day, sections were washed three times 10 min each wash under agitation in 3 % BSA in 0.01 M PBS and incubated 2 h, RT under agitation with secondary fluorophore-conjugated AB in 0.01 M PBS. The list of secondary AB and their respective dilutions is given in table 2.4. Finally, sections were washed in 0.01 M PBS, counterstained with 4',6-diamidino-2-phenylindole (DAPI) and mounted with AquaPolymount (Polysciences).

2.3.6 Transmission electron microscopy

For the transmission electron microscopy (TEM) freshly isolated cortices were minced into 5-10 tiny pieces and post-fixed in 2 % glutaraldehyde/2 % fomaladehyde in 0.1 M cacodylate buffer (pH=7.3).

Subsequent, sample processing, embedding, contrasting, and cutting were performed at the CECAD Imaging facility by Ms. Janine Klask.

2.4 Image Capture, Analysis and Processing

2.4.1 Image capture

Brightfield images of TUNEL assay, H&E, and COX/SDH stained sections were taken with a slidescanner (Leica SCN400) at 20x magnification. IHC stained sections were imaged with a confocal laser-scanning microscope (TCS SP8 Leica Microsystems). Z-stack images were acquired following the Nyquist sampling in sequential mode.TEM micrographs were acquired together with Ms. Janine Klask at a transmission electron microscope (JEM 2100 Plus, JEOL), equipped with a OneView 4K camera (Gatan) and DigitalMicrograph software at 80 kV at RT. Western blot films and *in-gel* activity gels were scanned with the Epson V800 transparency scanner at 800 dpi.

2.4.2 Image analysis

Purkinje cell density was assessed by counting the number of PC and dividing it by the length of the cerebellar loop occupied by the counted cells. SHMT2 and ATPB expression in PC was evaluated at the single-cell level using Image Calculator plugin for Fiji (Fiji is Just ImageJ). Shortly, mitochondrial area showing immunoreactivity for SHMT2 in PC was found in a single-stack confocal images of the corresponding channel by using the equation: signal=min (ATPB, SHMT2). The pixel area in the resulting mask was quantified and subsequently normalized over the corresponding thresholded single-stack image of the ATPB channel, resulting in the fraction of mitochondria displaying SHMT2 expression.

The number of neurons per mm^2 of retrosplenial cortex was assessed by counting the number of NeuN positive cells in a ROI, defined in Fiji (Fiji is Just ImageJ) and dividing it by the area of ROI in mm^2.

To quantify the area fraction occupied by IBA-1 positive (IBA-1$^+$) microglia in cerebellum midsagittal sections of *Dars2_KO*^{PC}, *DKO*^{PC} and respective controls, 23-30 ROIs within 6-8 cerebellum loops were marked using Fiji (Fiji is Just ImageJ), thresholded, and automatic particle counting corresponding to IBA-1$^+$ microglia was performed with Analyze Particles menu command. The sum of area occupied by IBA-1$^+$ microglia in a cerebellum was divided by the total area of ROIs and normalised over the control. To quantify area fraction occupied by IBA-1$^+$ microglia in RSC, motor cortex (2-3 ROIs) and dentate gyrus of hippocampus (1 ROI) were selected in Fiji (Fiji is Just ImageJ) and particle analysis was performed as described before.

To measure protein expression levels, intensities of specific bands (dynamic range of grey scale per mm^2 of a scanned film), corresponding to the proteins of interest were determined by Image J. Densitometric values were normalised relative to control.

2.4.3 Image processing

Image J, Fiji (Fiji is Just ImageJ), Leica Application Suite X (version 3.7.1.21655) and CorelDRAW 2018 (version 20.1.0.708) were used to set up uniformly contrast and brightness. Figure preparation was done with CorelDRAW 2018. To create additional illustrations Biorender.com with Premium membership was used, figures created with Biorender.com are marked as such.

2.5 Statistical Analysis

All statistical analyses were performed using Graph Pad Prism 8.0.2 software. Details of statistical tests can be found at corresponding figure legends. Unless stated otherwise, all data are present as mean ± SD.

2.6 Data Accessibility

All data supporting the findings of this study are available within this dissertation. Experimental protocols, unprocessed images, and raw quantification data are deposited at nas9. uni-koeln.de — a storage of the University of Cologne, at the space allocated for the Prof. Aleksandra Trifunovic's lab (AG-Trifunovic) and available upon request. No libraries and omics data were generated and deposited in the public repositories.

2.7 Key Resources

2.7.1 Primary and Secondary Antibody

Table 2.3: Primary AB

Antibody	Source	Identifier	Application, Concentration
anti-ATPB	Abcam	cat.no ab5432	IHC 1:500
anti-CALBINDIN D1I4Q	Cell Signalling	cat. no 13176	IHC 1:1000 WB 1:1000
anti-CALBINDIN D-28 K	SWANT	cat. no 300	IHC 1:1000 WB 1:1000
anti-CALNEXIN, C-Terminal (575-593)	Sigma-Aldrich	cat. no 208880	WB 1:1000
anti-COXI	Invitrogen	cat. no 459600	WB 1:2000
anti-GFAP GA5	Cell Signalling	cat. no 3670	IHC 1:2000 WB 1:20000
anti-HSC70	Santa Cruz	cat. no sc-7298	WB 1:4000
anti-IBA-1	Fujifilm Wako Chemicals	cat. no 019-19741	IHC 1:2000 WB 1:500
anti-NDUFA9	Invitrogen	cat. no 459100	WB 1:5000
anti-NeuN, clone A60	Sigma-Aldrich	cat. no MAB377	IHC 1:1000
anti-SHMT2	Sigma-Aldrich	cat. no HPA020543	IHC 1:100

Table 2.4: Secondary AB

Antibody	Source	Identifier	Application, Concentration
goat anti-rabbit IgG (H+L)-Alexa fluor 546	Invitrogen	cat. no A-11035	IHC 1:2000
goat anti-mouse IgG (H+L)-Alexa fluor 488	Invitrogen	cat. no A-11001	IHC 1:2000
goat anti-mouse IgG-HRP	Sigma-Aldrich	cat. no A4416	WB 1:2000
goat anti-rabbit IgG-HRP	Sigma-Aldrich	cat. no A6154	WB 1:2000

*WB = western blot; IHC = immunohistochemistry

2.7.2 Chemicals

Name	Source
[^{35}S]-Methionine	Hartmann Analytic
2-Mercaptoethanol	Sigma Aldrich
2-Propanol	Applichem
Acetic Acid	AppliChem
Acetone	AppliChem
Adenosine-tri-phosphate ATP	Sigma Aldrich
ADP Adenosine 5'-diphosphate sodium Salt	Sigma Aldrich
Agarose NEEO Ultra-Quality	Roth
Alanine (L-)	Sigma Aldrich
Arginine mono-hydrochloride (L-)	Sigma Aldrich
Asparagine monohydrate (L-)	Sigma Aldrich
Aspartic Acid (L-)	Sigma Aldrich
Bradford	Sigma Aldrich
Bromophenol Blue	MERCK
BSA (Albumin from bovine serum) fatty acid free	Sigma Aldrich
Catalase, bovine liver	Sigma Aldrich
Coomassie Brilliant Blue R250	MERCK
Creatine Phosphokinase Type III, bovine	Sigma Aldrich
Cysteine hydrochloride monohydrate (L-)	Sigma Aldrich
Cytochrome c, equine heart	Sigma Aldrich
DAB	Vector

DAPI	AppliChem
DDM Dodecyl-β-maltosicyl	Roth
dNTPs	Promega
DreamTaq™ buffer (10x)	ThermoFischer Scientific
DreamTaq™ polymerase	ThermoFischer Scientific
EDTA Ethylenediaminetetraacetic acid	Sigma Aldrich
Entellan®	Merck Millipore
Eosin	Sigma Aldrich
Ethanol	AppliChem
Ethidium bromide	Sigma Aldrich
Gelantine, cold water fish skin	Sigma Aldrich
Glutamine (L-)	Sigma Aldrich
Glycerol	Sigma Aldrich
Glycine Molecular Biology grade	AppliChem
GoTaq® buffer (5x)	Promega
GoTaq® polymerase	Promega
GTP Guanosine 5'triphosphate sodium salt	Sigma Aldrich
H_2O_2 30%	Fluka
HCl 37%	VWR
HEPES-Molecular biology grade	AppliChem
Histidine mono hydrochloride monohydrate (L-)	Sigma Aldrich
Isoleucine (L-)	Sigma Aldrich
Ketamin hydrochloride CIIIN	Sigma Aldrich
Leucine (L-)	Sigma Aldrich
Lysine mono-hydrochloride (L-)	Sigma Aldrich
Magnesium chloride hexahydrate	Fluka Analytical
Mannitol	AppliChem
Mayer's haemotoxylin	Sigma Aldrich
Methionine (L-)	Sigma Aldrich
$MgCl_2$ 25 mM	Promega
Milk powder	AppliChem
Nitrotetrazolium Blue	Sigma Aldrich
NP-40 Nonidet P40	AppliChem
Paraformaldehyde Powder 95%	Sigma Aldrich
PBS Buffer (10X Dulbecco's) Powder	AppliChem
Phenylalanine (L-)	Sigma Aldrich
PMS (Phenazine methosulfate)	Sigma Aldrich
Ponceau S	Abcam

Potassium chloride	AppliChem
Potassium phosphate monobasic	Sigma Aldrich
Proline (L-)	Sigma Aldrich
Protease Inhibitor tablets EDTA free	Roche
Protein Standard	Sigma Aldrich
Proteinase K	AppliChem
SDS granules	Sigma Aldrich
Serine (L-)	Sigma Aldrich
Sodium azide	AppliChem
Sodium chloride for molecular biology	Sigma Aldrich
Sodium deoxycholate	AppliChem
Sodium hydroxide	Sigma Aldrich
Sodium phosphate dibasic	Sigma Aldrich
Sodium phosphate dibasic dihydrate	Sigma Aldrich
Sodium phosphate monobasic	Sigma Aldrich
Sodium succinate dibasic hexahydrate	Sigma Aldrich
Sucrose	Sigma Aldrich
TEMED	Sigma Aldrich
Threonine (L-)	Sigma Aldrich
Tri-sodium citrate dihydrate	AppliChem
Triton™ X 100	Sigma Aldrich
Trizma® Base (Tris)	Sigma Aldrich
Tryptophan (L-)	Sigma Aldrich
Tween® 20	VWR
Tyrosine (L-)	Sigma Aldrich
Valine (L-)	Sigma Aldrich
Xylazine Hydrochloride	Sigma Aldrich
Xylol	Roth

3 Results

3.1 DARS2 loss in Purkinje cells leads to progressive cerebellar ataxia and neuroinflammation

3.1.1 Generation of Dars2 Purkinje cell-specific knockout mouse model

To date, the vast majority of DARS2 patients suffering from LBSL was reported to have a compound heterozygous mutation, one of which was predominantly intron 2 mutation, leading to incorrect exon 3 splicing (Isohanni et al., 2010; Scheper et al., 2007). Intriguingly, neuronal cells were demonstrated to have lower wild-type DARS2 exon 3 inclusion (van Berge et al., 2012). The defect in splicing arising from the intron 2 mutation exacerbated further the exon 3 skipping (van Berge et al., 2012), prompting us to speculate that neurons are most susceptible to DARS2 mutations than the other cell types.

Previously, we have established that DARS2 deficiency cannot be recapitulated globally in mice: DARS2 is essential for embryonic development, and embryos lacking it die *in utero* before E8.5 (Dogan et al., 2014). Therefore, we turned to tissue-specific *Dars2* knock-out (KO) mouse models.

Recently characterised forebrain neuron-specific *Dars2*_KO (henceforth referred to as *Dars2_KO*^{FbNe}) mouse model (Aradjanski et al., 2017) is indispensable to study DARS2 depletion effect on forebrain neurons in a generalized manner but does not give insights on LBSL-associated neuronal cell type-specific vulnerability. To address this important question, a novel Purkinje cell (PC)-specific knockout mouse model was generated (henceforth referred as *Dars2_KO*^{PC}) by breeding *Dars2*$^{loxP/loxP}$ mice to *L7-Cre* transgenic mice (Fig. 3.1). *Cre*-mediated recombination under control of *L7* promoter starts at postnatal day 5-7 and is fully established at 2-3 weeks of age (Barski et al., 2000). The presence of the transgene and loxP sites were verified by PCR (Materials and Methods).

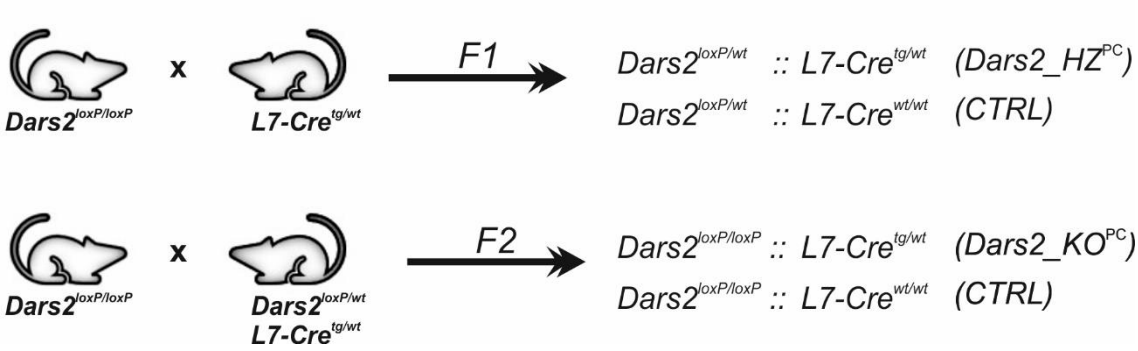

Figure 3.1: Generation of PC-specific *Dars2* knock-out mice (*Dars2_KO*^{PC}). F1 and F2 breeding strategy**.**

Dars2_KO^{PC} mice were born at Mendelian ratio; animals of both sexes were viable and indistinguishable from control (*CTRL*) mice. However, at about 15 weeks of age, *Dars2_KO*^{PC} mice showed visible motor impairment, manifested as loss of equilibrium, incoordination, and unsteady gait. *Dars2_KO*^{PC} mice survived to 25-28 weeks of age, at which time they had to be sacrificed due to severe ataxia. To study dynamic changes imposed by DARS2 deficiency in PCs, we set a time-course analysis of PC morphology, starting from 6 weeks, when no behavioural manifestations were observed, to 15 weeks (Rumyantseva et al., 2020).

Analysis of the PC layer by haematoxylin-eosin (H&E) staining in *Dars2_KO*^{PC} mice disclosed no apparent changes at 6 and 8 weeks of age (Fig. 3.2). In contrast, we observed a prominent loss of PC, resulting in the PC layer disruption in *Dars2_KO*^{PC} mice at 15 weeks (Fig. 3.2).

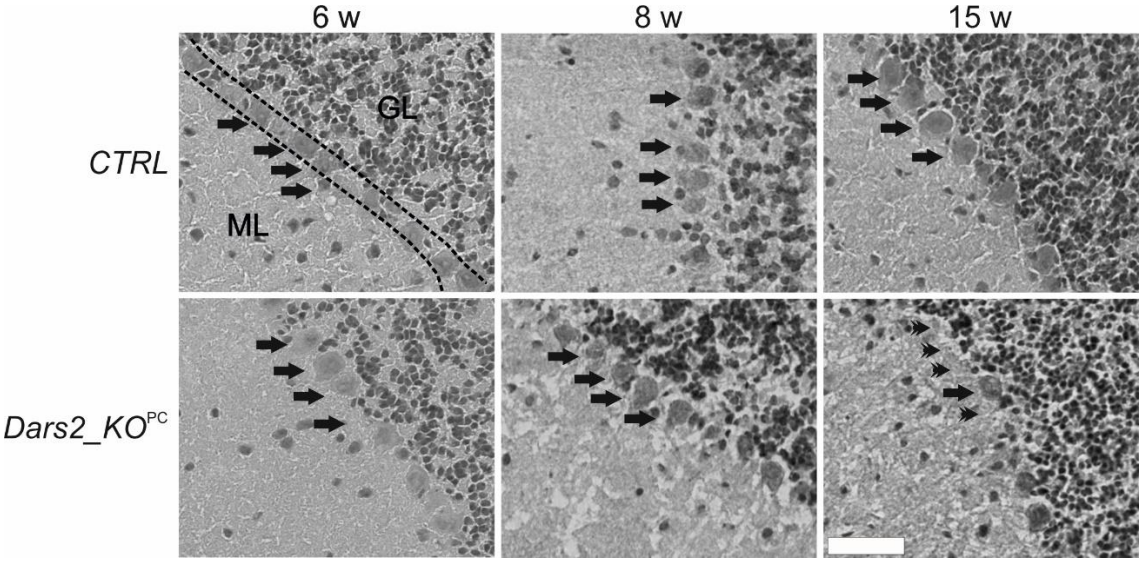

Figure 3.2: General cerebellar morphology of *Dars2_KO*^{PC}. Representative images of H&E staining at the indicated time points, arrowheads indicate PC; GL: granular cell layer; ML: molecular cell layer; scale bar=100 µm. *Unmodified from (Rumyantseva et al., 2020)*

As *Dars2_KO*^{FbNe} mice were reported to have progressively decreased brain weight and body weight (Aradjanski et al., 2017), we evaluated these general parameters in *Dars2_KO*^{PC} animals.

The brain mass and the bodyweight of were not affected at any of the analysed time-points (Fig. 3.3A and B). Notably, despite the overt loss of PC in 15-weeks-old *Dars2_KO*^{PC} mice, the cerebellar size was not different (Fig. 3.2C), indicating that postnatal DARS2 depletion in PCs did not affect cerebellar growth or induced massive atrophy (Rumyantseva et al., 2020).

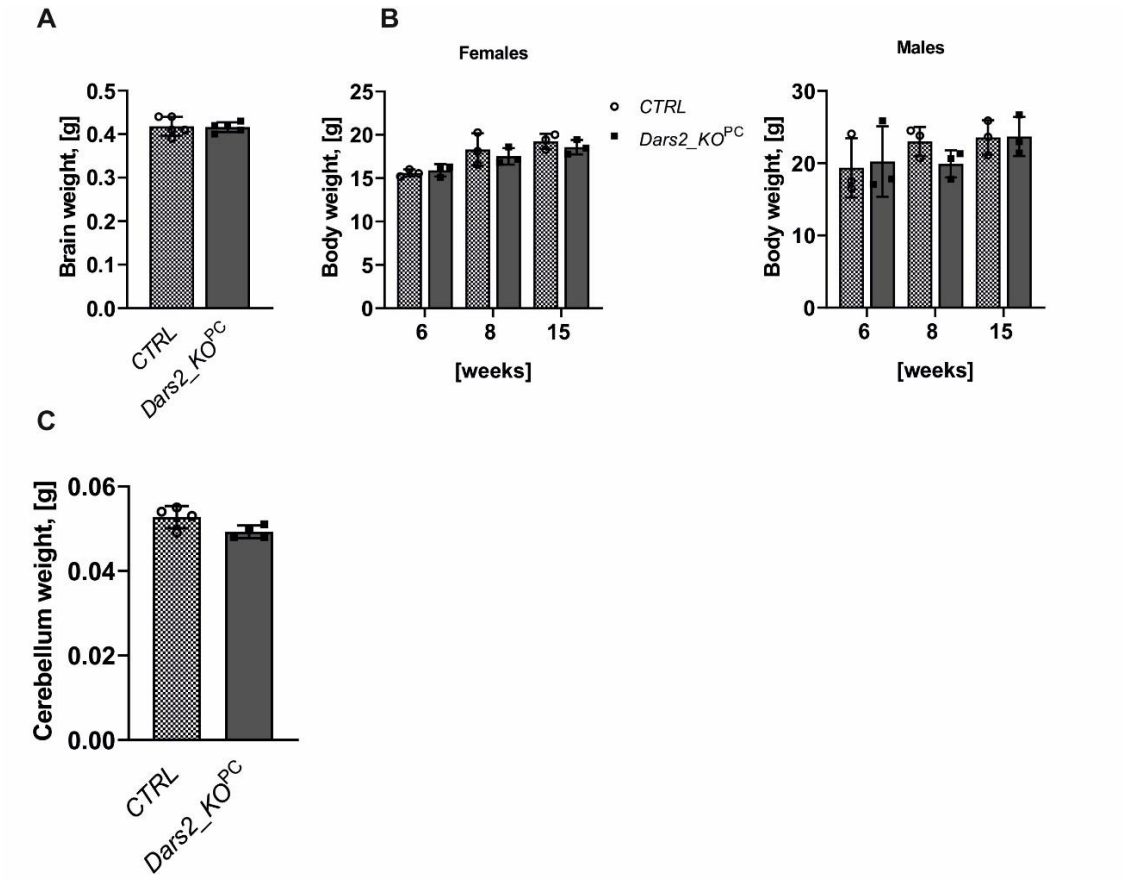

Figure 3.3: General characteristics of *Dars2_KO*^{PC}. (A) Brain weight of *CTRL* and *Dars2_KO*^{PC} at 15 w of age data presented as mean ± SD. **(B)** Bodyweight gain from 6 to 15 w of female and male mice *CTRL* vs *Dars2_KO*^{PC}, data presented as mean ± SD (n=3-5 mice per genotype per time point). **(C)** Cerebellum weight in *CTRL* vs *Dars2_KO*^{PC} at 15 w of age data presented as mean ± SD (n=3-4 mice per genotype and time point). *Unmodified from (Rumyantseva et al., 2020)*

3.1.2. Massive PC loss leads to motor skill deterioration

To analyse cytoarchitecture of cerebella, we took advantage of PC specific marker calbindin. Calbindin is expressed abundantly in the PC somata and dendrites, enabling to perform immunofluorescent (IF) staining on midsagittal cerebellar sections (Fig. 3.4A). In agreement with H&E staining, 8-weeks-old *Dars2_KO* ^{PC} mice did not exhibit either PC loss or changes in PC dendrite morphology. In sharp contrast, 15-weeks-old

Dars2_KO^{PC} mice had PC numbers decreased significantly, making up only 50 % of the *CTRL* animals (Fig. 3.4A and B).

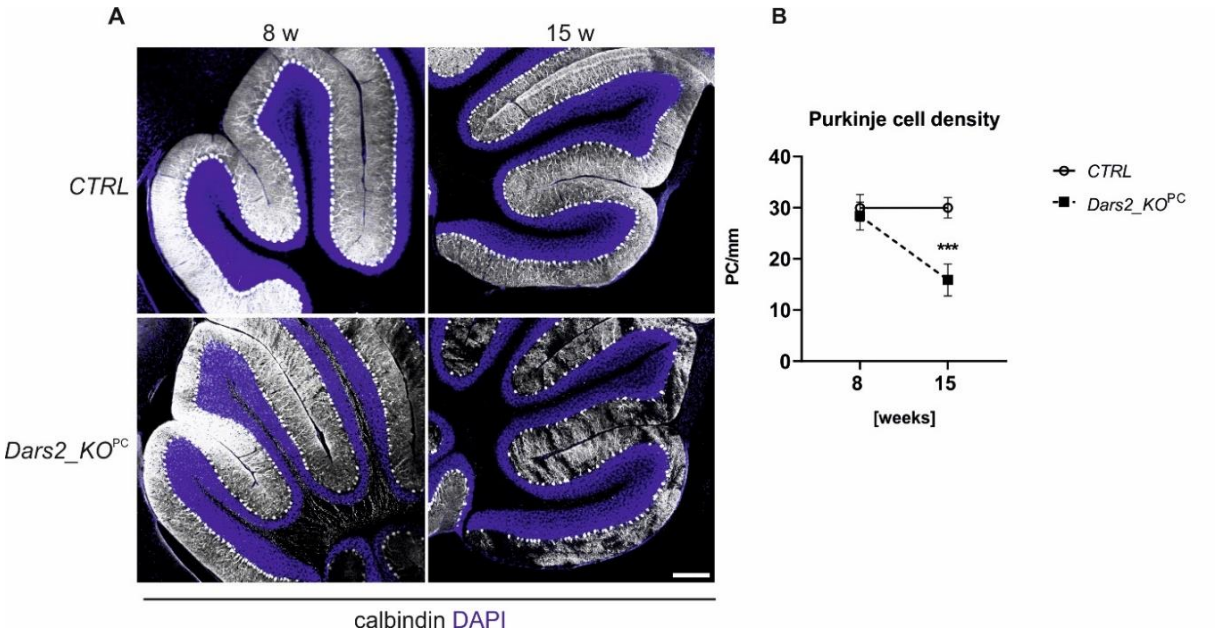

Figure 3.4: Massive PC loss in *Dars2_KO*^{PC} by 15 w of age. (A) Representative confocal images of midsagittal sections of cerebellar vermis lobules II-III of *CTRL* and *Dars2_KO*^{PC}at the indicated time points labelled immunofluorescently with an antibody against calbindin (grey, Purkinje-specific marker) and DAPI (blue, nuclei) scale bar=200 µm. **(B)** Quantification of PC density from (A), data presented as mean ± SD (One-way ANOVA, ***p < 0.001, n=5-7 lobules from three mice, per genotype and time point). *Unmodified from (Rumyantseva et al., 2020)*

Furthermore, the organisation of dendritic arbours of the remaining PCs in *Dars2_KO*^{PC} mice was highly impaired, displaying signs of severing and fragmentation that potentially affected cerebellar connectivity (Fig. 3.5A). Notably, cerebellar lobules displayed variable severity of PC loss. The most prominent PC loss was observed in the anterior (lobules I-V) and central zone (lobules VI-VII), whereas lobules IX and X had more Purkinje neurons preserved (Fig. 3.5B).

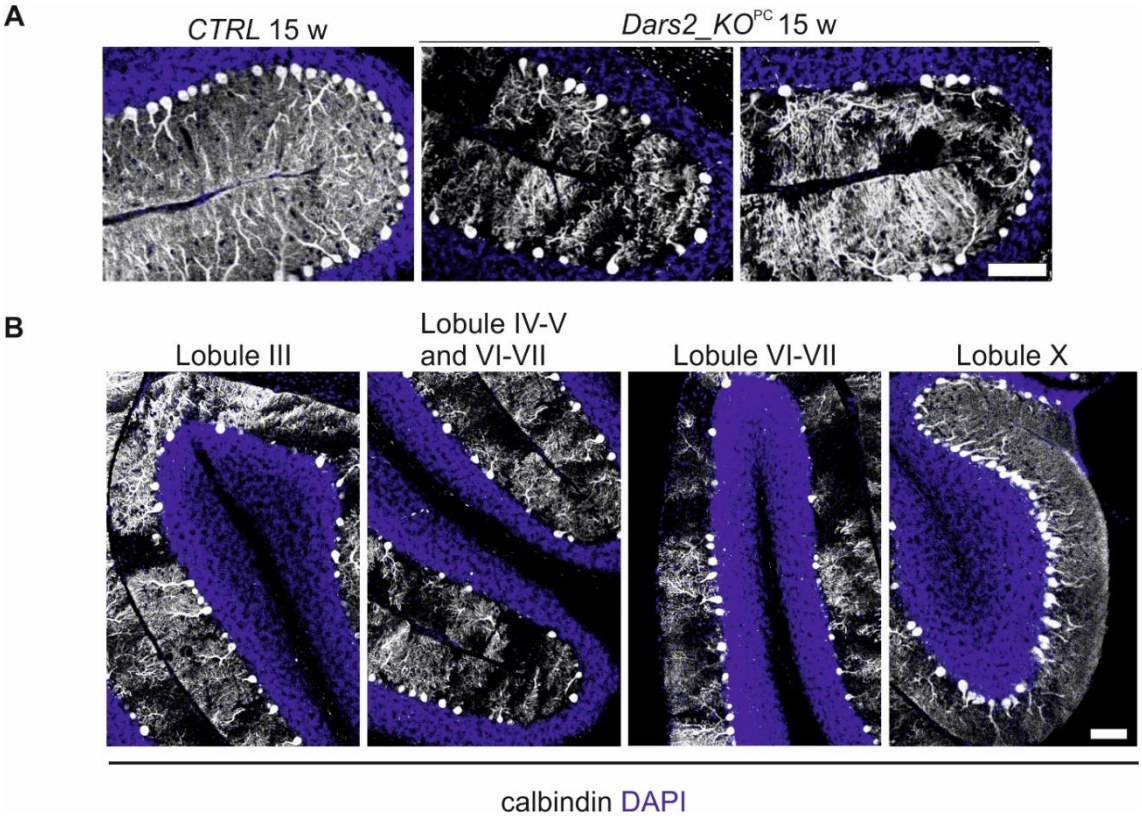

Figure 3.5: Spatial heterogeneity of PC loss in *Dars2_KO*^{PC} at 15 w of age. (A) Close-ups of PC layer in 15 w old *CTRL* and *Dars2_KO*^{PC} mice (lobules VI-VII and VIII) labelled immunofluorescently with the antibody against calbindin (grey, Purkinje-specific marker) and DAPI (blue, nuclei) scale bar=100 µm. **(B)** Representative confocal images of lobules III, IV-V, VI-VII and X are shown. Scale bar=200 µm. *Unmodified from (Rumyantseva et al., 2020)*

Predictably, this striking decrease in PC numbers impaired motor performance, evaluated by measurements of Ledge Test, Hind Limb Test, Gait Test, and occurrence of kyphosis. At 15 weeks of age, *Dars2_KO*^{PC} mice were unable to keep their balance when walking on the ledge, receiving a significantly higher score than the age-matching *CTRL* mice (Fig. 3.6A). Consistently, lack of balance and coordination manifested in the Gait Test for *Dars2_KO*^{PC} mice. At 15 weeks of age, they showed disturbed, unsteady gait while walking on a flat surface (Fig. 3.6B). However, the 15-week-old *Dars2_KO*^{PC} mice did not show any difference in the hind limb clasping response (Fig. 3.6C). Similarly, kyphosis was

observed only in some animals of this age (Fig. 3.6D). Notably, *Dars2_KO*^{PC} mice exhibited progressive deterioration of motor skills, confirmed by significantly higher scores in all tests, excepting kyphosis evaluation, at 22 weeks of age (Fig. 3.6A-D). Together these results demonstrate that the defect in mitochondrial translation, caused by DARS2 deficiency triggers PC loss after 8 weeks of age and results in severe ataxic phenotype of *Dars2_KO*^{PC} mice.

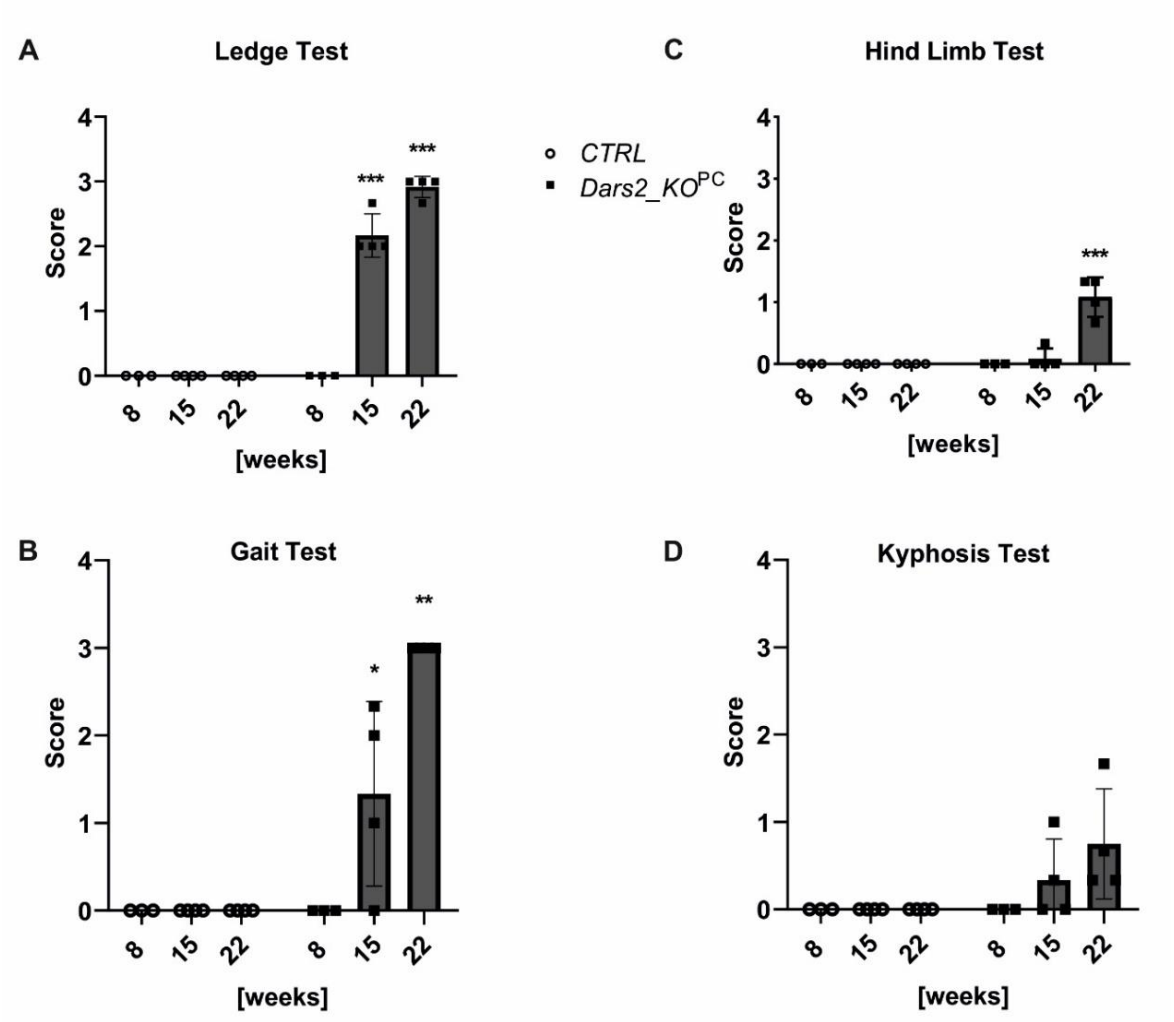

Figure 3.6: Simple composite phenotype scoring. (A) Ledge Test **(B)** Gait Test **(C)** Hind Limb Test **(D)** Kyphosis Test of *CTRL* and *Dars2_KO*^{PC} at the indicated time points, data presented as mean ± SD (One-way ANOVA,*p<0.05; ** p<0.01; ***p < 0.001; n=3-4 per genotype and time point). *Unmodified from (Rumyantseva et al., 2020)*

3.1.3 Strong respiratory chain dysfunction coincides with massive PC loss in Dars2_KO^{PC} mice

The impaired function of the respiratory chain (RC) enzymes, following the loss of DARS2, has been previously shown in heart and skeletal muscle-specific *Dars2_KO* (Dogan et al., 2014) and in *Dars2_KO*^{FbNe} mouse models (Aradjanski et al., 2017). To assess activities of RC enzymes, we took advantage of COX/SDH double staining. This histochemical technique allows sequential analysis of enzymatic activities of Complex IV (cytochrome c oxidase, COX) and Complex II (succinate dehydrogenase, SDH) *in situ*. While COX activity is highly dependent on the mitochondrial gene expression, as its core subunits are encoded by mtDNA, SDH is entirely encoded by nuclear DNA, and its activity is typically unaltered, or even upregulated, by impaired mitochondrial gene expression (Ross, 2011). As expected, cerebella of *CTRL* mice, including PC layer, displayed uniformly a saturate brown staining at all analysed time points, indicating functioning COX (Fig. 3.7 upper panel). Notably, first signs of COX deficiency (indicated by blue colour) in individual PC were detected already in 6 and 8-weeks old *Dars2_KO*^{PC} mice, (Fig. 3.6A lower panel). Moreover, the elaborated dendrites of PCs, which are almost entirely occupied by mitochondria (Chen et al., 2007), occasionally had a characteristic blue colour, pinpointing RC dysfunction. Remarkably, at 15 weeks of age, all remaining PCs of *Dars2_KO*^{PC} mice had intense blue staining, implying exacerbation of RC function.

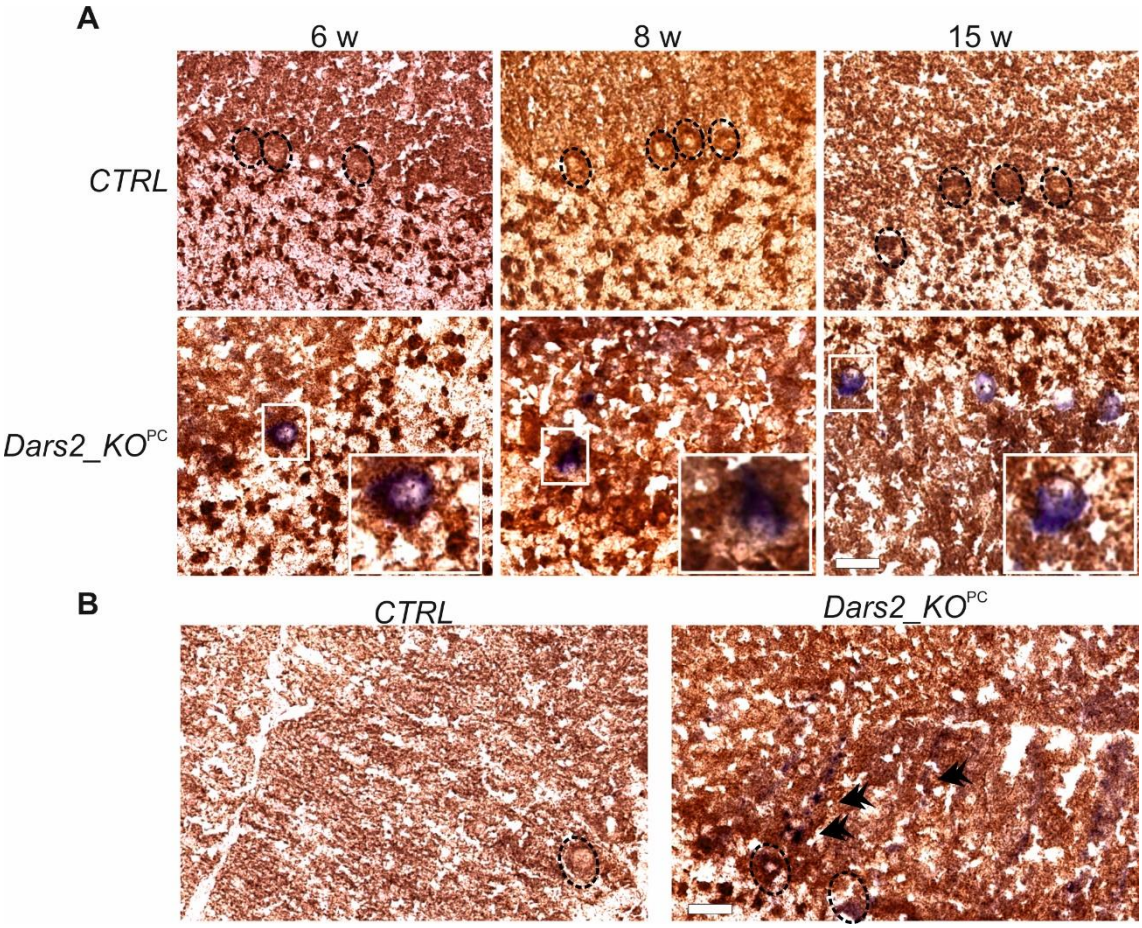

Figure 3.7: Strong respiratory chain dysfunction coincides with massive PC loss in *Dars2_KO*^{PC} mice. **(A)** Representative images of midsagittal sections of cerebellar vermis stained for COX/SDH activity at the time points, PCs are marked by a dashed circle in *CTRL* mice, close-up of SDH-positive PCs in *Dars2_KO*^{PC} in white squares, scale bar=100 µm. **(B)** Representative images of midsagittal sections of cerebellar vermis stained for COX/SDH activity showing PC (dashed circles), cerebellar molecular layer, and PC dendrites (double arrowheads), scale bar=100 µm. *Unmodified from (Rumyantseva et al., 2020)*

To corroborate COX/SDH staining data and to further probe the mitochondrial function, we analysed the levels of ATP synthetase beta subunit (ATPB). No overt difference in immunoreactivity was observed in *Dars2_KO*^{PC} mice at 8 weeks of age compared to age-matched controls (Fig. 3.8). However, when we performed immunohistochemistry at a 15-week-old, a decrease in PC numbers in *Dars2_KO*^{PC} coincided with diminished ATPB levels in the remaining PC and apparent mitochondrial network fragmentation (Fig. 3.8). These results highlight the importance

of DARS2 for maintaining OXPHOS function in PCs, which otherwise leads to the neuronal loss (Rumyantseva et al., 2020).

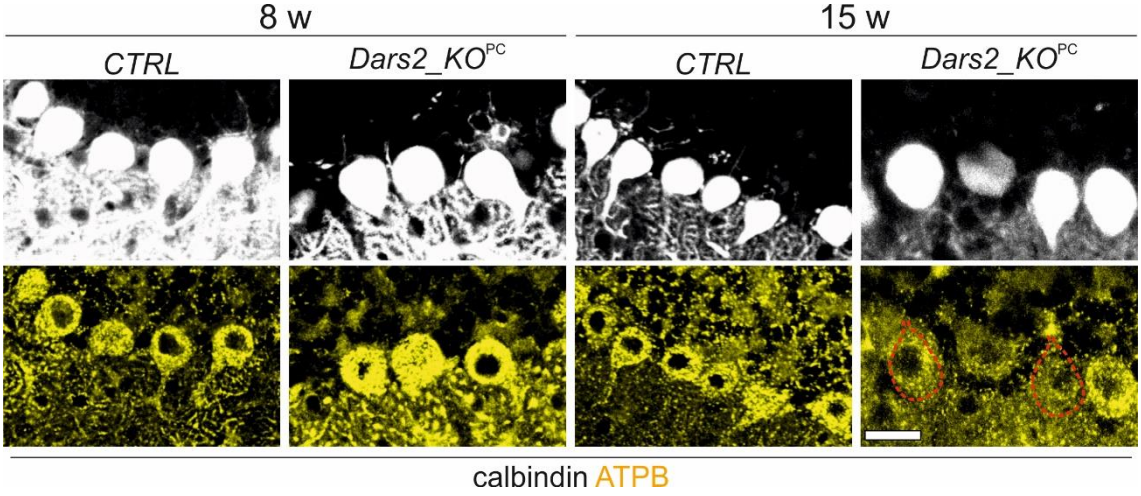

Figure 3.8: Diminished ATPB levels in *Dars2_KO*^{PC} mice at 15 w of age. Representative confocal images of midsagittal sections of cerebellar vermis lobule VI-VII of *CTRL* and *Dars2_KO*^{PC} at the indicated time points labelled immunofluorescently with antibodies against calbindin (grey, Purkinje-specific marker) and ATPB (yellow, mitochondria) scale bar=25 µm. *Unmodified from (Rumyantseva et al., 2020)*

3.1.4 Dars2 haploinsufficiency in PCs does not lead to aberrant phenotype

Previous studies in *Afg3l2* haploinsufficient mice showed a progressive decline in motor coordination, late-onset PC degeneration and cerebellar dysfunction correlating with the decreased assembly of RC complexes and altered mitochondria morphology (Maltecca et al., 2009).

To test, if PCs are sensitive to the reduced *Dars2* dosage, we followed PC-specific *Dars2* haploinsufficient mice (*Dars2_Hz*^{PC}) up to 38 weeks of age. *Dars2_Hz*^{PC} developed normally and were fertile up to 52 weeks of age. Not only PC layer was intact (Fig. 3.9A), but also no signs of decreased OXPHOS function were detected by COX/SDH double staining (Fig. 3.9B). Remarkably, *Dars2_Hz*^{PC} were indistinguishable from wildtype (WT) control littermates at 28 and 38 weeks of age (Fig. 3.9C) and did not display any behavioural signs associated with cerebellar impairment

(data not shown). These results indicate that one copy of *Dars2* gene is sufficient to maintain RC function, and only entire postnatal deletion of it

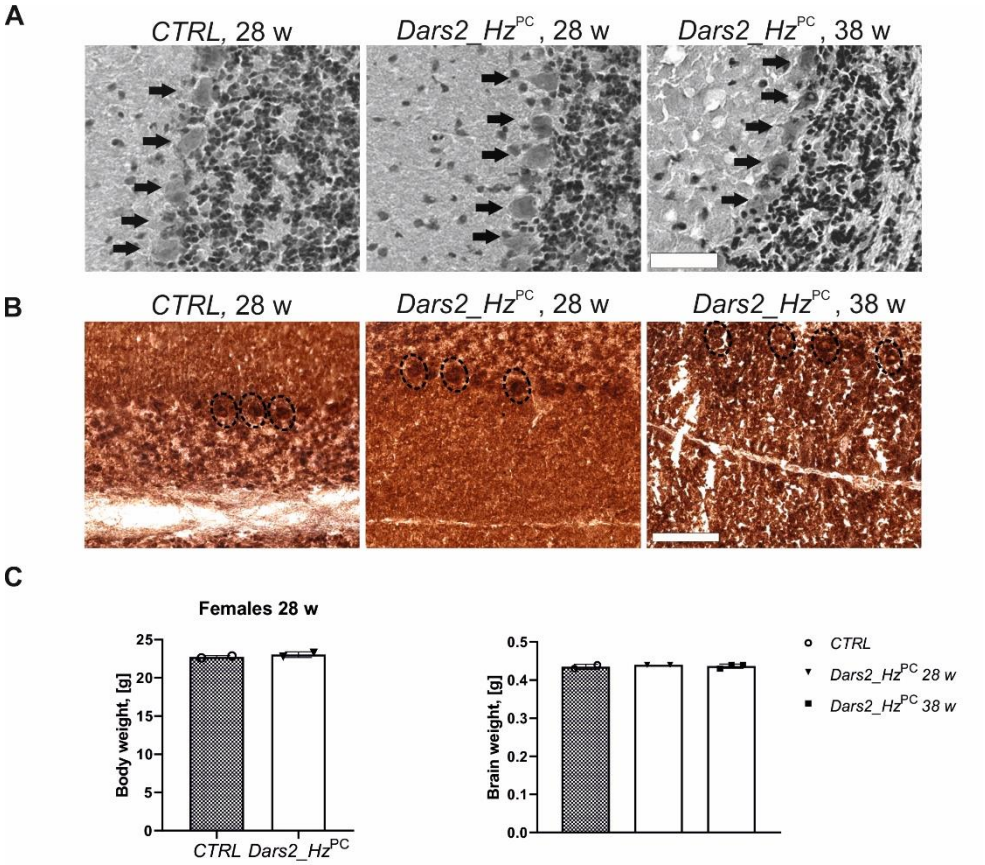

leads to severe mitochondrial dysfunction and dramatic loss of PCs.

Figure 3.9: PC-specific *Dars2* heterozygous mice (*Dars2_Hz*^{PC}) are not different from WT control littermates (*CTRL*). **(A)** Representative images of midsagittal sections of the cerebellar vermis of H&E staining at the indicated time points, arrowheads indicate PC; scale bar=100 µm. **(B)** Representative images of midsagittal sections of cerebellar vermis COX/SDH staining at the time points, PCs are marked by a dashed circle scale bar=100 µm **(C)** Body and brain weight of *CTRL* and *Dars2_KO*^{PC} at indicated time points data presented as mean ± SD (n=2 mice per genotype and time point). *Unmodified from (Rumyantseva et al., 2020)*

3.1.5 PC loss evokes neuroinflammation

A growing body of evidence supports the notion that neuroinflammation not only accompanies the neurodegeneration but precedes massive neuronal loss, further abrogating neuron-glial communication and underlying the progression of neurodegeneration (Ransohoff, 2016). We

anticipated that impaired cerebellar homeostasis following OXPHOS dysfunction in PC would result in the hypertrophy of astrocytes (astrogliosis) and microglial cells (microgliosis).

Interestingly, protein levels of glial fibrillary protein (GFAP), a marker of Bergmann glia, unipolar astrocytes around PC somata were unaltered in *Dars2_KO*^{PC} mice at 6 weeks of age, despite commenced mitochondrial dysfunction (Fig. 3.10A and B).

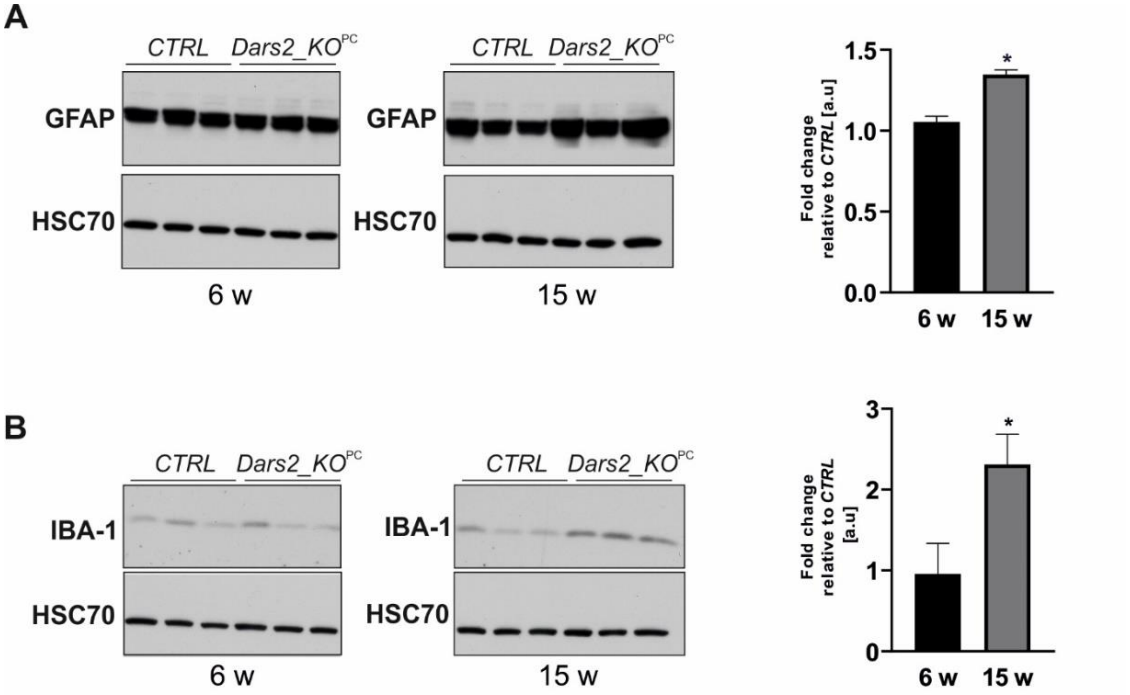

Figure 3.10: PC loss causes upregulation of neuroinflammation markers on a protein level at 15 w of age. (A) Immunoblot of whole cerebellar lysates *CTRL* vs *Dars2_KO*^{PC} 6 and 15 w for an astrocytes marker (GFAP) **(B)** Immunoblots of whole cerebellar lysates *CTRL* vs *Dars2_KO*^{PC} at 6 and 15 w for a microglia marker (IBA-1), quantification presented as mean ± SEM, Student's t-test, *p < 0.05 (n=3 mice per genotype and time point). *Unmodified from (Rumyantseva et al., 2020)*

Moreover, we did not detect increased levels of ionized calcium-binding adaptor protein-1 (IBA-1). Strikingly, the 2.5-fold increase in lBA-1, paired with the significant increase in GFAP levels, was observed in *Dars2_KO*^{PC} mice at 15 weeks of age. Conversely, the previous study in *Afg3l2* PC-specific knockout mice reported the increase in hypertrophic Bergmann glial and microglia prior to the loss of PC and functional signs of neurodegeneration (Almajan et al., 2012). To investigate, if neuroinflammatory changes and astrogliosis take place before the significant decrease in PC number, protein levels of GFAP and IBA-1 were checked at two additional time points: 9 and 13 weeks of age (Fig. 3.11A and B).

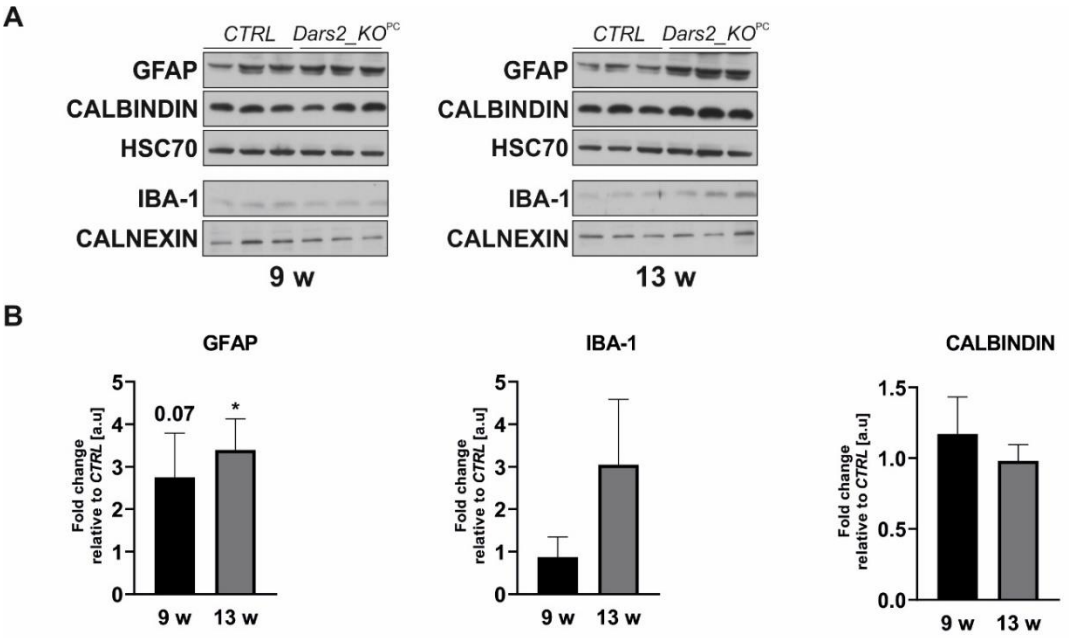

Figure 3.11: Gradual increase of GFAP-positive Bergman glia cells in *Dars2_KO*^{PC} at 9 and 13 w of age. (A) Immunoblots of whole cerebellar lysates *CTRL* vs *Dars2_KO*^{PC} at 9 and 13 w for a microglia marker (IBA-1), astrocytes marker (GFAP), and PC marker (CALBINDIN) **(B)** Quantification of **(A)** presented as mean ± SEM, Student's t-test, *p < 0.05 (n=3 mice per genotype per time point). *Unmodified from (Rumyantseva et al., 2020)*

The increase in neuroinflammation seems to be somewhat gradual, as we detected increased levels in the amount of Bergman glia at 9 and 13 weeks of age, but no significant changes in the amount of microglia, due to a high variation in individual animals (Fig. 3.11A and B). Remarkably, a marker of PC calbindin was not significantly different in *Dars2_KO*^{PC} mice at 13 weeks of age, comparing to control mice, suggesting that PC loss occurs very rapidly at 14-15 weeks of age.

Robust morphology alterations in astrocyte and microglia cells highlight their switch from the resting to the activated state. To test, if Bergmann glia and microglia undergo morphological changes, IF staining was performed. Consistently, with the immunoblot data, the immunoreactivities of IBA-1 and GFAP were unchanged in *Dars2_KO*^{PC} mice at 8 weeks of age. In both, *Dars2_KO*^{PC} and control mice, IBA-1 positive (IBA-1^{+}) microglial cells were sparsely scattered across cerebellar vermis and had resting, ramified morphology (Fig. 3.12A, white square). Similarly, only the ubiquitous weak signal of Bergmann glial marker GFAP was present in *Dars2_KO*^{PC} mice at 8 weeks of age (Fig. 3.12B). However, when we turned to *Dars2_KO*^{PC} 15 weeks old mice, the drastic changes in astrocyte and microglial morphology were evident. Both cell types exhibited signs of hypertrophy (Fig. 3.12A and B). The morphology of IBA-1^{+} cells in *Dars2_KO*^{PC} 15 weeks old mice differed dramatically from the control mice. Most of the microglial cells, lost their long thin processes, a hallmark of the ramified state, and were ameboid (Fig. 3.12A, white squares). Similarly, GFAP-labelled Bergmann glia appeared hypertrophic in PC and molecular layers (Fig. 3.12B).

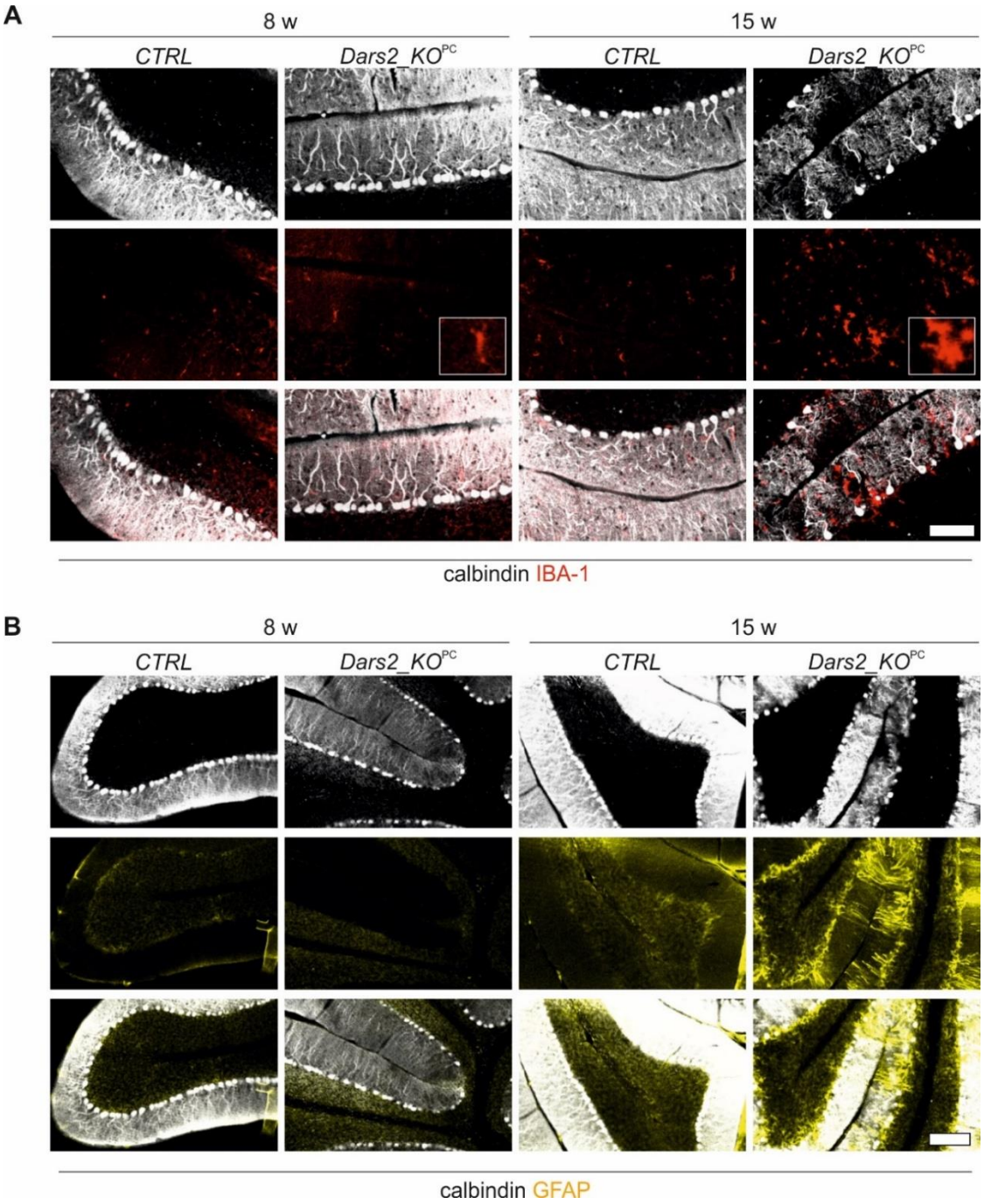

Figure 3.12: PC death leads to neuroinflammation. **(A)** Representative confocal images of midsagittal sections of the cerebellar vermis of *CTRL* and *Dars2_KO*^{PC} at the indicated time points (lobule IV-V at 8 w; lobule VI-VII at 15 w) labelled immunofluorescently with antibodies against calbindin (grey, Purkinje-specific marker) and IBA-1 (red, microglia) scale bar=100 µm **(B)** Representative confocal images of midsagittal sections of the cerebellar vermis of *CTRL* and *Dars2_KO*^{PC} at the indicated time points (lobule IV-V at 8 w; lobule VI-VII at 15 w) labelled immunofluorescently with antibodies against calbindin (grey, Purkinje-specific marker) and GFAP (yellow, astrocytes) scale bar=100 µm. *Unmodified from (Rumyantseva et al., 2020)*

Collectively, these results demonstrate that early events of OXPHOS dysfunction in PCs are insufficient to trigger the immune response and induce astrogliosis at 6 and 8 weeks of age in *Dars2_KO*^{PC}. However, the tendency of increased levels of GFAP-positive astrocytes was evident starting from 9 weeks of age, long before PC death takes place, suggesting that metabolic changes associated with the reduced mitochondrial function in PC stimulate astrogliosis.

3.1.6 Early 1C metabolism upregulation in Dars2_KO^{PC} mice

Intrigued by mild and localized to individual PCs OXPHOS dysfunction, on the one hand (Fig. 3.7A and 3.8), and gradual increase in astrocytes marker GFAP on the other hand (Fig. 3.10A and B), we sought to identify a stress signal that leads to astrogliosis, prior to the widespread OXPHOS defect. A compelling number *in vivo* and *in vitro* studies, carried out in last years, has established the alterations of one-carbon (1C) metabolism, as an immediate effect of mitochondrial dysfunction (Bao et al., 2016; Celardo et al., 2017; Nikkanen et al., 2016). 1C metabolism comprises a large network of biosynthetic reactions, compartmentalized to cytoplasm and mitochondria, responsible for 1C (methyl) units production that are broadly utilized in various cellular processes (Bao et al., 2016).

Previously, it has been demonstrated that enzymes controlling the mitochondrial branch of 1C flux exclusively are upregulated in cell models, the heart and skeletal muscles, and PCs of mouse models with mitochondrial dysfunction (Bao et al., 2016; Motori et al., 2020; Nikkanen et al., 2016).

In accordance with that, PCs of *Dars2_KO*^{PC} mice exhibited a strong IF signal for serine hydroxymethyltransferase 2 (SHMT2), a mitochondrial enzyme that catalyses the first step in mitochondrial 1C metabolism converting serine to glycine, accompanied by the production of 5,10-

methylenetetrahydrofolate (THF). (Fig. 3.13A). Remarkably, confocal microscopy revealed that SHMT2 reactivity was markedly increased in PCs of *Dars2_KO*^{PC} mice already at 8 weeks. Moreover, the intensity of SHMT2, when normalized over ATPB levels that were unaltered at 8 weeks of age (Fig. 3.8), was 9-fold higher in PCs of *Dars2_KO*^{PC} mice, than in controls that displayed weak SHMT2 signal (Fig. 3.13B). Higher levels of SHMT2 persisted in the remaining PCs of *Dars2_KO*^{PC} mice at 15 weeks of age (Fig. 3.13A).

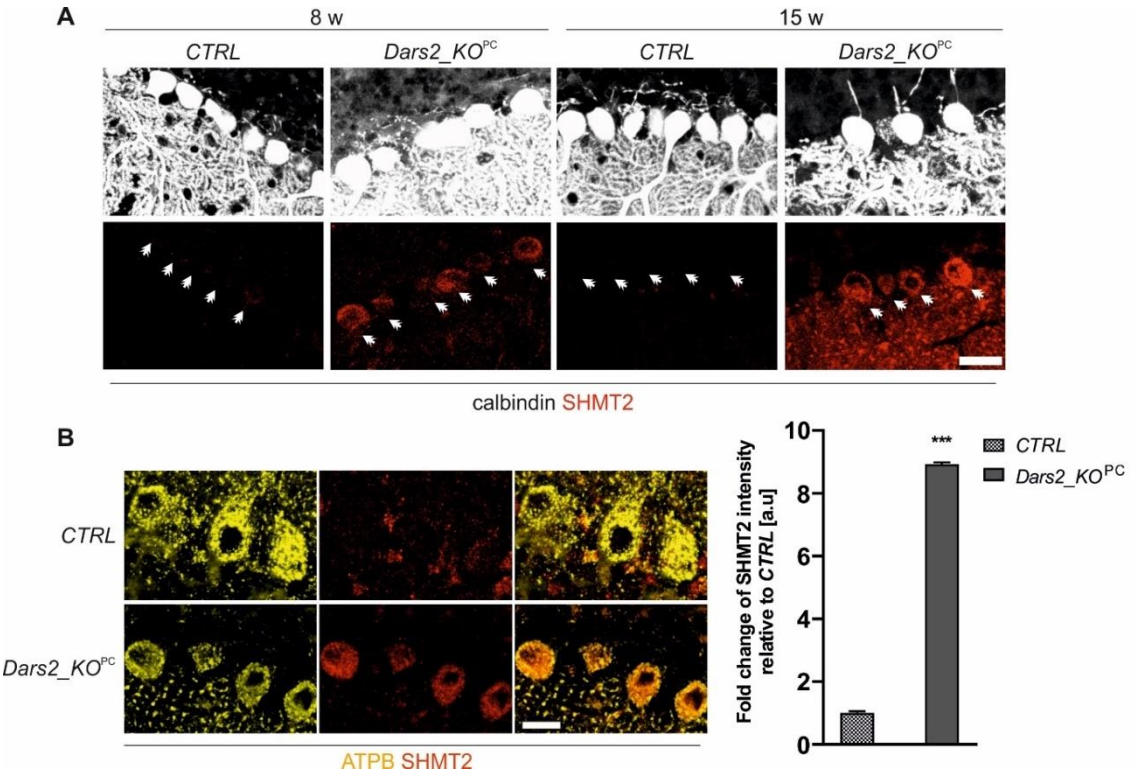

Figure 3.13: SHMT2 upregulation in *Dars2_KO*^{PC} mice. **(A)** Representative confocal images of midsagittal sections of cerebellar vermis lobule IV-V of *CTRL* and *Dars2_KO*^{PC} at the indicated time points labelled immunofluorescently with antibodies against calbindin (grey, Purkinje-specific marker) and SHMT2 (red) scale bar=25 µm. **(B)** Representative confocal images of sections of cerebellar vermis lobule III of *CTRL* and *Dars2_KO*^{PC} at 8 w labelled immunofluorescently with antibodies against ATPB (yellow, mitochondria) and SHMT2 (red) scale bar=25 µm. A fraction of mitochondria displaying SHMT2 expression was quantified and normalised over ATPB (Student's t-test; n=20 PCs from 2 mice per genotype). *Unmodified from (Rumyantseva et al., 2020)*

These findings suggest that rather altered metabolism, in particularly 1C cycle, than locally impaired OXPHOS lead to astrocytic reactivity that progressively increases with time, culminating with widespread neuroinflammation detected in *Dars2_KO*^{PC} mice at 15 weeks of age.

3.2 Effect of CLPP inhibition in mitochondrial encephalopathy models

3.2.2 Concomitant loss of mitochondrial matrix protease Clpp in *Dars2_KO*^{PC} mice delays cerebellar neurodegeneration

3.2.2.2 Generation of Dars2/Clpp Purkinje cell-specific double knockout mouse model

Intriguingly, we have recently demonstrated that strong mitochondrial cardiomyopathy and diminished respiration caused by the loss of DARS2 can be alleviated by the loss of mitochondrial matrix protease CLPP (Seiferling et al., 2016). To investigate, whether the beneficial effect of CLPP ablation can be extended to DARS2-deficient neurons, double knockout *Dars2/Clpp* PC-specific mouse model was generated (*DKO*^{PC}). Briefly, *Dars2*$^{loxP/loxP}$ *Clpp*$^{loxP/loxP}$ mice were bred to *L7-Cre* transgenic mice (Fig. 3.14A). The genotypes were verified by PCR (Material and Methods).

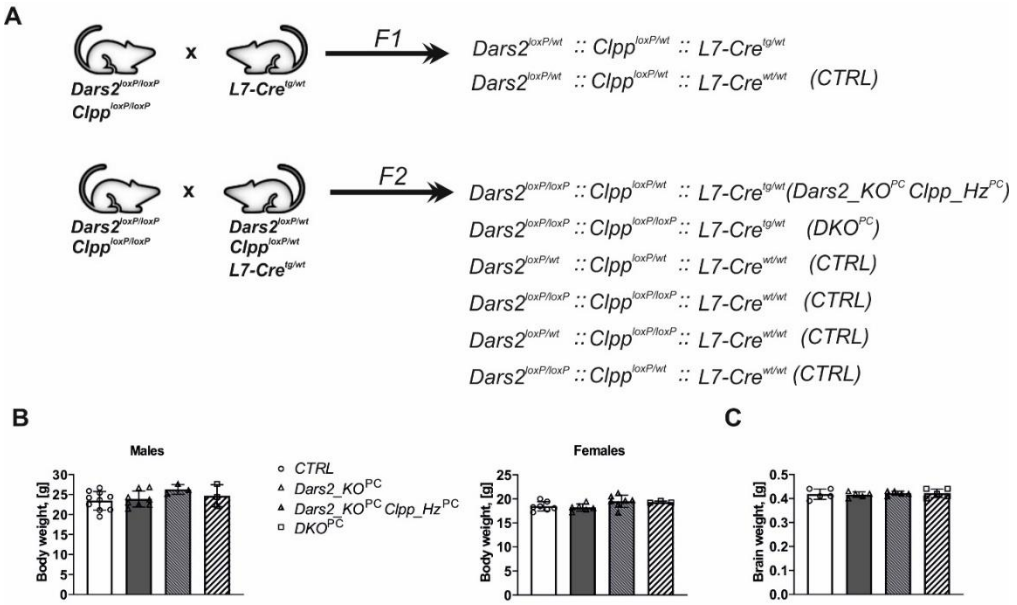

Figure 3.14: Generation and general characteristics of PC-specific *Dars2/Clpp* double knockout mice (*DKO*^{PC}). (A) F1 and F2 breeding strategy **(B)** Body weight of *CTRL, Dars2_KO*^{PC}, *Dars2_KO*^{PC} *Clpp_Hz*^{PC} and *DKO*^{PC} mice at 15 w of age data presented as mean ± SD (n=3-10 mice per genotype). **(C)** Brain weight of *CTRL, Dars2_KO*^{PC}, *Dars2_KO*^{PC} *Clpp_Hz*^{PC} and *DKO*^{PC} mice at 15 w of age data presented as mean ± SD. (n=5 mice per genotype).

DKO^{PC} mice were born in Mendelian ratio, appeared normal at weaning and were indistinguishable from control animals. No significant changes, compared to control and *Dars2_KO*^{PC} mice, in body weight of either sex and brain weight was detected (Fig. 3.14B and C).

DKO^{PC} mice did not display any behavioural phenotype at 8 weeks (data not shown); hence their motor skills were assessed at 15 weeks. At this age, *Dars2_KO*^{PC} mice displayed significant impairment in their ability to keep balance and unsteady gait (Fig. 3.15A and B). Strikingly, *DKO*^{PC} mice performed significantly better at the Ledge Test, receiving five times lower score comparing to *Dars2_KO*^{PC} (Fig. 3.15A). Interestingly, *Dars2_KO*^{PC} animals that were additionally haploinsufficient for Clpp (*Dars2_KO*^{PC} *Clpp_Hz*^{PC}) displayed a moderate alleviation of distorted equilibrium comparing to *Dars2_KO*^{PC} (Fig. 3.15A). Accordingly, we observed a striking improvement of gait in mice with one or both *Clpp* alleles ablated. Importantly, no signs of unsteadiness and ataxia were noticeable at 15 weeks of age in *DKO*^{PC} mice. Although *Dars2_KO*^{PC} *Clpp_Hz*^{PC} animals showed a tendency to have a reduced score, it did not differ significantly from *Dars2_KO*^{PC}, due to the variation between individual animals (Fig. 3.15B). All three observed genotypes did not exhibit hind limb clasping response (Fig. 3.15C) and only mild kyphosis in individual *Dars2_KO*^{PC,} and *Dars2_KO*^{PC} *Clpp_Hz*^{PC} mice was detected. Notably, no signs of kyphosis were observed in *DKO*^{PC} mice at 15 weeks of age (Fig. 3.15D). The dramatic deterioration of motor skills, and in particular the sense of equilibrium in 15-weeks-old *Dars2_KO*^{PC} was a result of marked PC loss (Fig. 3.4). Thereby, the improvement of motor skills in *DKO*^{PC} suggests a milder reduction in PC numbers and might indicate alleviation of neurodegeneration.

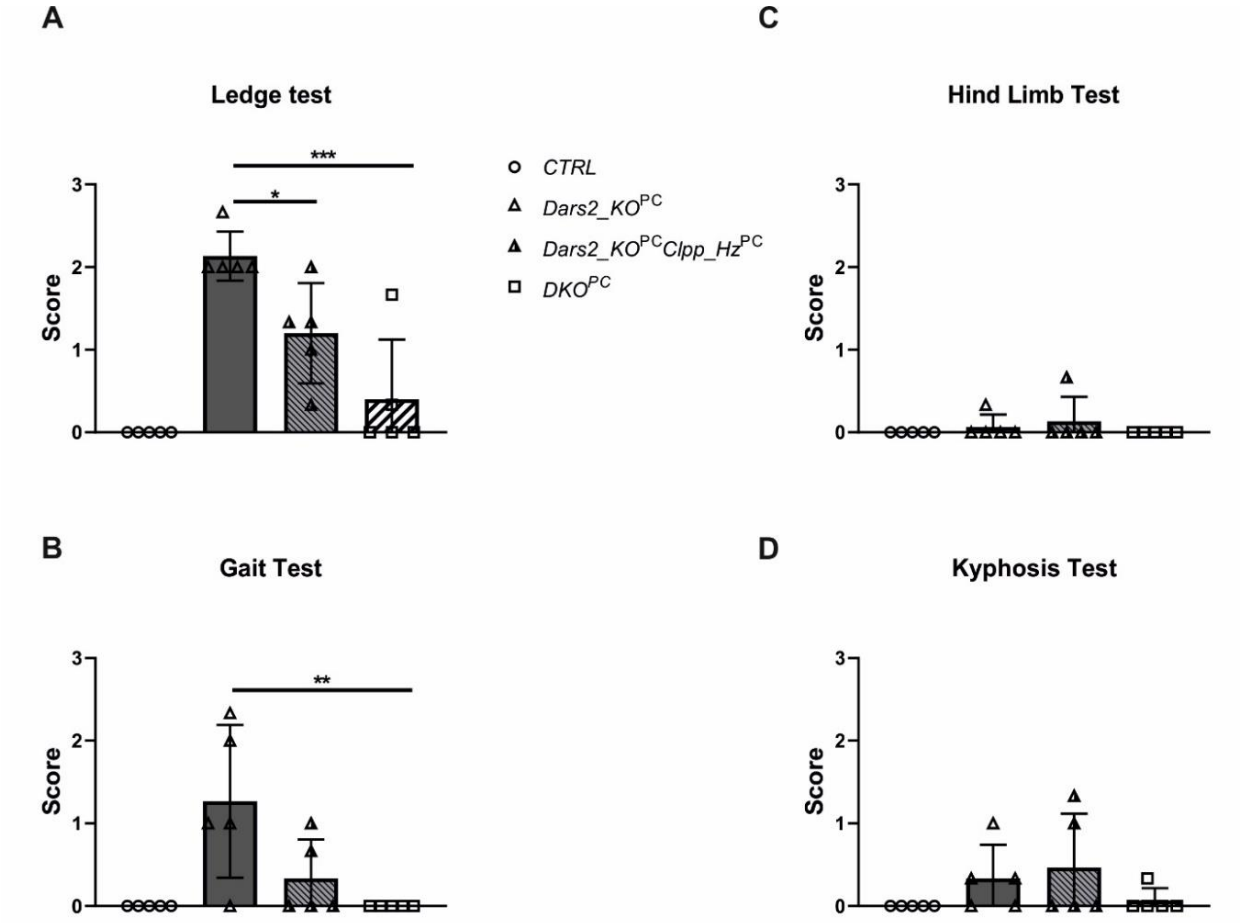

Figure 3.15: Simple composite phenotype scoring. (A) Ledge Test **(B)** Gait Test **(C)** Hind Limb Test **(D)** Kyphosis Test of *CTRL, Dars2_KO*^{PC}, *Dars2_KO*^{PC} *Clpp_Hz*^{PC} and *DKO*^{PC} at 15 w of age, data presented as mean ± SD (One-way ANOVA,*p<0.05; ** p<0.01; ***p < 0.001; n=5 per genotype).

3.2.2.3 PC loss and neuroinflammation are delayed in DKO^{PC}

Intrigued by the improved performance of *DKO*^{PC} at behavioural testing, we performed IF staining for PC specific marker calbindin. *DKO*^{PC} displayed a striking amelioration of PC loss (Fig. 3.16 A-C). At the age of 15 weeks, *DKO*^{PC} mice had 25 % more PCs than age-matching *Dars2_KO*^{PC} animals (Fig. 3.16C). In sharp contrast to *Dars2_KO*^{PC} mice that displayed a uniform PC loss, except for lobules IX and X, *DKO*^{PC} animals showed heterogeneous and patterned PC degeneration. The notable reduction of PC numbers occurred in a clustered manner in lobules III-VIII, while the most anterior (I-II) and posterior (IX-X) lobules appeared to be more protected against degeneration. Contrary to *Dars2_KO*^{PC} animals whose

survived PC displayed highly distorted and fragmented dendritic arbours, PCs in *DKO*^{PC} mice had a dense dendritic network, which appeared to be preserved at this age (Fig. 3.16B).

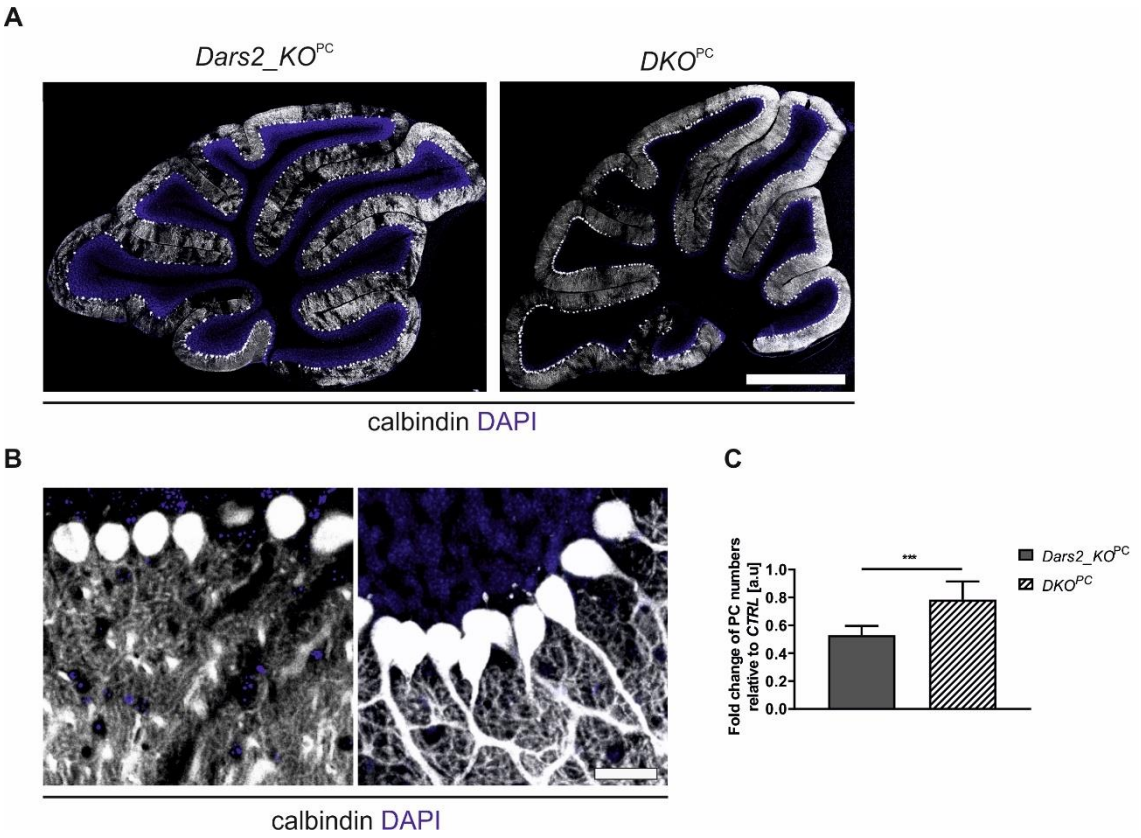

Figure 3.16: Delayed PC loss in *DKO*^{PC} mice at 15 w of age. (A) Representative confocal images of midsagittal sections of cerebellar vermis *Dars2_KO*^{PC} and *DKO*^{PC} at 15 w of age labelled immunofluorescently with the antibody against calbindin (grey, Purkinje-specific marker) and DAPI (blue, nuclei) scale bar=200 µm. **(B)** Close-ups of PC layer in 15 w old *Dars2_KO*^{PC} and *DKO*^{PC} mice labelled immunofluorescently with the antibody against calbindin (grey, Purkinje-specific marker) and DAPI (blue, nuclei) scale bar=50 µm **(C)** Quantification of PC density from (A), data presented as mean ± SD (One-way ANOVA, ***p < 0.001, n=5-7 lobules from three mice, per genotype).

To test, if partially prevented PC loss affects the degree of neuroinflammation, IF staining for microglia (IBA-1) marker was performed (3.17A and B).

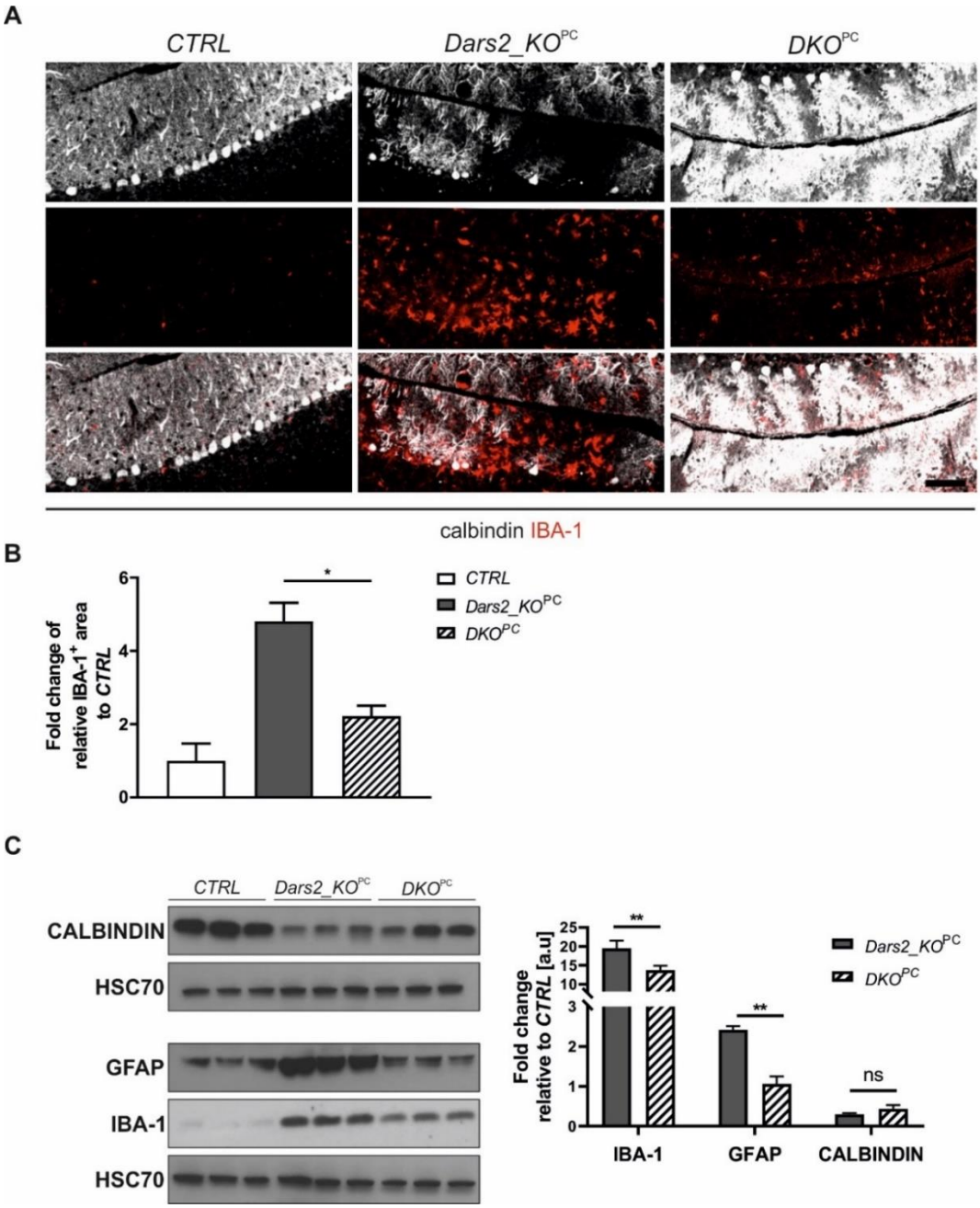

Figure 3.17: Ameliorated neuroinflammation in *DKO*^{PC} mice. **(A)** Representative confocal images of midsagittal sections of the cerebellar vermis of *CTRL, Dars2_KO*^{PC} and *DKO*^{PC} mice at 15 w of age (lobule IV-V and VI-VII) labelled immunofluorescently with antibodies against calbindin (grey, Purkinje-specific marker) and IBA-1 (red, microglia) scale bar=100 µm **(B)** A fraction of area occupied by IBA-1^{+} cells quantified across equally thresholded images from *CTRL, Dars2_KO*^{PC} and *DKO*^{PC} mice at 15 w of age and normalised over *CTRL*, data presented as mean ± SD (One-way ANOVA, *p < 0.05 (6-8 lobules from 2 mice per genotype) **(C)** Immunoblots of whole cerebellar lysates *CTRL* vs *Dars2_KO*^{PC} and *DKO*^{PC} at 18 w of age for a microglia marker (IBA-1), astrocytes marker (GFAP), and PC marker (CALBINDIN), quantification presented as mean ± SD (One-way ANOVA test **p < 0.01, n=3 mice per genotype).

Although an increase in IBA-1$^+$ microglia was detected in *DKO*^{PC} mice at 15 weeks of age comparing to control animals, the microgliosis was milder in *DKO*^{PC} comparing to *Dars2_KO*^{PC} animals. Not only IBA-1$^+$ cells were less numerous, but also the morphology did not undergo such pronounced changes. In fact, some of microglia were still in the ramified state in 15-weeks-old *DKO*^{PC} mice.

To follow the progression of neurodegeneration phenotype, levels of IBA-1, GFAP and calbindin were assessed at a later time point—18 weeks of age (Fig. 3.17C). Unsurprisingly, *Dars2_KO*^{PC} mice displayed a dramatic 19-fold and 2.5-fold increase in protein levels of IBA-1 and GFAP, respectively. Furthermore, 18-week-old *Dars2_KO*^{PC} animals had strongly diminished levels of PC-specific marker calbindin, making up only 30% of control mice. In stark contrast, the levels of both markers were significantly lower in *DKO*^{PC} mice, albeit they were elevated compared to control mice. Interestingly, 18-weeks old *DKO*^{PC} tended to have an increased level of PC-specific marker calbindin, comparing to *Dars2_KO*^{PC} animals. Altogether these results suggest that PC degeneration is delayed in *DKO*^{PC} mice and consequently that leads to decrease in neuroinflammatory response and alleviates impairment of motor skills.

3.2.3 Loss of CLPP improves phenotype of forebrain neuron-specific DARS2-deficient mice

3.2.3.1 Generation of Dars2/Clpp forebrain neuron-specific double knockout mouse model

To investigate if the beneficial effect of targeted ablation of CLPP is restricted to only the specific neuronal population of PC, we took advantage of another neuron-specific model of mitochondrial dysfunction. Recently, we have generated and described a DARS2 mitochondrial encephalopathy model (*Dars2_KO*^{FbNe}). The conditional knockout in *Dars2_KO*^{FbNe} was established under the control of calcium/calmodulin-dependent kinase II alpha promote (*CamKII*α), ensuring the *Dars2* depletion in forebrain neurons of cortex, hippocampus, and striatum with maximum recombination at 1 month of age. *Dars2_KO*^{FbNe} mice had a shorter life span of 28-30 weeks, owning to massive neuronal cell death and early onset of neuroinflammation. Severe respiratory chain dysfunction, detected by a double enzymatic COX/SDH staining was observed already at 15 weeks of age, peaking at 20 weeks (Aradjanski et al., 2017). To investigate, if the delayed decline of DARS2-deficient neurons upon concomitant loss of CLPP was restricted to PC population, we generated and analysed forebrain-neuron specific *Dars2/Clpp* DKO (*DKO*^{FbNe}) mouse model (Fig.3.16A and B).

DKO^{FbNe} mice were born in Mendelian ratio, were healthy at weaning and indistinguishable from control animals. They developed normally, however after 20 weeks of age mutant mice appeared visibly smaller. By 25 weeks of age *Dars2_KO*^{FbNe}, *Dars2_KO*^{FbNe} *Clpp_Hz*^{FbNe} and *DKO*^{FbNe} female mice were significantly 13-14 % smaller, than control females. Interestingly, the body weight of three analysed mutant genotypes

Dars2_KO^{FbNe}, *Dars2_KO*^{FbNe} *Clpp_Hz*^{FbNe} and *DKO*^{FbNe} did not significantly differ from each other (Fig.3.16C).

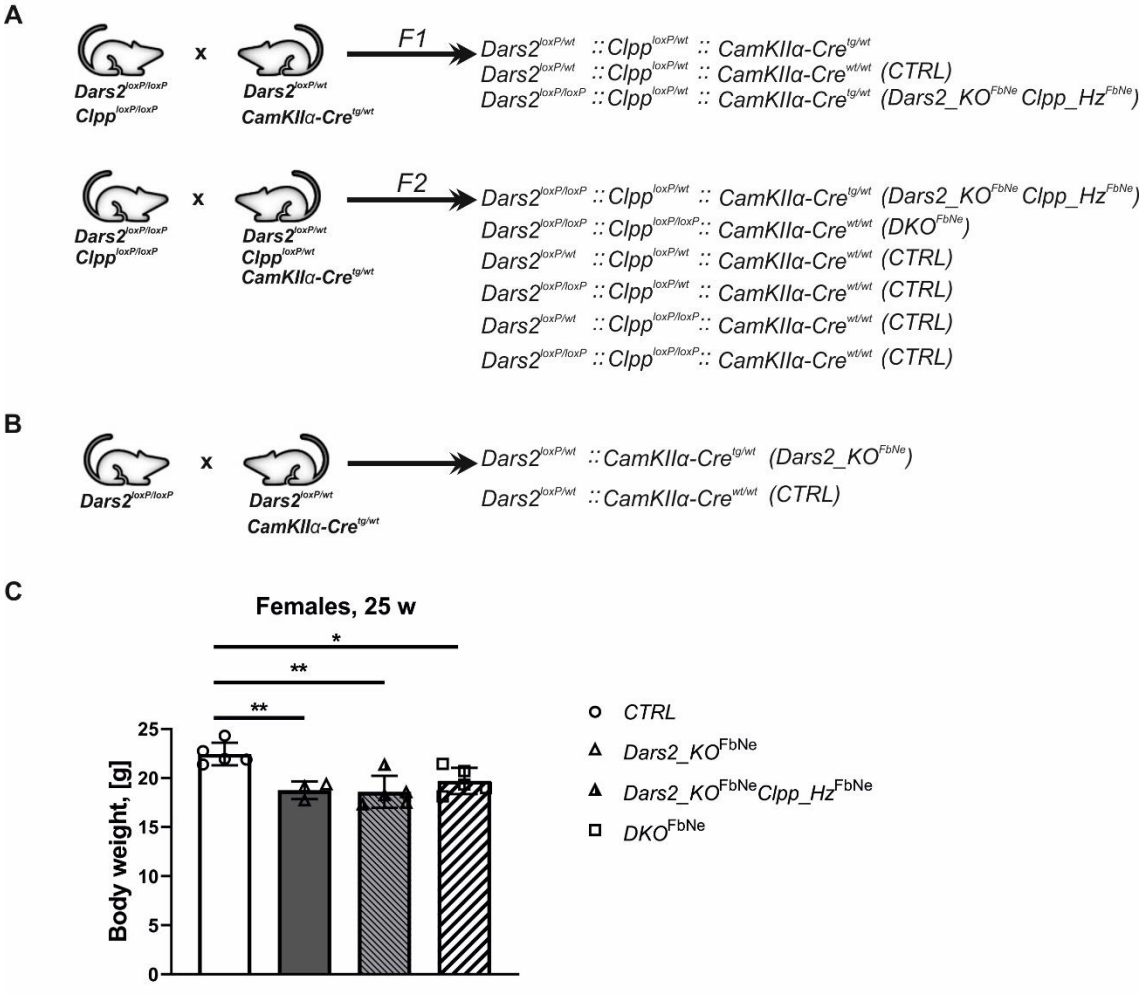

Figure 3.18: Generation and body weight of forebrain neuron-specific Dars2/Clpp double knockout mice (*DKO*^{FbNe}). (A) F1 and F2 breeding strategy **(B)** Breeding strategy of *Dars2_KO*^{FbNe} mice. **(C)** Body weight of *CTRL, Dars2_KO*^{FbNe}, *Dars2_KO*^{FbNe} *Clpp_Hz*^{FbNe} and *DKO*^{FbNe} female mice at 25 w of age data presented as mean ± SD. (One-way ANOVA, *p<0.05; ** p<0.01; n=3-5 mice per genotype).

To follow the progression of the phenotype, and to study the effect of CLPP loss in forebrain neuron DARS2-deficient background the following time-points were chosen: *(i)* 15 weeks, an early time point at which first signs of COX-deficiency were observed in *Dars2_KO*^{FbNe}; *(ii)* 20 weeks, a time point, which was characterized by widespread COX-deficient neurons in cortex and hippocampus and onset of motor impairment skills

in *Dars2_KO*^{FbNe} mice; *(iii)* 25 weeks, a time point at which brain size and cortical thickness of *Dars2_KO*^{FbNe} were significantly reduced resulting from a massive neuronal cell death; and finally *(iv)* 28-30 weeks, a terminal time point for *Dars2_KO*^{FbNe} mice at which they had to be sacrificed, as they severely wound themselves by scratching their muzzles and did not let wounds to heal.

3.2.3.2 Partially restored RC function and alleviated neuroinflammation in DKO^{FbNe} mice

Impaired mitochondrial translation upon DARS2-deficiency has been reported to lead to sever OXPHOS dysfunction in previously described heart and skeletal muscles, forebrain-neuron, and PC-specific mouse models (Aradjanski et al., 2017; Dogan et al., 2014; Rumyantseva et al., 2020).

To analyse the degree of RC dysfunction, COX/SDH double enzymatic staining was performed. In agreement with previously published data (Aradjanski et al., 2017) *Dars2_KO*^{FbNe}*, Dars2_KO*^{FbNe} *Clpp_Hz*^{FbNe} mice showed a marked increase in COX deficient neurons at 15 (Fig. 3.17A) and 20 weeks of age (Fig. 3.17B). The widespread COX-deficiency was present in restrosplenial cortex (RSC), hippocampus and was spanning layers of motor and somatosensory cortex. In striking contrast, COX-deficient neurons were not detected in 15-weeks old *DKO*^{FbNe} mice, which displayed saturated brown staining at this age, a sign of functional RC (Fig. 3.17A). Moreover, 20-weeks-old *DKO*^{FbNe} mice demonstrated an increase in COX-activity comparing to Dars2_KO^{FbNe} and Dars2_KO^{FbNe} Clpp_Hz^{FbNe} animals. However, at this age, the presence of some COX-deficient cells was visible in the hippocampus (Fig. 3.17B).

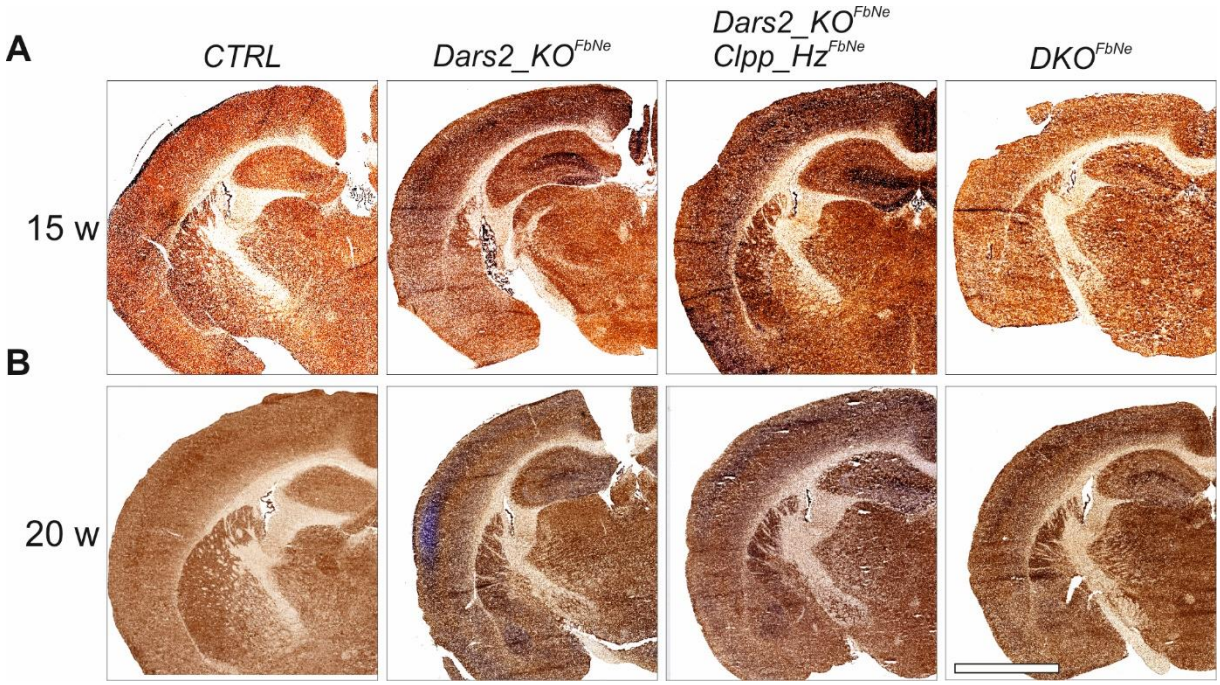

Figure 3.19: Partially restored respiratory chain dysfunction in *DKO*^{FbNe} mice. (A) Representative images of coronal forebrain sections of *CTRL*, *Dars2_KO*^{FbNe}, *Dars2_KO*^{FbNe} *Clpp_Hz*^{FbNe} and *DKO*^{FbNe} mice stained for COX/SDH activity at 15 w of age **(B)** Representative images of coronal forebrain sections stained for COX/SDH activity at 20 w of age, scale bar=2000 µm.

The moderate reduction of COX-deficiency, a result of an improved mitochondrial function in *DKO*^{FbNe} mice, suggested an amelioration of mitochondrial morphology. To characterise mitochondrial ultrastructural changes, transmission electron microscopy (TEM) was performed on ultrathin cortical slices of 20-weeks-old *Dars2_KO*^{FbNe} *Clpp_Hz*^{FbNe} and *DKO*^{FbNe} mice. Interestingly, while *Dars2_KO*^{FbNe} *Clpp_Hz*^{FbNe} appeared to have abnormal “swollen” mitochondria, devoided on cristae, mitochondria in *DKO*^{FbNe} mice revealed to have a cristae organisation at this age, resembling mitochondria of the control mice.

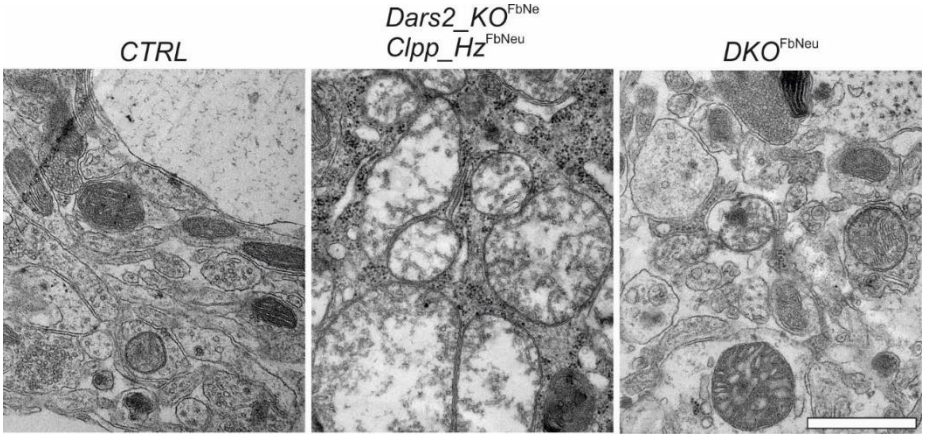

Figure 3.20: Ultrastructural imaging of mitochondria. Representative images of ultrathin cortical slices of *CTRL*, *Dars2_KO*^{FbNe} *Clpp_Hz*^{FbNe} and *DKO*^{FbNe} acquired with TEM; scale bar =1 µm

A massive OXPHOS dysfunction in cortex and hippocampus of *Dars2_KO*^{FbNe} was accompanied by neuroinflammation (Aradjanski et al., 2017). To investigate, if the microgliosis was changed alongside ameliorated RC function, we performed IF staining for microglial (IBA-1) marker and in parallel analyzed its protein level in whole tissue lysates of cortex and hippocampus.

Consistently with the previously published data (Aradjanski et al., 2017), 20-weeks-old *Dars2_KO*^{FbNe} mice displayed a marked upregulation in microglial marker level in cortex and hippocampus. Accordingly, the increase on the protein level and a larger area fraction occupied IBA-1^{+} cells was accompanied by immense changes in their morphology, highlighting their switch to the activated state. Strikingly, *DKO*^{FbNe} mice showed lower protein levels of IBA-1 in both cortex and hippocampus. Furthermore, 20-weeks-old *DKO*^{FbNe} mice displayed significantly lower abundance of IBA-1^{+} cells in the motor cortex and dentate gyrus (DG) region of the hippocampus, suggesting a moderate alleviation of neuroinflammatory response.

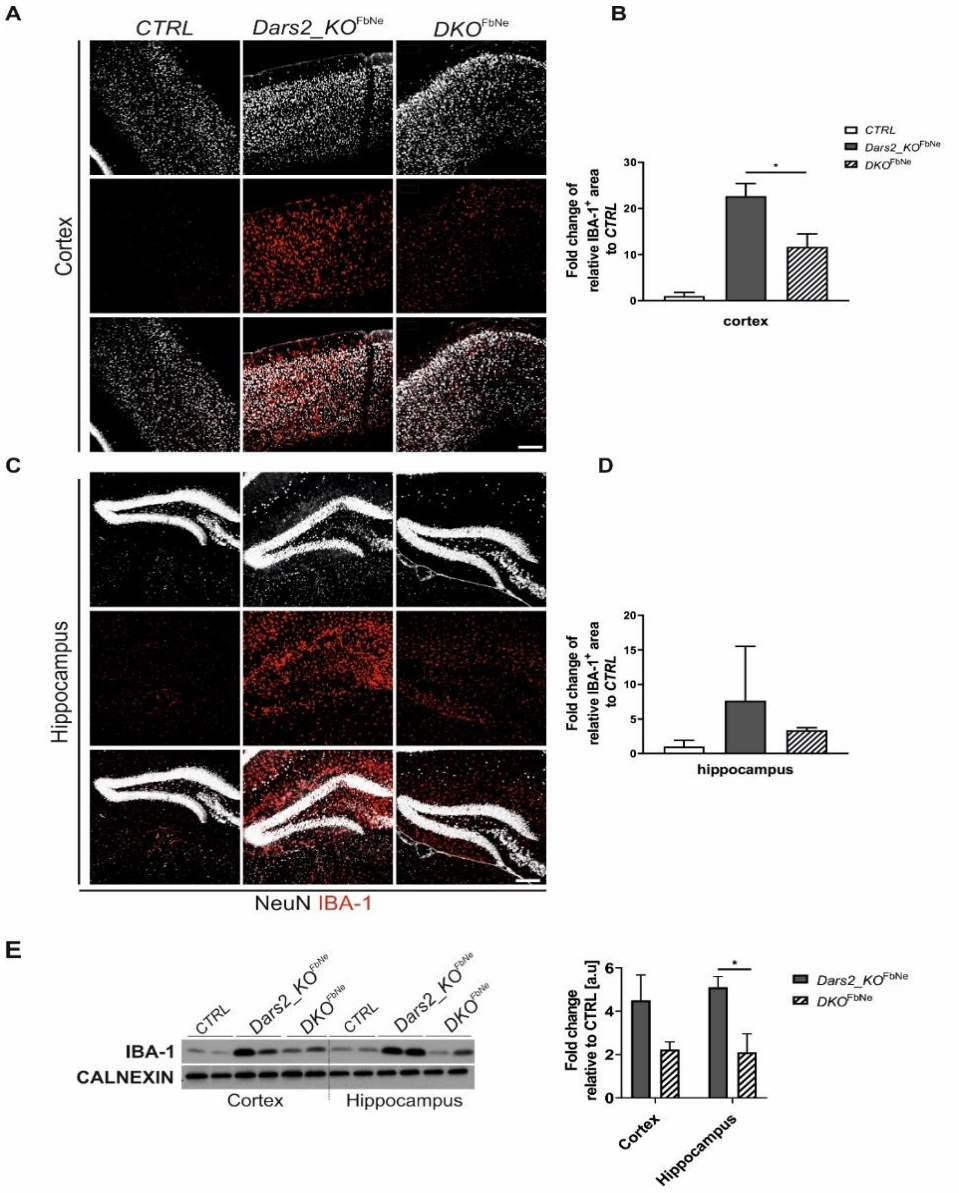

Figure 3.21: Alleviated neuroinflammation in *DKO*^{FbNe} mice. **(A)** Representative confocal images of coronal sections of cortex *CTRL, Dars2_KO*^{FbNe} and *DKO*^{FbNe} mice at 20 w of age labeled immunofluorescently with antibodies against NeuN (grey, neuron-specific marker) and IBA-1 (red, microglia) scale bar=100 µm **(B)** Fraction of area occupied by IBA-1^{+} cells in cortex quantified across equally thresholded images from *CTRL, Dars2_KO*^{FbNe} and *DKO*^{FbNe} mice at 20 w of age and normalised over *CTRL*, data presented as mean ± SD (One-way ANOVA, *p < 0.05 (n=2 mice per genotype) **(C)** Representative confocal images of coronal sections of hippocampal dentate gyrus of *CTRL, Dars2_KO*^{FbNe} and *DKO*^{FbNe} mice at 20 w of age labeled immunofluorescently with antibodies against NeuN (grey, neuron-specific marker) and IBA-1 (red, microglia) scale bar=100 µm **(D)** Fraction of area occupied by IBA-1^{+} cells in hippocampal dentate gyrus quantified across equally thresholded images from *CTRL, Dars2_KO*^{FbNe} and *DKO*^{FbNe} mice at 20 w of age and normalised over *CTRL*, data presented as mean ± SD (One-way ANOVA, *p < 0.05 (n=2 mice per genotype) **(E)** Immunoblots of whole cortex and hippocampus lysates *CTRL* vs. *Dars2_KO*^{FbNe} and *DKO*^{FbNe} at 20 w of age for a microglia marker (IBA-1) quantification presented as mean ± SD (One-way ANOVA test *p < 0.05, n=2 mice per genotype).

3.2.3.3 Ameliorated decline of RSC neurons and behavioural improvement of DKO^{FbNe} mice

The peak of RC dysfunction in 20-weeks-old *Dars2_KO*^{FbNe} mice was reported to coincide with massive neuronal apoptosis and microgliosis in the cortex. Interestingly, RSC layers II/III showed a high selective vulnerability to DARS2 deficiency (Aradjanski et al., 2017).

To visualise cytoarchitecture of RSC, an IF staining with a neuronal nuclear protein (NeuN) was performed. All postmitotic neurons with a rare exception, like for example PCs, show immunoreactivity to NeuN, making it an excellent marker to detect neuronal loss (Mullen et al., 1992).

In line with the neuronal apoptosis data in RSC (Aradjanski et al., 2017), *Dars2_KO*^{FbNe} mice lost more than 50 % of NeuN-positive neurons at 20 weeks of age, comparing to controls (Fig. 3.22A and B). Consistently with the neuroinflammation analysis in the motor cortex and DG region of the hippocampus (Fig. 3.21A-D), this massive neuronal death in RSC of 20-weeks-old *Dars2_KO*^{FbNe} mice was accompanied with a prominent microgliosis, characterized by the increased number of IBA-1^{+} microglia and their changed morphology from ramified (as in control mice) to ameboid (Fig. 3.22A and C). Remarkably, *DKO*^{FbNe} had significantly more NeuN-positive neurons preserved at 20 weeks of age, comparing to *Dars2_KO*^{FbNe} mice. Moreover, decreased abundance of IBA-1^{+} cells, suggests that improved preservation of neuronal cells leads to milder microgliosis.

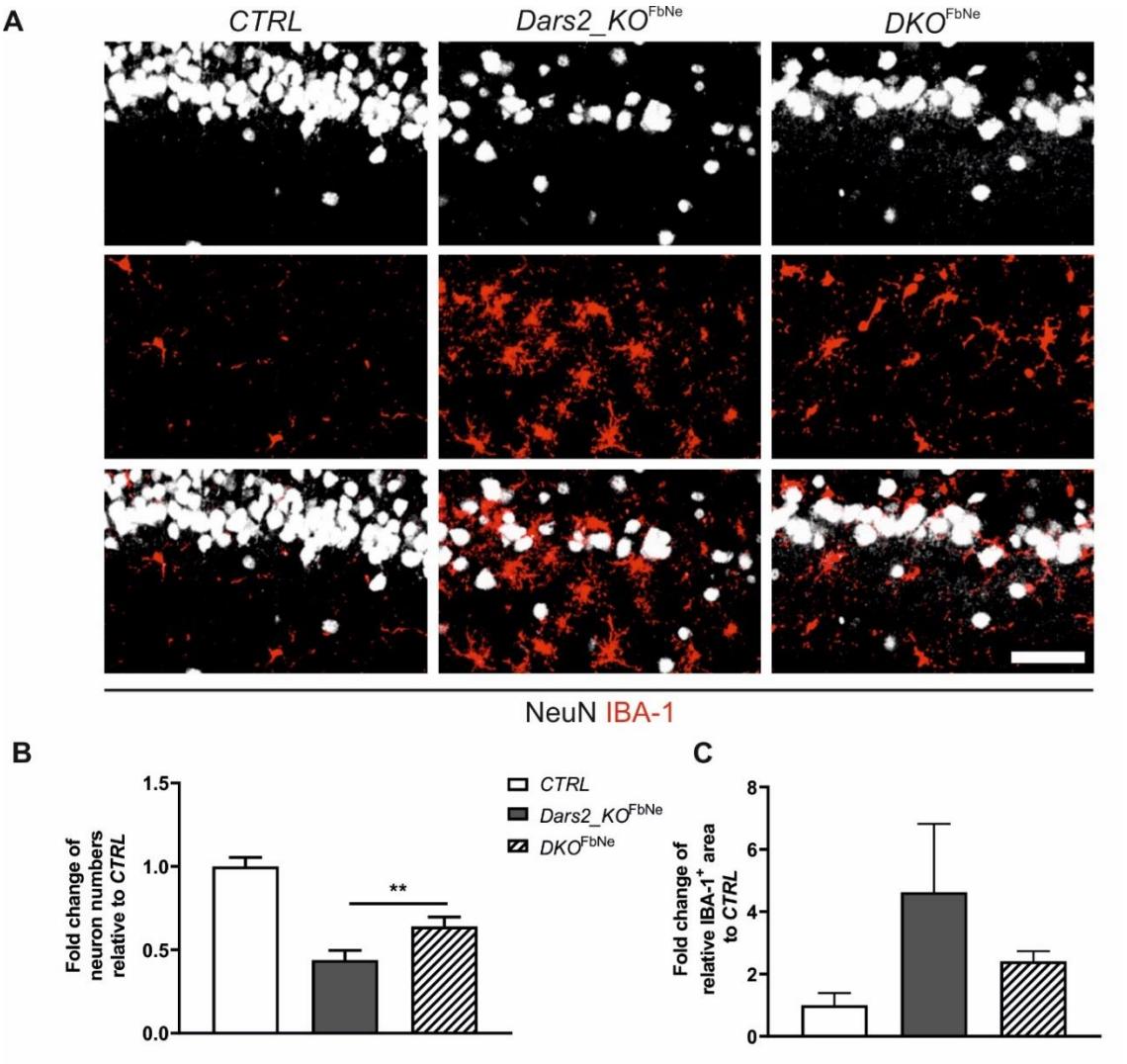

Figure 3.22: Ameliorated decline of RSC neurons in *DKO*^{FbNe} mice at 20 w of age. (A) Representative confocal images of coronal sections of RSC *CTRL, Dars2_KO*^{FbNe} and *DKO*^{FbNe} mice at 20 w of age labelled immunofluorescently with antibodies against NeuN (grey, neuron-specific marker) and IBA-1 (red, microglia) scale bar=50 µm **(B)** Quantification of NeuN^{+} neurons in RSC from (A), data presented as mean ± SD (One-way ANOVA, **p < 0.01, n=2 mice, per genotype). **(C)** A fraction of area occupied by IBA-1^{+} cells in RSC quantified across equally thresholded images from *CTRL, Dars2_KO*^{FbNe} and *DKO*^{FbNe} mice at 20 w of age and normalised over *CTRL*, data presented as mean ± SD (One-way ANOVA, **p < 0.01, n=2 mice per genotype)

The widespread neuronal RC dysfunction, apoptosis and neuroinflammation were reported to lead to motor dysfunction in *Dars2_KO*^{FbNe} mice at 20 weeks of age (Aradjanski et al., 2017). Notably, their sense of balance was affected, resulting in significantly worse performance in the Ledge Test (Fig. 3.23A). Intriguingly, *DKO*^{FbNe} mice

displayed significantly better motor coordination, implying that ameliorated RC dysfunction and neuroinflammation, and preserved neurons in RSC improve their behavioural phenotype (Fig. 3.23A).

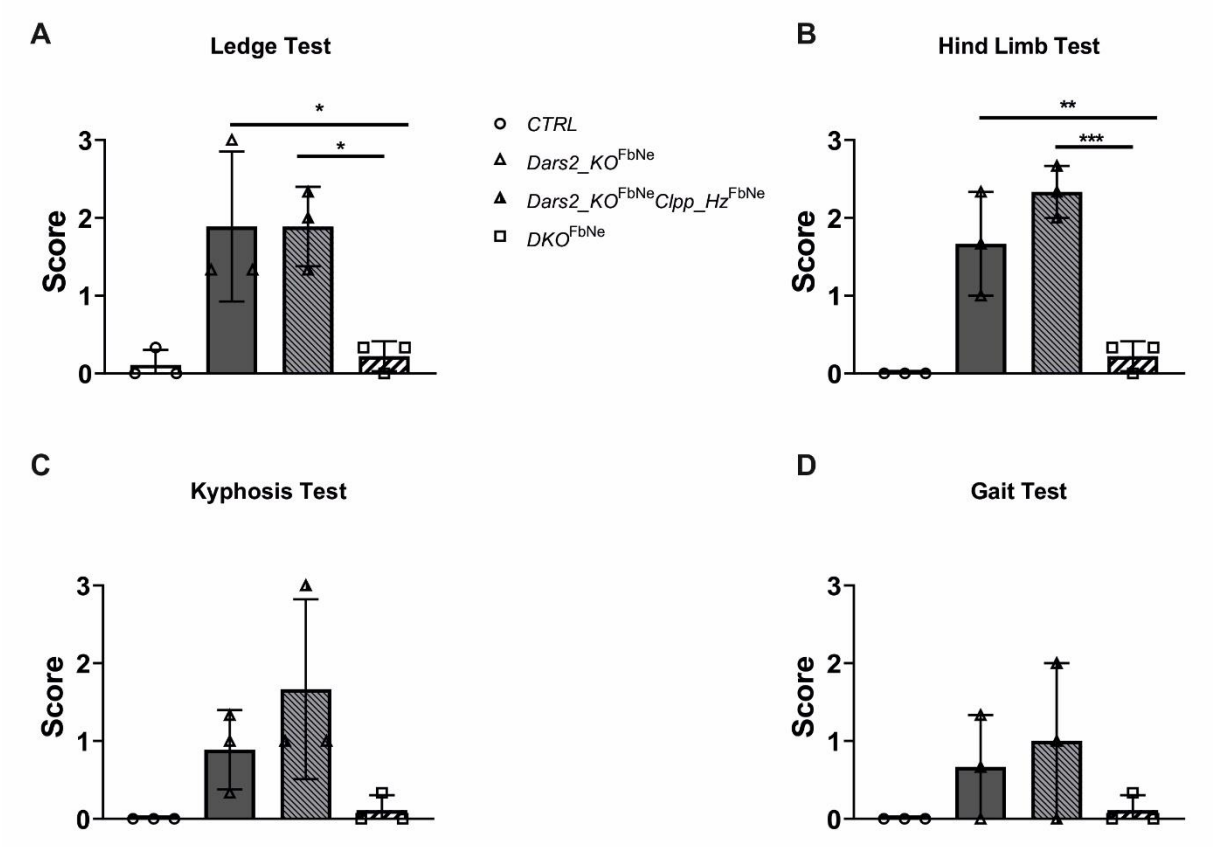

Figure 3.23: Simple composite phenotype scoring. (A) Ledge Test **(B)** Hind Limb Test **(C)** Kyphosis Test **(D)** Gait Test of *CTRL*, *Dars2_KO*^{FbNe}, *Dars2_KO*^{FbNe} *Clpp_Hz*^{FbNe} and *DKO*^{FbNe} mice at 20 w of age, data presented as mean ± SD (One-way ANOVA,*p<0.05; ** p<0.01; ***p < 0.001; n=3 per genotype).

Altogether these results suggest that the loss of CLPP leads to milder development of DARS2-deficiency associated phenotype, partially restoring RC function, and ameliorating neuroinflammatory response in cortex and hippocampus. Interestingly, the findings in RSC indicate that some neuronal populations are particularly vulnerable to DARS2-deficiency and might benefit to a larger extent from the concomitant loss of CLPP.

3.2.3.4 Loss of CLPP does not cause respiratory deficiency in forebrain

Previously, we discovered that the concomitant loss of CLPP in DARS2-deficient hearts improved cardiomyopathy phenotype, by acting on mitochondrial protein synthesis level. Briefly, CLPP-deficiency increased levels of proficiently synthesised OXPHOS subunits, leading to a mild increase in the respiratory function in DARS2-deficient hearts (Seiferling et al., 2016). Intrigued by the beneficial effect of CLPP loss on the progression of the neurodegeneration in two different neuronal models of mitochondrial dysfunction, we sought to investigate how the loss of CLPP affects respiratory function in the forebrain.

To this end, we employed Clpp whole-body KO mouse model (*Clpp_KO*^{WB}). *Clpp_KO*^{WB} mice were shown to recapitulate human Perrault syndrome (Gispert et al., 2013). Already at weaning *Clpp_KO*^{WB} mice are significantly smaller than the control animals and have 25-30 % reduced weight throughout the lifetime. Furthermore, Clpp_*KO*^{WB} mice exhibited resistance to high-fat diet (HFD), cold intolerance, infertility in both sexes due to a defect in spermatogenesis and ovarian failure, and later in life loss of the hearing (Becker et al., 2018; Bhaskaran et al., 2018; Gispert et al., 2013). The mild upregulation of inflammatory signatures ubiquitously in different tissues of *Clpp_KO*^{WB} animals was also described (Gispert et al., 2013). Previously we have reported that loss of CLPP leads to mild RC dysfunction in hearts of *Clpp_KO*^{WB} mice (Szczepanowska et al., 2016) and brown adipose tissue (Becker et al., 2018). To analyze if RC is affected in the forebrain of *Clpp_KO*^{WB} animals, we performed COX/SDH staining at 20-week-old animals. Remarkably, no signs of COX-deficiency were detected. Unlike RSC and DG region of the hippocampus in *Dars2_KO*^{FbNe} and *Dars2_KO*^{FbNe} *Clpp_Hz*^{FbNe} that showed intense blue stain already at 15 weeks, all visible regions of the brain of *Clpp_KO*^{WB} mice displayed ubiquitous and saturated brown stain at 20 weeks of age (Fig. 3.24A).

To assess levels of OXPHOS supercomplexes directly, BN-PAGE, followed by western blot, was performed on mitochondria isolated from forebrains. Interestingly, no considerable changes in the amount of supercomplexes, consisting of complex I (CI) and complex IV (IV) were detected in *Clpp_KO*^{WB} forebrains. Conversely, our previous results from heart mitochondria of *Clpp_KO*^{WB} mice demonstrated an apparent reduction in complexes abundance. Notably, CI levels were significantly downregulated already in 15-weeks-old hearts, followed by detectable CIV decrease at 35 weeks of age (Szczepanowska et al., 2016). This result might indicate the tissues-specificity in response to CLPP loss. Observing no alterations in supercomplexes levels and composition, we sought to determine whether activities of CI and CIV were affected by performing in-gel activity assay. Importantly CI or CIV activities were unaltered in forebrain mitochondria of *Clpp_KO*^{WB} mice (Fig, 3.24C). The decrease in complexes levels in hearts of *Clpp_KO*^{WB} mice was attributed to a general downregulation of mitochondrial translation, resulting from a decrease in the amount of fully assembled mitoribosomes (Szczepanowska et al., 2016). Puzzled by unaltered OXPHOS complexes levels in the forebrain of *Clpp_KO*^{WB} mice, we analysed the rate of *de novo* mitochondria protein synthesis (pulse) and degradation (chase) in CLPP-deficient forebrains, by performing *in organello* translation assay using radioactively labelled methionine ([^{35}S]-methionine) to mark *de novo* synthesised OXPHOS complexes subunits. Remarkably, overall protein synthesis in CLPP-deficient forebrains was not changed, comparing to controls. Moreover, no difference between forebrains of *Clpp_KO*^{WB} and control animals were detected after 3 hours of chase, implying that the turnover rate of newly

synthesised OXPHOS complexes subunits is not affected in forebrain of *Clpp_KO*^{WB} mice.

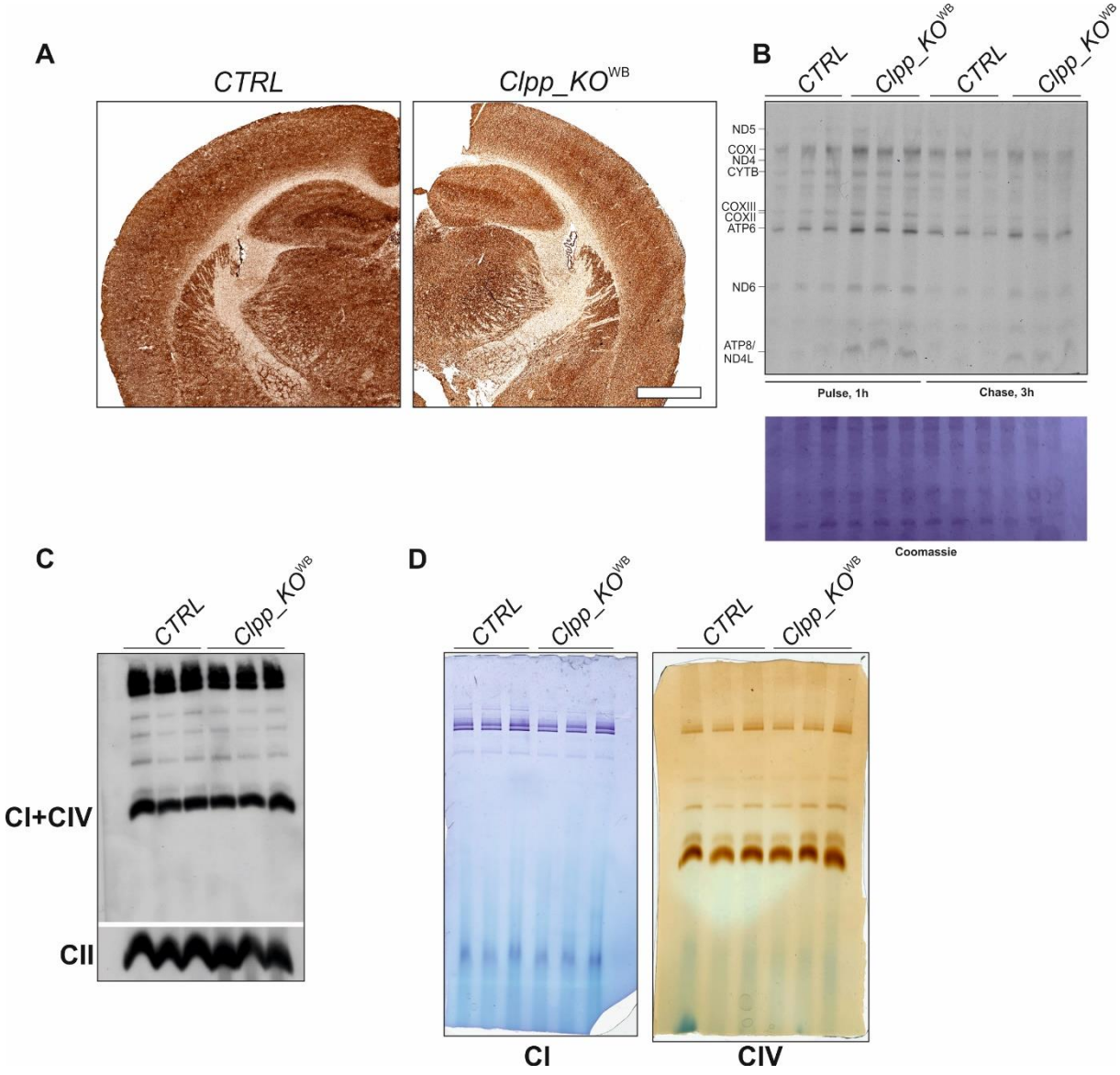

Figure 3.24: Loss of CLPP does not affect RC function in the forebrain. **(A)** Representative images of coronal forebrain sections of *CTRL* and *Clpp_KO*^{WB} mice stained for COX/SDH activity at 15 w of age, scale bar = 1000 µm **(B)** Autoradiograph of in organello translation assay of mitochondria isolated from the whole forebrain. Newly synthesized mitochondria-encoded OXPHOS subunits were pulsed labelled with [35]S-methionine for 1 h and were chased in the absence of [^{35}]S-methionine for 3 h. Translation products were separated on a 15% SDS-polyacrylamide gel. **(C)** BN-PAGE and subsequent western blot analysis of CI and CIV supercomplexes. **(D)** *In-gel* activity assay of CI and CIV separated by BN-PAGE

In contrast to the previously reported effect of CLPP ablation in mouse hearts, no changes in mitochondrial *de novo* protein synthesis rate and turnover were detected in the forebrain of *Clpp_KO*^{WB} mice. Accordingly, neither OXPHOS complexes levels nor their activities were altered in the forebrain of *Clpp_KO*^{WB} mice. Altogether these results argue that the loss of CLPP affects various tissues differently, and further experiments are needed to unravel neuron-specific response to CLPP deletion.

3.2.3.5 Improved phenotype of DKO^{FbNe} mice is preserved later in life

Partially rescued mitochondrial dysfunction and neuroinflammation raised a question, whether the beneficial effect of CLPP loss would be conserved at a later time point. To answer this question, we turned to 25 and 28-30-weeks-old mice. In accordance with previous findings (Aradjanski et al., 2017), At the age of 25 weeks, *Dars2_KO*^{FbNe} mice demonstrated a significant decrease in their total brain weight, resulting from massive apoptosis that led to a shrinkage of the cortex (Fig. 3.25A and B). Intriguingly, *DKO*^{FbNe} mice had significantly large brains at this age, likely owning to significantly better-preserved cortex (Fig. 3.25A and B).

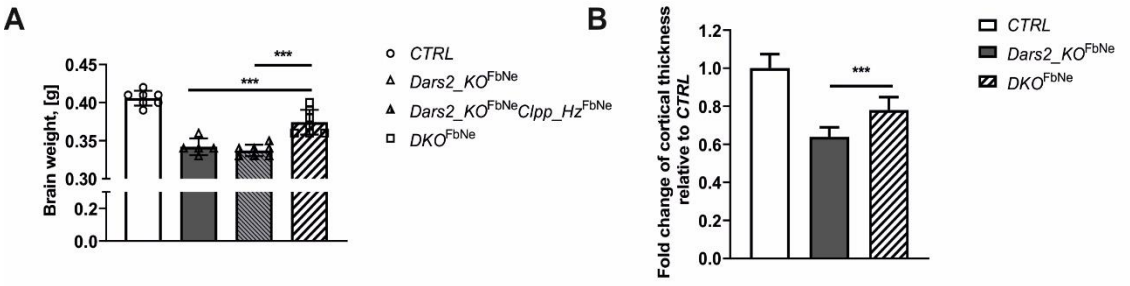

Figure 3.25: Diminished forebrain atrophy in *DKO*^{FbNe} mice by 25 w of age. (A) Brain weight of *CTRL, Dars2_KO*^{FbNe}, *Dars2_KO*^{FbNe} *Clpp_Hz*^{FbNe} and *DKO*^{FbNe} mice at 25 w of age data presented as mean ± SD. (One-way ANOVA, *** p<0.001; n=5-7 mice per genotype). **(B)** Fold change of cortical thickness of *CTRL, Dars2_KO*^{FbNe} and *DKO*^{FbNe} mice at 25 w of age data presented as mean ± SD. (One-way ANOVA *** p<0.001; n=3-7 mice per genotype).

Particularly vulnerable to DARS2 deficiency neurons of RSC demonstrated a further decline in *Dars2_KO*^{FbNe} mice, making up only 33% of RSC neurons in control animals (Fig. 3.26A and B). Interestingly, 25-weeks-old *DKO*^{FbNe} mice showed significantly milder degeneration of RSC neurons, albeit their numbers were strikingly reduced, comparing to control (Fig. 3.26A and B).

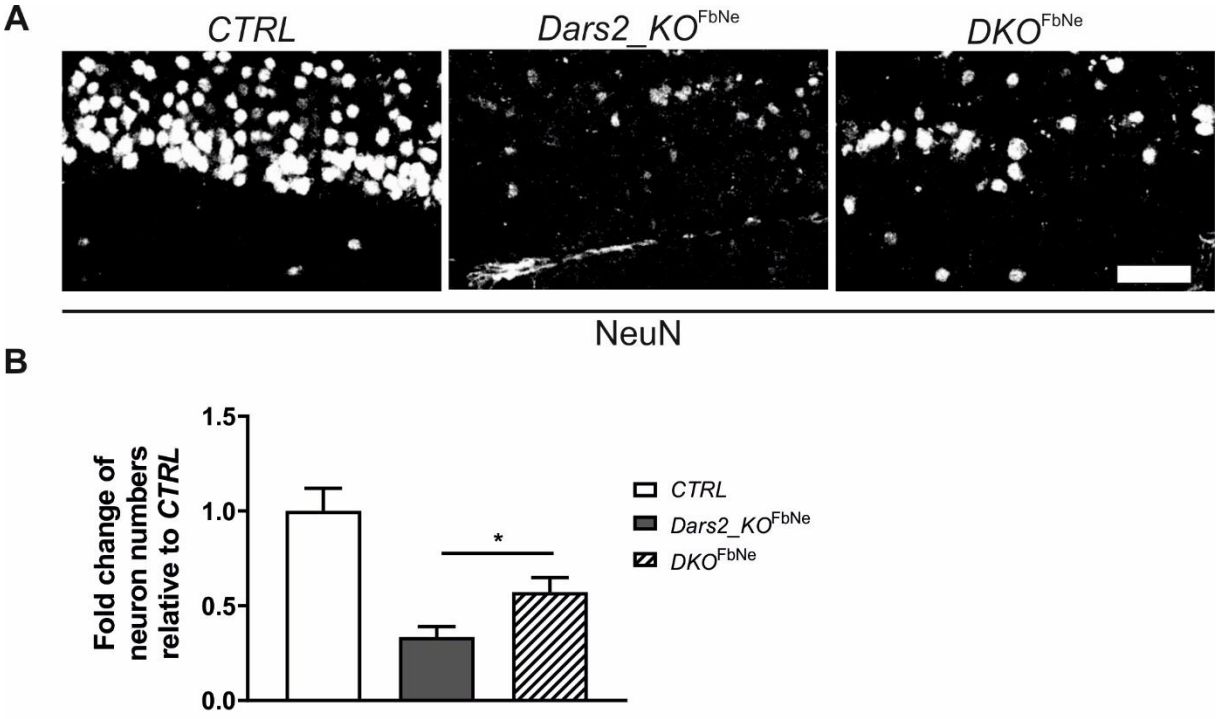

Figure 3.26: Ameliorated decline of RSC neurons in *DKO*^{FbNe} mice at 25 w of age. (A) Representative confocal images of coronal sections of RSC *CTRL, Dars2_KO*^{FbNe} and *DKO*^{FbNe} mice at 20 w of age labelled immunofluorescently with the antibody against NeuN (grey, neuron-specific marker) scale bar=50 µm **(B)** Quantification of NeuN^{+} neurons in RSC from (A), data presented as mean ± SD (One-way ANOVA, *$p < 0.05$, n=2 mice per genotype).

The vast majority of *Dars2_KO*^{FbNe} and *Dars2_KO*^{FbNe} *Clpp_Hz*^{FbNe} mice had to be sacrificed at 28 weeks of age due to the severity of the phenotype. Not only they exhibited considerable impairment of the motor skills (Fig. 3.25A-D), but they also repeatedly scratched their muzzles and did not let wounds to heal. *DKO*^{FbNe} mice lived past 28 weeks and demonstrated a partial improvement at behavioural tests (Fig. 3.27A-D). Notably, their

coordination was less affected, resulting in significantly better performance at the Ledge and Gait Tests (Fig. 3.27A and D). Notably, hind limb clasping response and degree of kyphosis did not show any significant difference across analysed mutant genotypes (Fig. 3.27B and C).

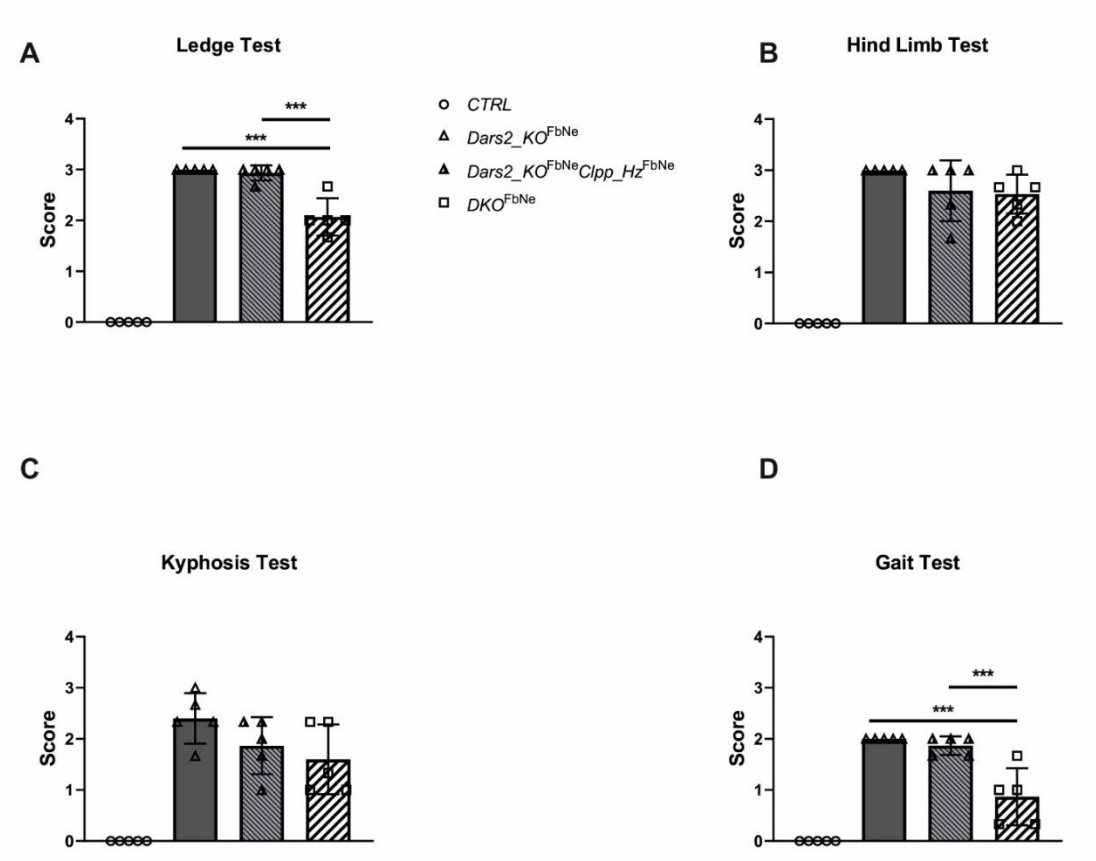

Figure 3.27: Simple composite phenotype scoring. (A) Ledge Test **(B)** Hind Limb Test **(C)** Kyphosis Test **(D)** Gait Test of *CTRL*, *Dars2_KO*^{FbNe}, *Dars2_KO*^{FbNe} *Clpp_Hz*^{FbNe} and *DKO*^{FbNe} mice at 28-30 w of age, data presented as mean ± SD (One-way ANOVA, ***p < 0.001; n=5 mice per genotype).

Previously, we have reported that cortical and hippocampal neurons in *Dars2_KO*^{FbNe} mice undergo a different cell death dynamic. The number of apoptotic cells in cortex reaches its maximum at 20 weeks of age. Contrary to that, hippocampal neurons and, in particular, neurons of DG are more resistant to death showing a massive increase in dead cells only after 25 weeks, despite persistent COX-deficiency from 15 weeks of age

(Aradjanski et al., 2017). To visualise the neuronal cell death, we performed the TUNEL assay that enables the detection of nuclear DNA fragmentation, a hallmark of apoptotic cell death. In line with the previous findings, TUNEL assay in both DG and corni ammonis 1 (CA1) region of the hippocampus of *Dars2_KO*^{FbNe} mice depicted a striking increase in apoptotic cell numbers (Fig. 3.28). Moreover, the CA1 region of *Dars2_KO*^{FbNe} mice appeared to be thinner and have fewer neuronal nuclei comparing to control animals. Remarkably, *DKO*^{FbNe} mice not only had better-preserved CA1, but they also showed fewer apoptotic cells in hippocampal CA1 and DG, indicating that CA1 and DG neurons benefit from the concomitant loss of CLPP (Fig. 3.28).

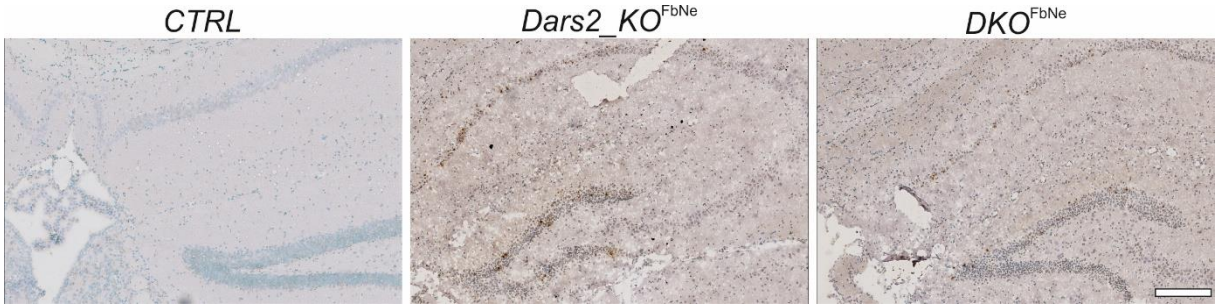

Figure 3.28: DKO^{FbNe} mice have fewer apoptotic neurons in CA1 and DG regions of the hippocampus at 28 w of age. Representative images of TUNEL assay in forebrain coronal sections of *CTRL, Dars2_KO*^{FbNe} and *DKO*^{FbNe} mice at 28 w of age, nuclei counterstained with methyl green, scale bar = 200 µm.

Altogether, these results demonstrate that the loss of CLPP improves the phenotype of both analysed models of mitochondrial encephalopathy, caused by DARS2 depletion. Remarkably, CLPP deficiency extends the life of several DARS2-deficient neuronal populations like PCs, neurons of RSC and CA1 and DG neurons. Delaying onset of neurodegeneration exerts overall beneficial effect, manifested by the amended performance at behavioural tests, and it is associated with ameliorated neuroinflammatory response. Remarkably, these findings provide further evidence of differential susceptibility of various neuronal populations to

mitochondrial dysfunction, and future experiments should aim to elucidate the precise mechanism underlying the beneficial effect of concomitant CLPP loss in DARS2-deficient background.

4 Discussion

Mitochondrial dysfunction has been proven to play a critical role in the pathogenesis of a variety of disorders. Indeed, the pathophysiological significance of mitochondria was reported for virtually all metabolic, neurodegenerative, ischaemic-reperfusion, and cancer morbidities spanning all tissues and organs (Murphy and Hartley, 2018). Unsurprisingly, the concept of mitochondria as a target of therapeutic strategy, or more precisely as a drug target has emerged over the last years (Gorman et al., 2016; Murphy and Hartley, 2018). The considerable efforts have been consolidated in the past two decades on the discovery of approaches to augment or repress certain intersection of mitochondrial physiology for the beneficial therapeutic outcome. Even though the substantial success has been achieved in alleviating some clinical symptoms through diet-supplement interventions and life style changes (Gorman et al., 2016; Parikh et al., 2009; Wijburg et al., 1992), currently neither the U.S Food and Drug Administration (FDA) nor any other governmental agency around the world has approved a drug able to cure a mitochondrial disease permanently (Weissig, 2020). As an idea of the discovery of any drug-based effective and everlasting cure of

mitochondrial diseases remains elusive, novel therapeutic approaches aiming to prevent disease progression must be investigated.

4.1 Loss of CLPP delays ataxia and neuroinflammation in *Dars2_KO*^{PC}

Recently, we have uncovered the beneficial effect of genetic ablation of mitochondrial matrix Clp protease proteolytic subunit (CLPP) in a model of mitochondrial cardiomyopathy caused by DARS2 deficiency. Not only the loss of CLPP does not affect the mitochondrial unfolded protein response (UPRmt), questioning the role of mammalian CLPP in UPRmt activation, but it also leads to the unexpected and striking alleviation of cardiomyopathy and increases the lifespan of *Dars2/Clpp* heart-specific double knock-out (KO) mice (Seiferling et al., 2016).

Given the fact that all reported DARS2 human patients do not develop cardiomyopathy, but, in contrast, exhibit severe, debilitating neuropathology culminating in LBSL (van Berge et al., 2014), this study aimed to explore a therapeutic potential of CLPP depletion in two distinct mouse models of mitochondrial encephalopathy. Remarkably, we have previously shown that even though LBSL in patients is predominantly manifested with white matter abnormalities, oligodendrocyte-specific *Dars2* KO mice do not display either demyelination pattern, or secondary neurodegeneration (Aradjanski et al., 2017). In contrast to this, DARS2 forebrain neuron-specific depletion, driven by *CamKIIα-Cre*, results in pronounced cerebral atrophy by 25 weeks of age, steered by dramatic neuronal death and accompanied by severe neuroinflammation (Aradjanski et al., 2017). Similarly, the other study, utilizing DARS2 KO-CamKIIα, has discovered induction of cell-stress response signalling, activation of inflammatory pathways, coinciding with cerebral atrophy (Nemeth et al., 2019). This evidence suggests that neurons and not adult

oligodendrocytes are the primary culprit in LBSL disorder. Intriguingly, most of the DARS2 patients develop slowly progressing cerebellar ataxia, associated with defects in the cerebellum. Moreover, cases accompanied by the loss of inhibitory neurons of cerebellum, Purkinje cells (PCs), have been described, highlighting the potential essentiality of DARS2 for PCs survival (Yamashita et al., 2013). In line with this, a recent study in mice has reported a 1.5-fold increase of *Dars2* transcript levels in the cerebellum (Fröhlich et al., 2018). Bearing in mind that PCs are sole efferents of the cerebellar cortex, it is unsurprising that they play a pivotal role in cerebellum functioning and PC pathology elicits loss of balance, coordination, and motor skills impairment (Kemp et al., 2016). However, the number of mouse models investigating primary mitochondrial dysfunction targeting PC remains limited to date. To address this shortcoming and to explore the contribution of cerebellar impairment to LBSL phenotype, we investigated the consequences of DARS2 PC-specific depletion (Rumyantseva et al., 2020).

This study shows that loss of DARS2 results in severe mitochondrial dysfunction culminating in the massive PC loss accompanied by the upregulation of one-carbon metabolism, neuroinflammation, and rapidly deteriorating motor skills (Fig.4.1).

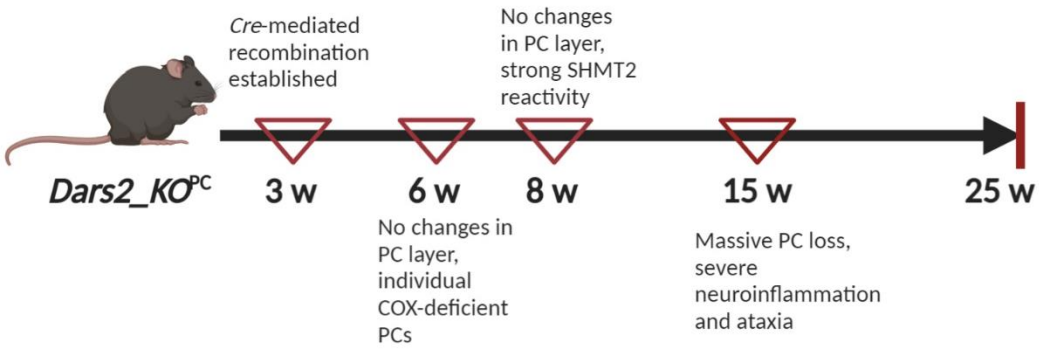

Figure 4.1: Purkinje cell-specific Dars2 knock-out (*Dars2_KO*^{PC}) mouse model.

made with Biorender.com

Pioneering studies in conditional PC-specific mouse models with mitochondrial dysfunction emphasised PC reliance on mitochondrial dynamics (Chen et al., 2007; Kageyama et al., 2012) and mitochondrial quality control (Almajan et al., 2012). Although the respiratory chain (RC) activity is impaired in those models, it is unclear whether OXPHOS defect in those mice primarily underlies pervasive PC loss (Almajan et al., 2012; Chen et al., 2010).

Despite the number of reports suggesting a temporal lag between the onset of a strong mitochondrial OXPHOS dysfunction and neurodegeneration (Ignatenko et al., 2018; Sorensen et al., 2001), it should be borne in mind that distinct neuronal populations might have different energy demands and be more vulnerable to RC dysfunction and oxidative stress (Kageyama et al., 2012; Motori et al., 2020). In line with this, a recent elegant study has reported a diverse effect of the selective NDUFS4 ablation on distinct neuronal populations (Bolea et al., 2019). While mice with NDUFS4-deficient cholinergic neurons are phenotypically equivalent to controls, animals lacking NDUFS4 in glutamatergic and GABAergic neurons have reduced lifespan and LS associated pathology (Bolea et al., 2019). It is not unreasonable to speculate that, given their central role in the cerebellar function and their unique highly-arbourised, mitochondria-rich dendritic morphology, PC cannot tolerate mitochondrial dysfunction for a prolonged time. Consistently, the loss of mitochondrial fission protein DRP1 has little effect on the survival of CA1 hippocampal neurons, while its deficiency results in marked PC degeneration (Kageyama et al., 2012; Shields et al., 2015). Additionally, we cannot exclude that PCs -are specifically sensitive to loss of DARS2 and that mitochondrial protein synthesis resulting from DARS2 depletion cannot be compensated for prolonged periods (Rumyantseva et al., 2020). Although the massive PC loss in our model leads predictably to

severely compromised motor skills of mice, especially their sense of equilibrium and gait, it does not culminate in the early death of mice. In fact, *Dars2_KO*^{PC} mice can live until 25-28 weeks of age, when they must be sacrificed due to severe ataxia (Rumyantseva et al., 2020). Accordingly, previous studies also have shown that despite progressively escalating ataxia, cerebellar defects alone rarely cause death (Quintana et al., 2010; Timmann et al., 2003).

Strikingly, the concomitant loss of CLPP in DARS2-deficient PCs partially ameliorated their degeneration. Intriguingly, *DKO*^{PC} show spatially altered degenerative pattern, revealing a clustered loss of PCs. Consistently, several reports have also described the compartmentalized PC degeneration in Niemann-Pick type C1 (NPC) disease mouse models BALB/c npc(nih) and C57BLKS/J spm and the Lurcher mutant mouse. Interestingly, the specific immunoreactivity for the small heat shock protein 25 (HSP25) has been implicated in the preferential survival of PC subpopulation in these models of cerebellar degeneration (Duffin et al., 2010; Martin et al., 2019; Sarna et al., 2003). HSP25 expression has been demonstrated to confer resistance against reactive oxygen species (ROS) by augmenting glutathione (GSH) concentration and modulating the glucose 6-phosphate dehydrogenase (G6PD) activity (Préville et al., 1999; Yan et al., 2002). The high susceptibility of PCs to oxidative damage has been highlighted through reports in ataxia-telangiectasia (A-T) patients (Reichenbach et al., 2002) and studies in A-T mouse model (Chen et al., 2003), and PC-specific *Mfn2* KO (Motori et al., 2020). Intriguingly, our previous results have revealed that CLPP depletion lowers ROS production (Szczepanowska et al., 2020) making it tempting to speculate that the preserved PCs in *DKO*^{PC} mice benefit from the loss of CLPP that downregulates ROS production.

Similarly to other studies that reported activation of glial cells in almost every primary and secondary mitochondrial neurodegenerative disease including, but not limited to Alzheimer's disease (Guillot-Sestier and Town, 2013), Parkinson's disease (L'Episcopo et al., 2013) and spinocerebellar ataxia type 1 (Cvetanovic et al., 2015), *Dars2* KO in PCs leads to local cerebellar neuroinflammation. In line with this, previous studies in mouse models of cerebellar ataxia have reported a robust PC loss coupled with the upregulation of neuroinflammatory markers (Aikawa et al., 2015; Almajan et al., 2012; Kavetsky et al., 2019). The potential release of damage-associated molecular patterns, upon mitochondrial dysfunction, might promote migration and activation of microglia, thereby amplifying neuroinflammation (Rumyantseva et al., 2020). Remarkably, previous studies have demonstrated that activated microglia are capable of phagocytosing dendrites and axons of living neurons, further amplifying neurodegeneration (Garber et al., 2019; Vilalta and Brown, 2018). In *Dars2_KO*^{PC} we observed PC somata with shrunken or almost disappeared dendritic network, while at the same time, the molecular layer where these dendrites were projected was strongly infiltrated by microglia, further supporting the notion that active phagocytosis of dendrites by microglia might play a role in the cerebellar pathology observed in *Dars2_KO*^{PC} mice (Rumyantseva et al., 2020). In sharp contrast to this, the dendrites of *DKO*^{PC} appeared to be preserved at 15 weeks of age, correlating with decreased microgliosis observed in *DKO*^{PC} mice. This result lends further credence to the notion that excessive neuroinflammation is detrimental to neurons.

Numerous studies in patients, animal models and cultured cells established the initiation of the broad, integrated stress response (ISR) program as an imminent effect of mitochondrial dysfunction (Bao et al., 2016; Celardo et al., 2017; Fujita et al., 2007; Khan et al., 2017; Kühl et al.,

2017; Mick et al., 2020; Quirós et al., 2017; Silva et al., 2009; Tyynismaa et al., 2010). Although the precise ISR-induced transcriptional program might vary across species and tissues (Mick et al., 2020); the activation of the mitochondrial one-carbon (1C) pathway was consistently identified as OXPHOS dysfunction hallmark (Bao et al., 2016; Mick et al., 2020; Nikkanen et al., 2016; Tyynismaa et al., 2010).

Recent studies in mice and *Drosophila melanogaster* have shown that the upregulation of 1C metabolism occurs at the early phase ISR in ATF4-dependent manner (Celardo et al., 2017; Forsström et al., 2019; Nikkanen et al., 2016). Interestingly, we have previously demonstrated a strong upregulation of ATF4 levels in DARS2-deficient hearts (Dogan et al., 2014; Kaspar, 2019). Here, we provide evidence that the SHMT2 upregulation precedes PC loss and massive inflammation, and instead coincides with initial signs of OXPHOS dysfunction, which is rapidly followed by increased levels of the astrocytic marker GFAP. In agreement with this result, a recent detailed study of Motori *et al*. on FACS-sorted PCs of *Mfn*2 KO model has demonstrated TCA anaplerosis and 1C metabolism rewiring occurring prior to the major loss of PCs (Motori et al., 2020). Our result lends further credence that remodelling of 1C metabolism occurs early during mitochondrial dysfunction and that this process is also conserved for DARS2 deficiency in PCs (Rumyantseva et al., 2020). Intriguingly, an adeno-associated viral (AAV) reintroduction of *Mfn2*, after main metabolic changes took place, can overturn PC degeneration (Motori et al., 2020). In line with this, recent studies have demonstrated that AAV delivery of *Ndufs4* after the onset of symptoms can delay neurodegeneration and prolong the lifespan of NDUFS4 KO mice (Reynaud-Dulaurier et al., 2020; Silva-Pinheiro et al., 2020). It would be of interest to determine if the reintroduction of *Dars2* after commenced mitochondrial dysfunction would prevent PCs loss and the neuroinflammation.

Importantly, a recent study has shed light on the contribution of imbalanced 1C metabolism to the inflammatory response. Namely, it has proposed that insufficient NAD^+ production resulting from CI deficiency leads to impaired 1C metabolism, which in its turn affects NADPH production, whose deficiency underlies activation of inflammatory kinases p38 and JNK (Balsa et al., 2020). Several reports have also provided evidence of boosting cellular NAD^+ levels, through its precursor vitamin B3 supplementation, as a potential therapy for mitochondrial diseases (Katsyuba et al., 2018; Khan et al., 2014; Pirinen et al., 2020). In line with this, a recent study has shown that the overexpression of the yeast enzyme NADH dehydrogenase (NDI1) regenerates cellular NAD^+ levels, reduces inflammation and rescues the lifespan of NDUFS4 KO mice (McElroy et al., 2020). Intriguingly, we have previously made two important observations. Firstly, we have identified 1C metabolism enzyme ALDH1L2, which is one of the main contributors to the cellular NADPH production (Balsa et al., 2020; Ducker et al., 2016; Fan et al., 2014), as a substrate candidate of CLPP (Szczepanowska et al., 2016). Secondly, we have suggested that N-module accumulation mediated by the absence of CLPP provides means to maintain NAD^+ levels, even when CI is compromised (Szczepanowska et al., 2020). The preceding observations and our current data make us hypothesize that concomitant *Clpp* deficiency in both our models decreases upregulation of inflammatory signatures emanating from neurons by increasing NADPH levels through simultaneously elevated levels of ALDH1L2 and NAD^+. Future experiments should aim to unravel the precise effect of CLPP inhibition in neuron-specific DARS2-deficient background on 1C metabolism enzymes and NAD^+, NADPH levels.

4.2 Loss of CLPP delays neurodegeneration in *Dars2_KO*^{FbNe}

PCs represent a very morphologically-specific population of GABAergic inhibitory neurons, confined to a cerebellum. To corroborate the observations of the beneficial effect of CLPP loss in *Dars2_KO*^{PC}, we generated a double KO under control of *CamkIIα-Cre* that drives postnatal deletion of the floxed alleles in a broader, compared to *L7-Cre*, manner, affecting neurons of forebrain, mainly in cortex and hippocampus (Diaz et al., 2012). Interestingly, *DKO*^{FbNe} mice have increased COX-activity at 15 and 20 weeks of age comparing to *Dars2_KO*^{FbNe} mice. Strikingly, *Dars2_KO*^{FbNe} mice have COX-deficient neurons in their cortices and hippocampi at 15 weeks, whereas *DKO*^{FbNe} displayed weak blue signal restricted to only hippocampal area at 15 weeks. Notably, the milder COX-deficiency in COX/SDH staining has been demonstrated previously in the heart-specific *Dars2/Clpp* double knock-out, implicating beneficial effect of the improved OXPHOS function also in that model (Seiferling et al., 2016). The observed discrepancy in OXPHOS function between *DKO*^{FbNe} and *Dars2_KO*^{FbNe} might be a direct consequence of previously uncovered stabilizing effect of CLPP deficiency on CI-containing supercomplexes (Szczepanowska et al., 2020). Unsurprisingly, the stability and incorporation of CI into supercomplexes was shown to play a pivotal role in neuronal respiration (Lopez-Fabuel et al., 2016). Remarkably, in the sharp contrast to *Dars2_KO*^{FbNe} mice that have “swollen”, devoided of cristae mitochondria, *DKO*^{FbNe} mice display partially rescued mitochondrial morphology, retaining cristae structures at 20 weeks. On the one hand, the organised cristae structures were demonstrated to stabilize RC supercomplexes, and thus might account for milder OXPHOS dysfunction (Cogliati et al., 2013). On the other hand, anterograde and retrograde trafficking of large and empty mitochondria of *Dars2_KO*^{FbNe} mice might be impaired, making it difficult to deliver them at

presynapses, where their ATP-producing activity is needed the most in such polarized cells as neurons (Hall et al., 2012; Lees et al., 2019). Hence, improved mitochondrial morphology might facilitate mitochondrial anterograde transport in *DKO*^{FbNe} mice, sustaining synaptic connection and therefore, potentiating neuronal survival that otherwise would not be possible (Verhage et al., 2000).

One of the first structural changes in the brain following *CamKIIα*-driven DARS2 deficiency occurs in retrosplenial cortex (RSC), which has more than 50 % neurons lost by 20 weeks of age in *Dars2_KO*^{FbNe}. This data is in agreement with our previous report, demonstrating a progressive increase in TUNEL-positive cell numbers from 15 to 20 weeks of age in *Dars2_KO*^{FbNe} mice, particularly in RSC (Aradjanski et al., 2017). In line with our findings in *DKO*^{PC} mice that have delayed decline of PCs, we also observed partially rescued the loss of RSC neurons in *DKO*^{FbNe} at 20 weeks of age. Potentially, the enhanced perseverance of RSC neurons is a direct consequence of milder COX-deficiency, observed in *DKO*^{FbNe}. However, a synergetic effect might take place, as it was shown that RSC neurons are selectively vulnerable to damage in their afferents located in a hippocampus (Poirier et al., 2011; van Groen and Wyss, 1990, 1992). Thus, it is reasonable to suggest that milder OXPHOS dysfunction in hippocampus of *DKO*^{FbNe} mice contributes to partial rescue of RSC neurons. Remarkably, even 25-weeks-old *DKO*^{FbNe} mice display milder brain atrophy in general and reduced loss of RSC neurons in particular.

Moreover, in the present study, we observed differential cell death dynamic in the CA1 hippocampal region. While *Dars2_KO*^{FbNe} mice have multiple TUNEL-positive cells in CA1 at the terminal stage at 28 weeks of age, *DKO*^{FbNe} mice exhibit fewer apoptotic neurons in CA1. Even though hippocampal neurons are among the first to show COX-deficiency, we

have noticed their robustness in our *Dars2_KO*^{FbNe} mouse model. Notably, apoptotic neurons in the hippocampus of *Dars2_KO*^{FbNe} mice appear much later in the disease progression, and the spike in their numbers correlates with the terminal stage when *Dars2_KO*^{FbNe} mice have to be sacrificed due to the severity of the phenotype (Aradjanski et al., 2017). Of a note, recent studies in MFN2 KO mice, utilising *CamkII*-*Cre* conditional recombination strategy have demonstrated the specific vulnerability of CA1 neurons to MFN2 depletion, with almost all CA1 neurons gone by the age of 18 weeks, highlighting the importance of mitochondrial fusion for CA1 neurons (Jiang et al., 2018). Notably, before degeneration, CA1 neurons in *Mnf2* KO model exhibited a progressive decrease in microtubule-associated protein 2 (MAP2), a cytoskeletal protein, which ensures the stability of dendritic processes (Di Stefano et al., 2001; Jiang et al., 2018). An intriguing possibility is that the dendritic network and interconnectivity within hippocampus might be less affected in *DKO*^{FbNe} mice comparing to *Dars2_KO*^{FbNe} mice and future experiments should shed light on that. This results altogether strengthen further our hypothesis that CLPP depletion is beneficial in *Dars2*-deficient background and that the effect is not limited to only one neuronal population. Notably, both our models might display only partial recapitulation of DARS2 patients. Firstly, unlike our models, DARS2 patients carry a compound, heterozygous mutation of *DARS2* associated with decreased activity of the enzyme. Secondly, the conditional KO in both our models takes place postnatally, which makes it challenging to determine the effect of *Dars2* depletion on neuronal development. Lastly, even though all DARS2 patients diagnosed to date display LBSL, cell non-autonomous response arising from other organs affected by *DARS2* mutation, cannot be ruled out.

Despite our previous reports that in the absence of CLPP mitochondrial translation rate is decreased in the heart with (Seiferling et al., 2016) and without DARS2-deficiency background (Szczepanowska et al., 2016; Szczepanowska et al., 2020), we did not observe any changes in brain mitochondrial translation rate of *Clpp_KO*^{WB} mice. This apparent discrepancy may be due to previously unforeseen tissue-specific outcome of CLPP loss. Alternatively, we cannot exclude the possibility that any potential effect of CLPP ablation on neuronal mitochondrial translation rate was masked in our experiments, as we purified mitochondria from the whole forebrain. In this regard, future experiments on primary neuronal cultures bearing DARS2, CLPP and double deficiency should aim to elucidate the implications of CLPP loss on neuronal mitochondrial translation rate.

In the present study, we demonstrated that the loss of mitochondrial matrix protease proteolytic subunit CLPP is beneficial in two distinct models of mitochondria encephalopathy, driven by *Dars2*-deficiency. We successfully showed that in both models, the concomitant absence of CLPP delays degeneration of several neuronal populations, including PCs, neurons of RSC, and CA1 neurons. The delayed neuronal death and milder OXPHOS dysfunction, potentially lead to the decreased neuroinflammatory response observed in *DKO*^{PC} and *DKO*^{FbNe} mice. The reduced neuroinflammation and neurodegeneration significantly improve motor functions in both mouse models, and partially rescue brain atrophy in *DKO*^{FbNe} mice (Fig.4.2).

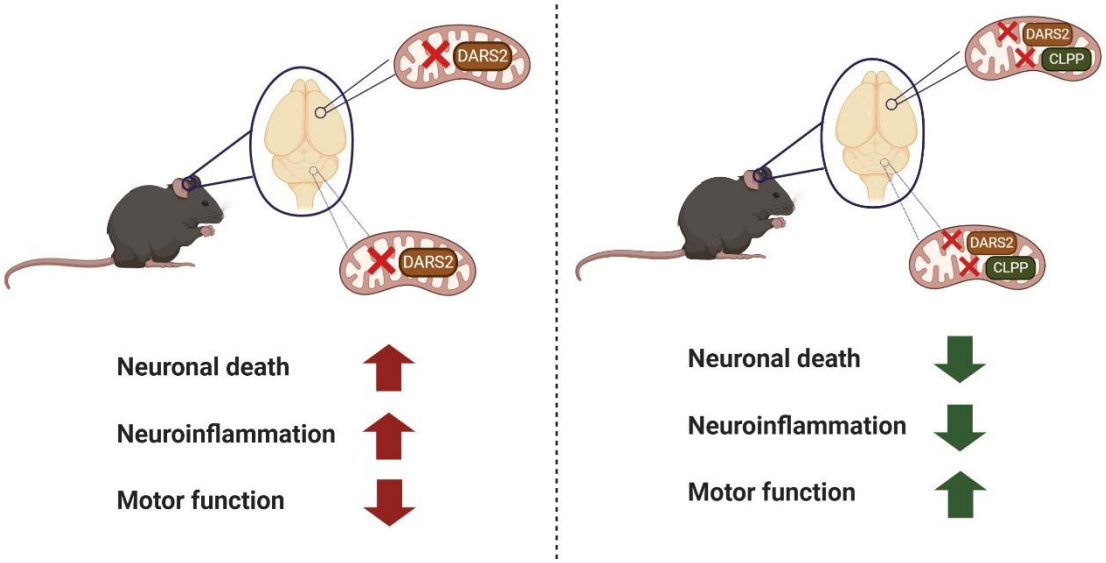

Figure 4.2 Beneficial effect of the CLPP loss in Purkinje cell-specific and forebrain-neuron-specific DARS2-deficient mice. *made with Biorender.com*

Notably, while the precise mechanism underlying the beneficial effect of CLPP loss in our encephalopathy models remains to be elucidated, we suggest three plausible explanations. First, the loss of CLPP prevents a build-up of deleterious ROS, thus reducing oxidative stress. Second, the increased stability of CI in the absence of CLPP ensures its partially restored activity, which coupled to the ability to accumulate free N-module to oxidize NADH, maintaining higher NAD^+ levels. Third, list of potential CLPP substrates includes not only components of the RC, but also proteins regulating metabolic processes of TCA, 1C cycle, carbohydrate, and lipid metabolism (Fischer et al., 2015; Szczepanowska et al., 2016). Thus, we cannot exclude the possibility that the loss of *Clpp* elicits metabolic rewiring that eventually improves the phenotype in our mouse models.

References

Accardi, M.V., Daniels, B.A., Brown, P.M., Fritschy, J.M., Tyagarajan, S.K., and Bowie, D. (2014). Mitochondrial reactive oxygen species regulate the strength of inhibitory GABA-mediated synaptic transmission. Nat Commun 5, 3168.

Aikawa, T., Mogushi, K., Iijima-Tsutsui, K., Ishikawa, K., Sakurai, M., Tanaka, H., Mizusawa, H., and Watase, K. (2015). Loss of MyD88 alters neuroinflammatory response and attenuates early Purkinje cell loss in a spinocerebellar ataxia type 6 mouse model. Hum Mol Genet 24, 4780-4791.

Almajan, E.R., Richter, R., Paeger, L., Martinelli, P., Barth, E., Decker, T., Larsson, N.G., Kloppenburg, P., Langer, T., and Rugarli, E.I. (2012). AFG3L2 supports mitochondrial protein synthesis and Purkinje cell survival. J Clin Invest 122, 4048-4058.

Almalki, A., Alston, C.L., Parker, A., Simonic, I., Mehta, S.G., He, L., Reza, M., Oliveira, J.M., Lightowlers, R.N., McFarland, R.*, et al.* (2014). Mutation of the human mitochondrial phenylalanine-tRNA synthetase causes infantile-onset epilepsy and cytochrome c oxidase deficiency. Biochim Biophys Acta 1842, 56-64.

Antonellis, A., Ellsworth, R.E., Sambuughin, N., Puls, I., Abel, A., Lee-Lin, S.Q., Jordanova, A., Kremensky, I., Christodoulou, K., Middleton, L.T.*, et al.* (2003). Glycyl tRNA synthetase mutations in Charcot-Marie-Tooth disease type 2D and distal spinal muscular atrophy type V. Am J Hum Genet 72, 1293-1299.

Antonellis, A., and Green, E.D. (2008). The role of aminoacyl-tRNA synthetases in genetic diseases. Annu Rev Genomics Hum Genet 9, 87-107.

Aradjanski, M., Dogan, S.A., Lotter, S., Wang, S., Hermans, S., Wibom, R., Rugarli, E., and Trifunovic, A. (2017). DARS2 protects against neuroinflammation and apoptotic neuronal loss, but is dispensable for myelin producing cells. Hum Mol Genet 26, 4181-4189.

Bacman, S.R., Kauppila, J.H.K., Pereira, C.V., Nissanka, N., Miranda, M., Pinto, M., Williams, S.L., Larsson, N.G., Stewart, J.B., and Moraes, C.T. (2018). MitoTALEN reduces mutant mtDNA load and restores tRNA. Nat Med 24, 1696-1700.

Balsa, E., Perry, E.A., Bennett, C.F., Jedrychowski, M., Gygi, S.P., Doench, J.G., and Puigserver, P. (2020). Defective NADPH production in mitochondrial disease complex I causes inflammation and cell death. Nat Commun 11, 2714.

Bao, X.R., Ong, S.E., Goldberger, O., Peng, J., Sharma, R., Thompson, D.A., Vafai, S.B., Cox, A.G., Marutani, E., Ichinose, F.*, et al.* (2016). Mitochondrial dysfunction remodels one-carbon metabolism in human cells. Elife 5.

Barriocanal-Casado, E., Hidalgo-Gutiérrez, A., Raimundo, N., González-García, P., Acuña-Castroviejo, D., Escames, G., and López, L.C. (2019). Rapamycin administration is not a valid therapeutic strategy for every case of mitochondrial disease. EBioMedicine 42, 511-523.

Barski, J.J., Dethleffsen, K., and Meyer, M. (2000). Cre recombinase expression in cerebellar Purkinje cells. Genesis 28, 93-98.

Bayat, V., Thiffault, I., Jaiswal, M., Tétreault, M., Donti, T., Sasarman, F., Bernard, G., Demers-Lamarche, J., Dicaire, M.J., Mathieu, J.*, et al.* (2012). Mutations in the mitochondrial methionyl-tRNA synthetase cause a neurodegenerative phenotype in flies and a recessive ataxia (ARSAL) in humans. PLoS Biol 10, e1001288.

Becker, C., Kukat, A., Szczepanowska, K., Hermans, S., Senft, K., Brandscheid, C.P., Maiti, P., and Trifunovic, A. (2018). CLPP deficiency protects against metabolic syndrome but hinders adaptive thermogenesis. EMBO Rep 19.

Beckervordersandforth, R., Ebert, B., Schäffner, I., Moss, J., Fiebig, C., Shin, J., Moore, D.L., Ghosh, L., Trinchero, M.F., Stockburger, C.*, et al.* (2017). Role of Mitochondrial Metabolism in the Control of Early Lineage Progression and Aging Phenotypes in Adult Hippocampal Neurogenesis. Neuron 93, 1518.

Belostotsky, R., Ben-Shalom, E., Rinat, C., Becker-Cohen, R., Feinstein, S., Zeligson, S., Segel, R., Elpeleg, O., Nassar, S., and Frishberg, Y. (2011). Mutations in the mitochondrial seryl-tRNA synthetase cause hyperuricemia, pulmonary hypertension, renal failure in infancy and alkalosis, HUPRA syndrome. Am J Hum Genet 88, 193-200.

Bhaskar, S., Sheshadri, P., Joseph, J.P., Potdar, C., Prasanna, J., and Kumar, A. (2020). Mitochondrial Superoxide Dismutase Specifies Early Neural Commitment by Modulating Mitochondrial Dynamics. iScience 23, 101564.

Bhaskaran, S., Pharaoh, G., Ranjit, R., Murphy, A., Matsuzaki, S., Nair, B.C., Forbes, B., Gispert, S., Auburger, G., Humphries, K.M.*, et al.* (2018). Loss of mitochondrial protease ClpP protects mice from diet-induced obesity and insulin resistance. EMBO Rep 19.

Billups, B., and Forsythe, I.D. (2002). Presynaptic mitochondrial calcium sequestration influences transmission at mammalian central synapses. J Neurosci 22, 5840-5847.

Bolea, I., Gella, A., Sanz, E., Prada-Dacasa, P., Menardy, F., Bard, A.M., Machuca-Márquez, P., Eraso-Pichot, A., Mòdol-Caballero, G., Navarro, X.*, et al.* (2019). Defined neuronal populations drive fatal phenotype in a mouse model of Leigh syndrome. Elife 8.

Bough, K.J., and Rho, J.M. (2007). Anticonvulsant mechanisms of the ketogenic diet. Epilepsia 48, 43-58.

Brusselmans, K., Compernolle, V., Tjwa, M., Wiesener, M.S., Maxwell, P.H., Collen, D., and Carmeliet, P. (2003). Heterozygous deficiency of hypoxia-inducible factor-2alpha protects mice against pulmonary hypertension and right ventricular dysfunction during prolonged hypoxia. J Clin Invest 111, 1519-1527.

Burke, E.A., Frucht, S.J., Thompson, K., Wolfe, L.A., Yokoyama, T., Bertoni, M., Huang, Y., Sincan, M., Adams, D.R., Taylor, R.W.*, et al.* (2018). Biallelic mutations in mitochondrial tryptophanyl-tRNA synthetase cause Levodopa-responsive infantile-onset Parkinsonism. Clin Genet 93, 712-718.

Bénard, G., Massa, F., Puente, N., Lourenço, J., Bellocchio, L., Soria-Gómez, E., Matias, I., Delamarre, A., Metna-Laurent, M., Cannich, A.*, et al.* (2012). Mitochondrial CB_1 receptors regulate neuronal energy metabolism. Nat Neurosci 15, 558-564.

Camandola, S., and Mattson, M.P. (2017). Brain metabolism in health, aging, and neurodegeneration. EMBO J 36, 1474-1492.

Cardoso, S.M., Santos, S., Swerdlow, R.H., and Oliveira, C.R. (2001). Functional mitochondria are required for amyloid beta-mediated neurotoxicity. FASEB J 15, 1439-1441.

Celardo, I., Lehmann, S., Costa, A.C., Loh, S.H., and Miguel Martins, L. (2017). dATF4 regulation of mitochondrial folate-mediated one-carbon metabolism is neuroprotective. Cell Death Differ 24, 638-648.

Cenini, G., and Voos, W. (2019). Mitochondria as Potential Targets in Alzheimer Disease Therapy: An Update. Front Pharmacol 10, 902.

Chen, C.T., Hsu, S.H., and Wei, Y.H. (2010). Upregulation of mitochondrial function and antioxidant defense in the differentiation of stem cells. Biochim Biophys Acta 1800, 257-263.

Chen, H., McCaffery, J.M., and Chan, D.C. (2007). Mitochondrial fusion protects against neurodegeneration in the cerebellum. Cell 130, 548-562.

Chen, P., Peng, C., Luff, J., Spring, K., Watters, D., Bottle, S., Furuya, S., and Lavin, M.F. (2003). Oxidative stress is responsible for deficient survival and dendritogenesis in purkinje neurons from ataxia-telangiectasia mutated mutant mice. J Neurosci 23, 11453-11460.

Chernova, T., Steinert, J.R., Guerin, C.J., Nicotera, P., Forsythe, I.D., and Smith, A.G. (2007). Neurite degeneration induced by heme deficiency mediated via inhibition of NMDA receptor-dependent extracellular signal-regulated kinase 1/2 activation. J Neurosci 27, 8475-8485.

Chol, M., Lebon, S., Bénit, P., Chretien, D., de Lonlay, P., Goldenberg, A., Odent, S., Hertz-Pannier, L., Vincent-Delorme, C., Cormier-Daire, V.*, et al.* (2003). The mitochondrial DNA G13513A MELAS mutation in the NADH dehydrogenase 5 gene is a frequent cause of Leigh-like syndrome with isolated complex I deficiency. J Med Genet 40, 188-191.

Civiletto, G., Dogan, S.A., Cerutti, R., Fagiolari, G., Moggio, M., Lamperti, C., Benincá, C., Viscomi, C., and Zeviani, M. (2018). Rapamycin rescues mitochondrial myopathy via coordinated activation of autophagy and lysosomal biogenesis. EMBO Mol Med 10.

Cogliati, S., Frezza, C., Soriano, M.E., Varanita, T., Quintana-Cabrera, R., Corrado, M., Cipolat, S., Costa, V., Casarin, A., Gomes, L.C.*, et al.* (2013). Mitochondrial cristae shape determines respiratory chain supercomplexes assembly and respiratory efficiency. Cell 155, 160-171.

Corder, E.H., Saunders, A.M., Strittmatter, W.J., Schmechel, D.E., Gaskell, P.C., Small, G.W., Roses, A.D., Haines, J.L., and Pericak-Vance, M.A. (1993). Gene dose of apolipoprotein E type 4 allele and the risk of Alzheimer's disease in late onset families. Science 261, 921-923.

Coughlin, C.R., Scharer, G.H., Friederich, M.W., Yu, H.C., Geiger, E.A., Creadon-Swindell, G., Collins, A.E., Vanlander, A.V., Coster, R.V., Powell, C.A.*, et al.* (2015). Mutations in the mitochondrial cysteinyl-tRNA synthase gene, CARS2, lead to a severe epileptic encephalopathy and complex movement disorder. J Med Genet 52, 532-540.

Cvetanovic, M., Ingram, M., Orr, H., and Opal, P. (2015). Early activation of microglia and astrocytes in mouse models of spinocerebellar ataxia type 1. Neuroscience 289, 289-299.

Cáceres, A., Banker, G.A., and Binder, L. (1986). Immunocytochemical localization of tubulin and microtubule-associated protein 2 during the development of hippocampal neurons in culture. J Neurosci 6, 714-722.

Cáceres, M., Lachuer, J., Zapala, M.A., Redmond, J.C., Kudo, L., Geschwind, D.H., Lockhart, D.J., Preuss, T.M., and Barlow, C. (2003). Elevated gene expression levels distinguish human from non-human primate brains. Proc Natl Acad Sci U S A 100, 13030-13035.

Dallabona, C., Diodato, D., Kevelam, S.H., Haack, T.B., Wong, L.J., Salomons, G.S., Baruffini, E., Melchionda, L., Mariotti, C., Strom, T.M.*, et al.* (2014). Novel (ovario) leukodystrophy related to AARS2 mutations. Neurology 82, 2063-2071.

Devine, M.J., and Kittler, J.T. (2018). Mitochondria at the neuronal presynapse in health and disease. Nat Rev Neurosci 19, 63-80.

Di Meo, I., Marchet, S., Lamperti, C., Zeviani, M., and Viscomi, C. (2017). AAV9-based gene therapy partially ameliorates the clinical phenotype of a mouse model of Leigh syndrome. Gene Ther 24, 661-667.

Di Stefano, G., Casoli, T., Fattoretti, P., Gracciotti, N., Solazzi, M., and Bertoni-Freddari, C. (2001). Distribution of map2 in hippocampus and cerebellum of young and old rats by quantitative immunohistochemistry. J Histochem Cytochem 49, 1065-1066.

Diaz, F., Garcia, S., Padgett, K.R., and Moraes, C.T. (2012). A defect in the mitochondrial complex III, but not complex IV, triggers early ROS-dependent damage in defined brain regions. Hum Mol Genet 21, 5066-5077.

DiMauro, S., and Schon, E.A. (2008). Mitochondrial disorders in the nervous system. Annu Rev Neurosci 31, 91-123.

Diodato, D., Ghezzi, D., and Tiranti, V. (2014a). The Mitochondrial Aminoacyl tRNA Synthetases: Genes and Syndromes. Int J Cell Biol 2014, 787956.

Diodato, D., Melchionda, L., Haack, T.B., Dallabona, C., Baruffini, E., Donnini, C., Granata, T., Ragona, F., Balestri, P., Margollicci, M.*, et al.* (2014b). VARS2 and TARS2 mutations in patients with mitochondrial encephalomyopathies. Hum Mutat 35, 983-989.

Dogan, S.A., Pujol, C., Maiti, P., Kukat, A., Wang, S., Hermans, S., Senft, K., Wibom, R., Rugarli, E.I., and Trifunovic, A. (2014). Tissue-specific loss of DARS2 activates stress responses independently of respiratory chain deficiency in the heart. Cell Metab 19, 458-469.

Dotti, C.G., Sullivan, C.A., and Banker, G.A. (1988). The establishment of polarity by hippocampal neurons in culture. J Neurosci 8, 1454-1468.

Dringen, R. (2000). Metabolism and functions of glutathione in brain. Prog Neurobiol 62, 649-671.

Duan, D., Sharma, P., Yang, J., Yue, Y., Dudus, L., Zhang, Y., Fisher, K.J., and Engelhardt, J.F. (1998). Circular intermediates of recombinant adeno-associated virus have defined structural characteristics responsible for long-term episomal persistence in muscle tissue. J Virol 72, 8568-8577.

Duchen, M.R. (1992). Ca(2+)-dependent changes in the mitochondrial energetics in single dissociated mouse sensory neurons. Biochem J 283 (Pt 1), 41-50.

Ducker, G.S., Chen, L., Morscher, R.J., Ghergurovich, J.M., Esposito, M., Teng, X., Kang, Y., and Rabinowitz, J.D. (2016). Reversal of Cytosolic One-Carbon Flux Compensates for Loss of the Mitochondrial Folate Pathway. Cell Metab 24, 640-641.

Duffin, C.A., McFarland, R., Sarna, J.R., Vogel, M.W., and Armstrong, C.L. (2010). Heat shock protein 25 expression and preferential Purkinje cell survival in the lurcher mutant mouse cerebellum. J Comp Neurol 518, 1892-1907.

Edvardson, S., Shaag, A., Kolesnikova, O., Gomori, J.M., Tarassov, I., Einbinder, T., Saada, A., and Elpeleg, O. (2007). Deleterious mutation in the mitochondrial arginyl-transfer RNA synthetase gene is associated with pontocerebellar hypoplasia. Am J Hum Genet 81, 857-862.

Elo, J.M., Yadavalli, S.S., Euro, L., Isohanni, P., Götz, A., Carroll, C.J., Valanne, L., Alkuraya, F.S., Uusimaa, J., Paetau, A., *et al.* (2012). Mitochondrial phenylalanyl-tRNA synthetase mutations underlie fatal infantile Alpers encephalopathy. Hum Mol Genet 21, 4521-4529.

Erecinska, M., Cherian, S., and Silver, I.A. (2004). Energy metabolism in mammalian brain during development. Prog Neurobiol 73, 397-445.

Fan, J., Ye, J., Kamphorst, J.J., Shlomi, T., Thompson, C.B., and Rabinowitz, J.D. (2014). Quantitative flux analysis reveals folate-dependent NADPH production. Nature 510, 298-302.

Felici, R., Buonvicino, D., Muzzi, M., Cavone, L., Guasti, D., Lapucci, A., Pratesi, S., De Cesaris, F., Luceri, F., and Chiarugi, A. (2017). Post onset, oral rapamycin treatment delays development of mitochondrial encephalopathy only at supramaximal doses. Neuropharmacology 117, 74-84.

Ferrari, M., Jain, I.H., Goldberger, O., Rezoagli, E., Thoonen, R., Cheng, K.H., Sosnovik, D.E., Scherrer-Crosbie, M., Mootha, V.K., and Zapol, W.M. (2017).

Hypoxia treatment reverses neurodegenerative disease in a mouse model of Leigh syndrome. Proc Natl Acad Sci U S A 114, E4241-E4250.

Fine, A.S., Nemeth, C.L., Kaufman, M.L., and Fatemi, A. (2019). Mitochondrial aminoacyl-tRNA synthetase disorders: an emerging group of developmental disorders of myelination. J Neurodev Disord 11, 29.

Fine, L.G., and Norman, J.T. (2008). Chronic hypoxia as a mechanism of progression of chronic kidney diseases: from hypothesis to novel therapeutics. Kidney Int 74, 867-872.

Finsterer, J. (2008). Leigh and Leigh-like syndrome in children and adults. Pediatr Neurol 39, 223-235.

Fischer, F., Langer, J.D., and Osiewacz, H.D. (2015). Identification of potential mitochondrial CLPXP protease interactors and substrates suggests its central role in energy metabolism. Sci Rep 5, 18375.

Flotte, T.R., and Berns, K.I. (2005). Adeno-associated virus: a ubiquitous commensal of mammals. Hum Gene Ther 16, 401-407.

Forsström, S., Jackson, C.B., Carroll, C.J., Kuronen, M., Pirinen, E., Pradhan, S., Marmyleva, A., Auranen, M., Kleine, I.M., Khan, N.A.*, et al.* (2019). Fibroblast Growth Factor 21 Drives Dynamics of Local and Systemic Stress Responses in Mitochondrial Myopathy with mtDNA Deletions. Cell Metab 30, 1040-1054.e1047.

Fröhlich, D., Suchowerska, A.K., Voss, C., He, R., Wolvetang, E., von Jonquieres, G., Simons, C., Fath, T., Housley, G.D., and Klugmann, M. (2018). Expression Pattern of the Aspartyl-tRNA Synthetase DARS in the Human Brain. Front Mol Neurosci 11, 81.

Fujita, Y., Ito, M., Nozawa, Y., Yoneda, M., Oshida, Y., and Tanaka, M. (2007). CHOP (C/EBP homologous protein) and ASNS (asparagine synthetase) induction in cybrid cells harboring MELAS and NARP mitochondrial DNA mutations. Mitochondrion 7, 80-88.

Gammage, P.A., Viscomi, C., Simard, M.L., Costa, A.S.H., Gaude, E., Powell, C.A., Van Haute, L., McCann, B.J., Rebelo-Guiomar, P., Cerutti, R.*, et al.* (2018). Genome editing in mitochondria corrects a pathogenic mtDNA mutation in vivo. Nat Med 24, 1691-1695.

Gao, G., Vandenberghe, L.H., and Wilson, J.M. (2005). New recombinant serotypes of AAV vectors. Curr Gene Ther 5, 285-297.

Garber, C., Soung, A., Vollmer, L.L., Kanmogne, M., Last, A., Brown, J., and Klein, R.S. (2019). T cells promote microglia-mediated synaptic elimination and cognitive dysfunction during recovery from neuropathogenic flaviviruses. Nat Neurosci 22, 1276-1288.

Ghezzi, D., Baruffini, E., Haack, T.B., Invernizzi, F., Melchionda, L., Dallabona, C., Strom, T.M., Parini, R., Burlina, A.B., Meitinger, T.*, et al.* (2012). Mutations of the mitochondrial-tRNA modifier MTO1 cause hypertrophic cardiomyopathy and lactic acidosis. Am J Hum Genet 90, 1079-1087.

Gispert, S., Parganlija, D., Klinkenberg, M., Dröse, S., Wittig, I., Mittelbronn, M., Grzmil, P., Koob, S., Hamann, A., Walter, M.*, et al.* (2013). Loss of mitochondrial peptidase Clpp leads to infertility, hearing loss plus growth retardation via accumulation of CLPX, mtDNA and inflammatory factors. Hum Mol Genet 22, 4871-4887.

Goedert, M., and Spillantini, M.G. (2006). A century of Alzheimer's disease. Science 314, 777-781.

Gorman, G.S., Chinnery, P.F., DiMauro, S., Hirano, M., Koga, Y., McFarland, R., Suomalainen, A., Thorburn, D.R., Zeviani, M., and Turnbull, D.M. (2016). Mitochondrial diseases. Nat Rev Dis Primers 2, 16080.

Gorman, G.S., Schaefer, A.M., Ng, Y., Gomez, N., Blakely, E.L., Alston, C.L., Feeney, C., Horvath, R., Yu-Wai-Man, P., Chinnery, P.F.*, et al.* (2015). Prevalence of nuclear and mitochondrial DNA mutations related to adult mitochondrial disease. Ann Neurol 77, 753-759.

Greenberg, S.B., Faerber, E.N., Riviello, J.J., de Leon, G., and Capitanio, M.A. (1990). Subacute necrotizing encephalomyelopathy (Leigh disease): CT and MRI appearances. Pediatr Radiol 21, 5-8.

Grossman, L.I., Schmidt, T.R., Wildman, D.E., and Goodman, M. (2001). Molecular evolution of aerobic energy metabolism in primates. Mol Phylogenet Evol 18, 26-36.

Guillot-Sestier, M.V., and Town, T. (2013). Innate immunity in Alzheimer's disease: a complex affair. CNS Neurol Disord Drug Targets 12, 593-607.

Guo, L., Tian, J., and Du, H. (2017). Mitochondrial Dysfunction and Synaptic Transmission Failure in Alzheimer's Disease. J Alzheimers Dis 57, 1071-1086.

Guyenet, S.J., Furrer, S.A., Damian, V.M., Baughan, T.D., La Spada, A.R., and Garden, G.A. (2010). A simple composite phenotype scoring system for evaluating mouse models of cerebellar ataxia. J Vis Exp.

Götz, A., Tyynismaa, H., Euro, L., Ellonen, P., Hyötyläinen, T., Ojala, T., Hämäläinen, R.H., Tommiska, J., Raivio, T., Oresic, M.*, et al.* (2011). Exome sequencing identifies mitochondrial alanyl-tRNA synthetase mutations in infantile mitochondrial cardiomyopathy. Am J Hum Genet 88, 635-642.

Halim, N.D., Mcfate, T., Mohyeldin, A., Okagaki, P., Korotchkina, L.G., Patel, M.S., Jeoung, N.H., Harris, R.A., Schell, M.J., and Verma, A. (2010). Phosphorylation status of pyruvate dehydrogenase distinguishes metabolic phenotypes of cultured rat brain astrocytes and neurons. Glia 58, 1168-1176.

Hall, C.N., Klein-Flügge, M.C., Howarth, C., and Attwell, D. (2012). Oxidative phosphorylation, not glycolysis, powers presynaptic and postsynaptic mechanisms underlying brain information processing. J Neurosci 32, 8940-8951.

Hallmann, K., Zsurka, G., Moskau-Hartmann, S., Kirschner, J., Korinthenberg, R., Ruppert, A.K., Ozdemir, O., Weber, Y., Becker, F., Lerche, H.*, et al.* (2014). A homozygous splice-site mutation in CARS2 is associated with progressive myoclonic epilepsy. Neurology 83, 2183-2187.

Hancock, D.B., Martin, E.R., Mayhew, G.M., Stajich, J.M., Jewett, R., Stacy, M.A., Scott, B.L., Vance, J.M., and Scott, W.K. (2008). Pesticide exposure and risk of Parkinson's disease: a family-based case-control study. BMC Neurol 8, 6.

Harris, J.J., Jolivet, R., and Attwell, D. (2012). Synaptic energy use and supply. Neuron 75, 762-777.

Hashimoto, M., Bacman, S.R., Peralta, S., Falk, M.J., Chomyn, A., Chan, D.C., Williams, S.L., and Moraes, C.T. (2015). MitoTALEN: A General Approach to Reduce Mutant mtDNA Loads and Restore Oxidative Phosphorylation Function in Mitochondrial Diseases. Mol Ther 23, 1592-1599.

Hebert-Chatelain, E., Desprez, T., Serrat, R., Bellocchio, L., Soria-Gomez, E., Busquets-Garcia, A., Pagano Zottola, A.C., Delamarre, A., Cannich, A., Vincent, P.*, et al.* (2016). A cannabinoid link between mitochondria and memory. Nature 539, 555-559.

Herrero-Mendez, A., Almeida, A., Fernández, E., Maestre, C., Moncada, S., and Bolaños, J.P. (2009). The bioenergetic and antioxidant status of neurons is controlled by continuous degradation of a key glycolytic enzyme by APC/C-Cdh1. Nat Cell Biol 11, 747-752.

Hirano, M., Emmanuele, V., and Quinzii, C.M. (2018). Emerging therapies for mitochondrial diseases. Essays Biochem 62, 467-481.

Hudson, G., Carelli, V., Spruijt, L., Gerards, M., Mowbray, C., Achilli, A., Pyle, A., Elson, J., Howell, N., La Morgia, C.*, et al.* (2007). Clinical expression of Leber hereditary optic neuropathy is affected by the mitochondrial DNA-haplogroup background. Am J Hum Genet 81, 228-233.

Huoponen, K. (2001). Leber hereditary optic neuropathy: clinical and molecular genetic findings. Neurogenetics 3, 119-125.

Hyder, F., Rothman, D.L., and Bennett, M.R. (2013). Cortical energy demands of signaling and nonsignaling components in brain are conserved across mammalian species and activity levels. Proc Natl Acad Sci U S A 110, 3549-3554.

Höglinger, G.U., Féger, J., Prigent, A., Michel, P.P., Parain, K., Champy, P., Ruberg, M., Oertel, W.H., and Hirsch, E.C. (2003). Chronic systemic complex I inhibition induces a hypokinetic multisystem degeneration in rats. J Neurochem 84, 491-502.

Ignatenko, O., Chilov, D., Paetau, I., de Miguel, E., Jackson, C.B., Capin, G., Paetau, A., Terzioglu, M., Euro, L., and Suomalainen, A. (2018). Loss of mtDNA activates astrocytes and leads to spongiotic encephalopathy. Nat Commun 9, 70.

Ignatenko, O., Nikkanen, J., Kononov, A., Zamboni, N., Ince-Dunn, G., and Suomalainen, A. (2020). Mitochondrial spongiotic brain disease: astrocytic stress and harmful rapamycin and ketosis effect. Life Sci Alliance 3.

Isler, K., and van Schaik, C. (2006). Costs of encephalization: the energy trade-off hypothesis tested on birds. J Hum Evol 51, 228-243.

Isohanni, P., Linnankivi, T., Buzkova, J., Lönnqvist, T., Pihko, H., Valanne, L., Tienari, P.J., Elovaara, I., Pirttilä, T., Reunanen, M.*, et al.* (2010). DARS2 mutations in mitochondrial leucoencephalopathy and multiple sclerosis. J Med Genet 47, 66-70.

Jain, I.H., Zazzeron, L., Goli, R., Alexa, K., Schatzman-Bone, S., Dhillon, H., Goldberger, O., Peng, J., Shalem, O., Sanjana, N.E.*, et al.* (2016). Hypoxia as a therapy for mitochondrial disease. Science 352, 54-61.

Jang, S., Nelson, J.C., Bend, E.G., Rodríguez-Laureano, L., Tueros, F.G., Cartagenova, L., Underwood, K., Jorgensen, E.M., and Colón-Ramos, D.A. (2016). Glycolytic Enzymes Localize to Synapses under Energy Stress to Support Synaptic Function. Neuron 90, 278-291.

Jiang, S., Nandy, P., Wang, W., Ma, X., Hsia, J., Wang, C., Wang, Z., Niu, M., Siedlak, S.L., Torres, S.*, et al.* (2018). Mfn2 ablation causes an oxidative stress

response and eventual neuronal death in the hippocampus and cortex. Mol Neurodegener 13, 5.

Johnson, S.C., Yanos, M.E., Kayser, E.B., Quintana, A., Sangesland, M., Castanza, A., Uhde, L., Hui, J., Wall, V.Z., Gagnidze, A.*, et al.* (2013). mTOR inhibition alleviates mitochondrial disease in a mouse model of Leigh syndrome. Science 342, 1524-1528.

Jun, A.S., Trounce, I.A., Brown, M.D., Shoffner, J.M., and Wallace, D.C. (1996). Use of transmitochondrial cybrids to assign a complex I defect to the mitochondrial DNA-encoded NADH dehydrogenase subunit 6 gene mutation at nucleotide pair 14459 that causes Leber hereditary optic neuropathy and dystonia. Mol Cell Biol 16, 771-777.

Jöbsis, F.F., and Rosenthal, M. (1978). Cerebral energy consumption and provision: the predominance of neuronal oxidative metabolic processes. Ciba Found Symp, 129-148.

Kageyama, Y., Zhang, Z., Roda, R., Fukaya, M., Wakabayashi, J., Wakabayashi, N., Kensler, T.W., Reddy, P.H., Iijima, M., and Sesaki, H. (2012). Mitochondrial division ensures the survival of postmitotic neurons by suppressing oxidative damage. J Cell Biol 197, 535-551.

Kaspar, S.M. (2019). Disentangling the Role of CHOP in Mitochondrial Dysfunction. In Faculty of Mathematics and Natural Sciences (Universität zu Köln, Universität zu Köln).

Katsyuba, E., Mottis, A., Zietak, M., De Franco, F., van der Velpen, V., Gariani, K., Ryu, D., Cialabrini, L., Matilainen, O., Liscio, P.*, et al.* (2018). De novo NAD. Nature 563, 354-359.

Kavetsky, L., Green, K.K., Boyle, B.R., Yousufzai, F.A.K., Padron, Z.M., Melli, S.E., Kuhnel, V.L., Jackson, H.M., Blanco, R.E., Howell, G.R., and Soto, I. (2019). Increased interactions and engulfment of dendrites by microglia precede Purkinje cell degeneration in a mouse model of Niemann Pick Type-C. Sci Rep 9, 14722.

Kemp, K.C., Cook, A.J., Redondo, J., Kurian, K.M., Scolding, N.J., and Wilkins, A. (2016). Purkinje cell injury, structural plasticity and fusion in patients with Friedreich's ataxia. Acta Neuropathol Commun 4, 53.

Khacho, M., Clark, A., Svoboda, D.S., Azzi, J., MacLaurin, J.G., Meghaizel, C., Sesaki, H., Lagace, D.C., Germain, M., Harper, M.E.*, et al.* (2016). Mitochondrial Dynamics Impacts Stem Cell Identity and Fate Decisions by Regulating a Nuclear Transcriptional Program. Cell Stem Cell 19, 232-247.

Khacho, M., Harris, R., and Slack, R.S. (2019). Mitochondria as central regulators of neural stem cell fate and cognitive function. Nat Rev Neurosci 20, 34-48.

Khan, N.A., Auranen, M., Paetau, I., Pirinen, E., Euro, L., Forsström, S., Pasila, L., Velagapudi, V., Carroll, C.J., Auwerx, J., and Suomalainen, A. (2014). Effective treatment of mitochondrial myopathy by nicotinamide riboside, a vitamin B3. EMBO Mol Med 6, 721-731.

Khan, N.A., Nikkanen, J., Yatsuga, S., Jackson, C., Wang, L., Pradhan, S., Kivelä, R., Pessia, A., Velagapudi, V., and Suomalainen, A. (2017). mTORC1 Regulates Mitochondrial Integrated Stress Response and Mitochondrial Myopathy Progression. Cell Metab 26, 419-428.e415.

Kirches, E. (2011). LHON: Mitochondrial Mutations and More. Curr Genomics 12, 44-54.

Kitada, T., Asakawa, S., Hattori, N., Matsumine, H., Yamamura, Y., Minoshima, S., Yokochi, M., Mizuno, Y., and Shimizu, N. (1998). Mutations in the parkin gene cause autosomal recessive juvenile parkinsonism. Nature 392, 605-608.

Klann, E., Roberson, E.D., Knapp, L.T., and Sweatt, J.D. (1998). A role for superoxide in protein kinase C activation and induction of long-term potentiation. J Biol Chem 273, 4516-4522.

Knapp, L.T., and Klann, E. (2002). Potentiation of hippocampal synaptic transmission by superoxide requires the oxidative activation of protein kinase C. J Neurosci 22, 674-683.

Kruse, S.E., Watt, W.C., Marcinek, D.J., Kapur, R.P., Schenkman, K.A., and Palmiter, R.D. (2008). Mice with mitochondrial complex I deficiency develop a fatal encephalomyopathy. Cell Metab 7, 312-320.

Kwon, N.H., Fox, P.L., and Kim, S. (2019). Aminoacyl-tRNA synthetases as therapeutic targets. Nat Rev Drug Discov 18, 629-650.

Kühl, I., Miranda, M., Atanassov, I., Kuznetsova, I., Hinze, Y., Mourier, A., Filipovska, A., and Larsson, N.G. (2017). Transcriptomic and proteomic landscape of mitochondrial dysfunction reveals secondary coenzyme Q deficiency in mammals. Elife 6.

L'Episcopo, F., Tirolo, C., Testa, N., Caniglia, S., Morale, M.C., Impagnatiello, F., Pluchino, S., and Marchetti, B. (2013). Aging-induced Nrf2-ARE pathway disruption in the subventricular zone drives neurogenic impairment in parkinsonian mice via PI3K-Wnt/β-catenin dysregulation. J Neurosci 33, 1462-1485.

La Rosa, P., Russo, M., D'Amico, J., Petrillo, S., Aquilano, K., Lettieri-Barbato, D., Turchi, R., Bertini, E.S., and Piemonte, F. (2019). Nrf2 Induction Re-establishes a Proper Neuronal Differentiation Program in Friedreich's Ataxia Neural Stem Cells. Front Cell Neurosci 13, 356.

Lee, M. (2012). The use of ketogenic diet in special situations: expanding use in intractable epilepsy and other neurologic disorders. Korean J Pediatr 55, 316-321.

Lees, R.M., Johnson, J.D., and Ashby, M.C. (2019). Presynaptic Boutons That Contain Mitochondria Are More Stable. Front Synaptic Neurosci 11, 37.

LEIGH, D. (1951). Subacute necrotizing encephalomyelopathy in an infant. J Neurol Neurosurg Psychiatry 14, 216-221.

Levin, E.D., Brady, T.C., Hochrein, E.C., Oury, T.D., Jonsson, L.M., Marklund, S.L., and Crapo, J.D. (1998). Molecular manipulations of extracellular superoxide dismutase: functional importance for learning. Behav Genet 28, 381-390.

Levy, M., Faas, G.C., Saggau, P., Craigen, W.J., and Sweatt, J.D. (2003). Mitochondrial regulation of synaptic plasticity in the hippocampus. J Biol Chem 278, 17727-17734.

Lin, C.S., Sharpley, M.S., Fan, W., Waymire, K.G., Sadun, A.A., Carelli, V., Ross-Cisneros, F.N., Baciu, P., Sung, E., McManus, M.J.*, et al.* (2012). Mouse mtDNA mutant model of Leber hereditary optic neuropathy. Proc Natl Acad Sci U S A 109, 20065-20070.

Linnankivi, T., Neupane, N., Richter, U., Isohanni, P., and Tyynismaa, H. (2016). Splicing Defect in Mitochondrial Seryl-tRNA Synthetase Gene Causes Progressive Spastic Paresis Instead of HUPRA Syndrome. Hum Mutat 37, 884-888.

Llorens-Bobadilla, E., Zhao, S., Baser, A., Saiz-Castro, G., Zwadlo, K., and Martin-Villalba, A. (2015). Single-Cell Transcriptomics Reveals a Population of Dormant Neural Stem Cells that Become Activated upon Brain Injury. Cell Stem Cell 17, 329-340.

Llorente-Folch, I., Rueda, C.B., Pardo, B., Szabadkai, G., Duchen, M.R., and Satrustegui, J. (2015). The regulation of neuronal mitochondrial metabolism by calcium. J Physiol 593, 3447-3462.

Lopez-Fabuel, I., Le Douce, J., Logan, A., James, A.M., Bonvento, G., Murphy, M.P., Almeida, A., and Bolaños, J.P. (2016). Complex I assembly into

supercomplexes determines differential mitochondrial ROS production in neurons and astrocytes. Proc Natl Acad Sci U S A 113, 13063-13068.

López, L.C., Luna-Sánchez, M., García-Corzo, L., Quinzii, C.M., and Hirano, M. (2014). Pathomechanisms in coenzyme q10-deficient human fibroblasts. Mol Syndromol 5, 163-169.

Maffezzini, C., Calvo-Garrido, J., Wredenberg, A., and Freyer, C. (2020). Metabolic regulation of neurodifferentiation in the adult brain. Cell Mol Life Sci 77, 2483-2496.

Malinow, R., Schulman, H., and Tsien, R.W. (1989). Inhibition of postsynaptic PKC or CaMKII blocks induction but not expression of LTP. Science 245, 862-866.

Maltecca, F., Magnoni, R., Cerri, F., Cox, G.A., Quattrini, A., and Casari, G. (2009). Haploinsufficiency of AFG3L2, the gene responsible for spinocerebellar ataxia type 28, causes mitochondria-mediated Purkinje cell dark degeneration. J Neurosci 29, 9244-9254.

Martin, K.B., Williams, I.M., Cluzeau, C.V., Cougnoux, A., Dale, R.K., Iben, J.R., Cawley, N.X., Wassif, C.A., and Porter, F.D. (2019). Identification of Novel Pathways Associated with Patterned Cerebellar Purkinje Neuron Degeneration in Niemann-Pick Disease, Type C1. Int J Mol Sci 21.

Martin, L.J., Pan, Y., Price, A.C., Sterling, W., Copeland, N.G., Jenkins, N.A., Price, D.L., and Lee, M.K. (2006). Parkinson's disease alpha-synuclein transgenic mice develop neuronal mitochondrial degeneration and cell death. J Neurosci 26, 41-50.

Mattson, M.P., Cheng, B., Davis, D., Bryant, K., Lieberburg, I., and Rydel, R.E. (1992). beta-Amyloid peptides destabilize calcium homeostasis and render human cortical neurons vulnerable to excitotoxicity. J Neurosci 12, 376-389.

Mattson, M.P., Gleichmann, M., and Cheng, A. (2008). Mitochondria in neuroplasticity and neurological disorders. Neuron 60, 748-766.

Mattson, M.P., and Partin, J. (1999). Evidence for mitochondrial control of neuronal polarity. J Neurosci Res 56, 8-20.

McElroy, G.S., Reczek, C.R., Reyfman, P.A., Mithal, D.S., Horbinski, C.M., and Chandel, N.S. (2020). NAD+ Regeneration Rescues Lifespan, but Not Ataxia, in a Mouse Model of Brain Mitochondrial Complex I Dysfunction. Cell Metab 32, 301-308.e306.

McFarland, R., Taylor, R.W., and Turnbull, D.M. (2010). A neurological perspective on mitochondrial disease. Lancet Neurol 9, 829-840.

McLaughlin, H.M., Sakaguchi, R., Liu, C., Igarashi, T., Pehlivan, D., Chu, K., Iyer, R., Cruz, P., Cherukuri, P.F., Hansen, N.F.*, et al.* (2010). Compound heterozygosity for loss-of-function lysyl-tRNA synthetase mutations in a patient with peripheral neuropathy. Am J Hum Genet 87, 560-566.

Mick, E., Titov, D.V., Skinner, O.S., Sharma, R., Jourdain, A.A., and Mootha, V.K. (2020). Distinct mitochondrial defects trigger the integrated stress response depending on the metabolic state of the cell. Elife 9.

Miller, V.J., LaFountain, R.A., Barnhart, E., Sapper, T.S., Short, J., Arnold, W.D., Hyde, P.N., Crabtree, C.D., Kackley, M.L., Kraemer, W.J.*, et al.* (2020). A ketogenic diet combined with exercise alters mitochondrial function in human skeletal muscle while improving metabolic health. Am J Physiol Endocrinol Metab 319, E995-E1007.

Mink, J.W., Blumenschine, R.J., and Adams, D.B. (1981). Ratio of central nervous system to body metabolism in vertebrates: its constancy and functional basis. Am J Physiol 241, R203-212.

Motori, E., Atanassov, I., Kochan, S.M.V., Folz-Donahue, K., Sakthivelu, V., Giavalisco, P., Toni, N., Puyal, J., and Larsson, N.G. (2020). Neuronal metabolic rewiring promotes resilience to neurodegeneration caused by mitochondrial dysfunction. Sci Adv 6, eaba8271.

Mouton-Liger, F., Jacoupy, M., Corvol, J.C., and Corti, O. (2017). PINK1/Parkin-Dependent Mitochondrial Surveillance: From Pleiotropy to Parkinson's Disease. Front Mol Neurosci 10, 120.

Mullen, R.J., Buck, C.R., and Smith, A.M. (1992). NeuN, a neuronal specific nuclear protein in vertebrates. Development 116, 201-211.

Murphy, M.P., and Hartley, R.C. (2018). Mitochondria as a therapeutic target for common pathologies. Nat Rev Drug Discov 17, 865-886.

Nagamatsu, S., Kornhauser, J.M., Burant, C.F., Seino, S., Mayo, K.E., and Bell, G.I. (1992). Glucose transporter expression in brain. cDNA sequence of mouse GLUT3, the brain facilitative glucose transporter isoform, and identification of sites of expression by in situ hybridization. J Biol Chem 267, 467-472.

Nehlig, A., and Pereira de Vasconcelos, A. (1993). Glucose and ketone body utilization by the brain of neonatal rats. Prog Neurobiol 40, 163-221.

Nemani, V.M., Lu, W., Berge, V., Nakamura, K., Onoa, B., Lee, M.K., Chaudhry, F.A., Nicoll, R.A., and Edwards, R.H. (2010). Increased expression of alpha-synuclein reduces neurotransmitter release by inhibiting synaptic vesicle reclustering after endocytosis. Neuron 65, 66-79.

Nesbitt, V., Morrison, P.J., Crushell, E., Donnelly, D.E., Alston, C.L., He, L., McFarland, R., and Taylor, R.W. (2012). The clinical spectrum of the m.10191T>C mutation in complex I-deficient Leigh syndrome. Dev Med Child Neurol 54, 500-506.

Ng, Y.S., Martikainen, M.H., Gorman, G.S., Blain, A., Bugiardini, E., Bunting, A., Schaefer, A.M., Alston, C.L., Blakely, E.L., Sharma, S.*, et al.* (2019). Pathogenic variants in MT-ATP6: A United Kingdom-based mitochondrial disease cohort study. Ann Neurol 86, 310-315.

Nie, A., Sun, B., Fu, Z., and Yu, D. (2019). Roles of aminoacyl-tRNA synthetases in immune regulation and immune diseases. Cell Death Dis 10, 901.

Nikkanen, J., Forsstrom, S., Euro, L., Paetau, I., Kohnz, R.A., Wang, L., Chilov, D., Viinamaki, J., Roivainen, A., Marjamaki, P.*, et al.* (2016). Mitochondrial DNA Replication Defects Disturb Cellular dNTP Pools and Remodel One-Carbon Metabolism. Cell Metab 23, 635-648.

Nishri, D., Goldberg-Stern, H., Noyman, I., Blumkin, L., Kivity, S., Saitsu, H., Nakashima, M., Matsumoto, N., Leshinsky-Silver, E., Lerman-Sagie, T., and Lev, D. (2016). RARS2 mutations cause early onset epileptic encephalopathy without ponto-cerebellar hypoplasia. Eur J Paediatr Neurol 20, 412-417.

Niyazov, D.M., Kahler, S.G., and Frye, R.E. (2016). Primary Mitochondrial Disease and Secondary Mitochondrial Dysfunction: Importance of Distinction for Diagnosis and Treatment. Mol Syndromol 7, 122-137.

Nouws, J., Wibrand, F., van den Brand, M., Venselaar, H., Duno, M., Lund, A.M., Trautner, S., Nijtmans, L., and Ostergard, E. (2014). A Patient with Complex I Deficiency Caused by a Novel ACAD9 Mutation Not Responding to Riboflavin Treatment. JIMD Rep 12, 37-45.

Nunnari, J., and Suomalainen, A. (2012). Mitochondria: in sickness and in health. Cell 148, 1145-1159.

Nussbaum, R.L., and Ellis, C.E. (2003). Alzheimer's disease and Parkinson's disease. N Engl J Med 348, 1356-1364.

O'Brien, L.C., Keeney, P.M., and Bennett, J.P. (2015). Differentiation of Human Neural Stem Cells into Motor Neurons Stimulates Mitochondrial Biogenesis and Decreases Glycolytic Flux. Stem Cells Dev 24, 1984-1994.

Ogasahara, S., Engel, A.G., Frens, D., and Mack, D. (1989). Muscle coenzyme Q deficiency in familial mitochondrial encephalomyopathy. Proc Natl Acad Sci U S A 86, 2379-2382.

Owen, O.E., Morgan, A.P., Kemp, H.G., Sullivan, J.M., Herrera, M.G., and Cahill, G.F. (1967). Brain metabolism during fasting. J Clin Invest 46, 1589-1595.

Parikh, S., Saneto, R., Falk, M.J., Anselm, I., Cohen, B.H., Haas, R., and Medicine Society, T.M. (2009). A modern approach to the treatment of mitochondrial disease. Curr Treat Options Neurol 11, 414-430.

Parker, W.D., Filley, C.M., and Parks, J.K. (1990). Cytochrome oxidase deficiency in Alzheimer's disease. Neurology 40, 1302-1303.

Parker, W.D., Parks, J.K., and Swerdlow, R.H. (2008). Complex I deficiency in Parkinson's disease frontal cortex. Brain Res 1189, 215-218.

Pathak, D., Shields, L.Y., Mendelsohn, B.A., Haddad, D., Lin, W., Gerencser, A.A., Kim, H., Brand, M.D., Edwards, R.H., and Nakamura, K. (2015). The role of mitochondrially derived ATP in synaptic vesicle recycling. J Biol Chem 290, 22325-22336.

Pereira, C., Santos, M.S., and Oliveira, C. (1998). Mitochondrial function impairment induced by amyloid beta-peptide on PC12 cells. Neuroreport 9, 1749-1755.

Pierce, S.B., Chisholm, K.M., Lynch, E.D., Lee, M.K., Walsh, T., Opitz, J.M., Li, W., Klevit, R.E., and King, M.C. (2011). Mutations in mitochondrial histidyl tRNA synthetase HARS2 cause ovarian dysgenesis and sensorineural hearing loss of Perrault syndrome. Proc Natl Acad Sci U S A 108, 6543-6548.

Pierce, S.B., Gersak, K., Michaelson-Cohen, R., Walsh, T., Lee, M.K., Malach, D., Klevit, R.E., King, M.C., and Levy-Lahad, E. (2013). Mutations in LARS2, encoding mitochondrial leucyl-tRNA synthetase, lead to premature ovarian failure and hearing loss in Perrault syndrome. Am J Hum Genet 92, 614-620.

Pirinen, E., Auranen, M., Khan, N.A., Brilhante, V., Urho, N., Pessia, A., Hakkarainen, A., Ulla Heinonen, J.K., Schmidt, M.S., Haimilahti, K.*, et al.* (2020). Niacin Cures Systemic NAD. Cell Metab 32, 144.

Poirier, G.L., Amin, E., Good, M.A., and Aggleton, J.P. (2011). Early-onset dysfunction of retrosplenial cortex precedes overt amyloid plaque formation in Tg2576 mice. Neuroscience 174, 71-83.

Polymeropoulos, M.H., Lavedan, C., Leroy, E., Ide, S.E., Dehejia, A., Dutra, A., Pike, B., Root, H., Rubenstein, J., Boyer, R.*, et al.* (1997). Mutation in the alpha-synuclein gene identified in families with Parkinson's disease. Science 276, 2045-2047.

Pouchieu, C., Piel, C., Carles, C., Gruber, A., Helmer, C., Tual, S., Marcotullio, E., Lebailly, P., and Baldi, I. (2018). Pesticide use in agriculture and Parkinson's disease in the AGRICAN cohort study. Int J Epidemiol 47, 299-310.

Préville, X., Salvemini, F., Giraud, S., Chaufour, S., Paul, C., Stepien, G., Ursini, M.V., and Arrigo, A.P. (1999). Mammalian small stress proteins protect against oxidative stress through their ability to increase glucose-6-phosphate dehydrogenase activity and by maintaining optimal cellular detoxifying machinery. Exp Cell Res 247, 61-78.

Quintana, A., Kruse, S.E., Kapur, R.P., Sanz, E., and Palmiter, R.D. (2010). Complex I deficiency due to loss of Ndufs4 in the brain results in progressive encephalopathy resembling Leigh syndrome. Proc Natl Acad Sci U S A 107, 10996-11001.

Quintana, A., Zanella, S., Koch, H., Kruse, S.E., Lee, D., Ramirez, J.M., and Palmiter, R.D. (2012). Fatal breathing dysfunction in a mouse model of Leigh syndrome. J Clin Invest 122, 2359-2368.

Quirós, P.M., Prado, M.A., Zamboni, N., D'Amico, D., Williams, R.W., Finley, D., Gygi, S.P., and Auwerx, J. (2017). Multi-omics analysis identifies ATF4 as a key regulator of the mitochondrial stress response in mammals. J Cell Biol 216, 2027-2045.

Rahman, S., Blok, R.B., Dahl, H.H., Danks, D.M., Kirby, D.M., Chow, C.W., Christodoulou, J., and Thorburn, D.R. (1996). Leigh syndrome: clinical features and biochemical and DNA abnormalities. Ann Neurol 39, 343-351.

Rangaraju, V., Lewis, T.L., Hirabayashi, Y., Bergami, M., Motori, E., Cartoni, R., Kwon, S.K., and Courchet, J. (2019). Pleiotropic Mitochondria: The Influence of Mitochondria on Neuronal Development and Disease. J Neurosci 39, 8200-8208.

Ransohoff, R.M. (2016). How neuroinflammation contributes to neurodegeneration. Science 353, 777-783.

Reichenbach, J., Schubert, R., Schindler, D., Müller, K., Böhles, H., and Zielen, S. (2002). Elevated oxidative stress in patients with ataxia telangiectasia. Antioxid Redox Signal 4, 465-469.

Reynaud-Dulaurier, R., Benegiamo, G., Marrocco, E., Al-Tannir, R., Surace, E.M., Auwerx, J., and Decressac, M. (2020). Gene replacement therapy provides benefit in an adult mouse model of Leigh syndrome. Brain 143, 1686-1696.

Riley, L.G., Cooper, S., Hickey, P., Rudinger-Thirion, J., McKenzie, M., Compton, A., Lim, S.C., Thorburn, D., Ryan, M.T., Giegé, R.*, et al.* (2010). Mutation of the mitochondrial tyrosyl-tRNA synthetase gene, YARS2, causes myopathy, lactic acidosis, and sideroblastic anemia--MLASA syndrome. Am J Hum Genet 87, 52-59.

Riley, L.G., Rudinger-Thirion, J., Schmitz-Abe, K., Thorburn, D.R., Davis, R.L., Teo, J., Arbuckle, S., Cooper, S.T., Campagna, D.R., Frugier, M.*, et al.* (2015). LARS2 Variants Associated with Hydrops, Lactic Acidosis, Sideroblastic Anemia, and Multisystem Failure. JIMD Rep.

Ross, J.M. (2011). Visualization of mitochondrial respiratory function using cytochrome c oxidase/succinate dehydrogenase (COX/SDH) double-labeling histochemistry. J Vis Exp, e3266.

Rumyantseva, A., Motori, E., and Trifunovic, A. (2020). DARS2 is indispensable for Purkinje cell survival and protects against cerebellar ataxia. Hum Mol Genet 29, 2845-2854.

Ruthel, G., and Hollenbeck, P.J. (2003). Response of mitochondrial traffic to axon determination and differential branch growth. J Neurosci 23, 8618-8624.

Sarna, J.R., Larouche, M., Marzban, H., Sillitoe, R.V., Rancourt, D.E., and Hawkes, R. (2003). Patterned Purkinje cell degeneration in mouse models of Niemann-Pick type C disease. J Comp Neurol 456, 279-291.

Schapira, A.H., Cooper, J.M., Dexter, D., Jenner, P., Clark, J.B., and Marsden, C.D. (1989). Mitochondrial complex I deficiency in Parkinson's disease. Lancet 1, 1269.

Scheper, G.C., van der Klok, T., van Andel, R.J., van Berkel, C.G., Sissler, M., Smet, J., Muravina, T.I., Serkov, S.V., Uziel, G., Bugiani, M.*, et al.* (2007). Mitochondrial aspartyl-tRNA synthetase deficiency causes leukoencephalopathy with brain stem and spinal cord involvement and lactate elevation. Nat Genet 39, 534-539.

Schimmel, P. (1987). Aminoacyl tRNA synthetases: general scheme of structure-function relationships in the polypeptides and recognition of transfer RNAs. Annu Rev Biochem 56, 125-158.

Schimmel, P. (2008). Development of tRNA synthetases and connection to genetic code and disease. Protein Sci 17, 1643-1652.

Schwartzentruber, J., Buhas, D., Majewski, J., Sasarman, F., Papillon-Cavanagh, S., Thiffault, I., Thiffaut, I., Sheldon, K.M., Massicotte, C., Patry, L.*, et al.* (2014). Mutation in the nuclear-encoded mitochondrial isoleucyl-tRNA synthetase IARS2 in patients with cataracts, growth hormone deficiency with short stature, partial sensorineural deafness, and peripheral neuropathy or with Leigh syndrome. Hum Mutat 35, 1285-1289.

Seager, R., Lee, L., Henley, J.M., and Wilkinson, K.A. (2020). Mechanisms and roles of mitochondrial localisation and dynamics in neuronal function. Neuronal Signal 4, NS20200008.

Seiferling, D., Szczepanowska, K., Becker, C., Senft, K., Hermans, S., Maiti, P., König, T., Kukat, A., and Trifunovic, A. (2016). Loss of CLPP alleviates mitochondrial cardiomyopathy without affecting the mammalian UPRmt. EMBO Rep 17, 953-964.

Sena, L.A., and Chandel, N.S. (2012). Physiological roles of mitochondrial reactive oxygen species. Mol Cell 48, 158-167.

Sherer, T.B., Betarbet, R., Testa, C.M., Seo, B.B., Richardson, J.R., Kim, J.H., Miller, G.W., Yagi, T., Matsuno-Yagi, A., and Greenamyre, J.T. (2003). Mechanism of toxicity in rotenone models of Parkinson's disease. J Neurosci 23, 10756-10764.

Shields, L.Y., Kim, H., Zhu, L., Haddad, D., Berthet, A., Pathak, D., Lam, M., Ponnusamy, R., Diaz-Ramirez, L.G., Gill, T.M.*, et al.* (2015). Dynamin-related protein 1 is required for normal mitochondrial bioenergetic and synaptic function in CA1 hippocampal neurons. Cell Death Dis 6, e1725.

Sibson, N.R., Dhankhar, A., Mason, G.F., Rothman, D.L., Behar, K.L., and Shulman, R.G. (1998). Stoichiometric coupling of brain glucose metabolism and glutamatergic neuronal activity. Proc Natl Acad Sci U S A 95, 316-321.

Silva, J.M., Wong, A., Carelli, V., and Cortopassi, G.A. (2009). Inhibition of mitochondrial function induces an integrated stress response in oligodendroglia. Neurobiol Dis 34, 357-365.

Silva-Pinheiro, P., Cerutti, R., Luna-Sanchez, M., Zeviani, M., and Viscomi, C. (2020). A Single Intravenous Injection of AAV-PHP.B-. Mol Ther Methods Clin Dev 17, 1071-1078.

Simon, M., Richard, E.M., Wang, X., Shahzad, M., Huang, V.H., Qaiser, T.A., Potluri, P., Mahl, S.E., Davila, A., Nazli, S.*, et al.* (2015). Mutations of human NARS2, encoding the mitochondrial asparaginyl-tRNA synthetase, cause nonsyndromic deafness and Leigh syndrome. PLoS Genet 11, e1005097.

Sissler, M., González-Serrano, L.E., and Westhof, E. (2017). Recent Advances in Mitochondrial Aminoacyl-tRNA Synthetases and Disease. Trends Mol Med 23, 693-708.

Smeyne, R.J., Breckenridge, C.B., Beck, M., Jiao, Y., Butt, M.T., Wolf, J.C., Zadory, D., Minnema, D.J., Sturgess, N.C., Travis, K.Z.*, et al.* (2016). Assessment of the Effects of MPTP and Paraquat on Dopaminergic Neurons and Microglia in the Substantia Nigra Pars Compacta of C57BL/6 Mice. PLoS One 11, e0164094.

Sofou, K., Kollberg, G., Holmström, M., Dávila, M., Darin, N., Gustafsson, C.M., Holme, E., Oldfors, A., Tulinius, M., and Asin-Cayuela, J. (2015). Whole exome sequencing reveals mutations in NARS2 and PARS2, encoding the mitochondrial asparaginyl-tRNA synthetase and prolyl-tRNA synthetase, in patients with Alpers syndrome. Mol Genet Genomic Med 3, 59-68.

Sorensen, L., Ekstrand, M., Silva, J.P., Lindqvist, E., Xu, B., Rustin, P., Olson, L., and Larsson, N.G. (2001). Late-onset corticohippocampal neurodepletion attributable to catastrophic failure of oxidative phosphorylation in MILON mice. J Neurosci 21, 8082-8090.

Spinelli, J.B., and Haigis, M.C. (2018). The multifaceted contributions of mitochondria to cellular metabolism. Nat Cell Biol 20, 745-754.

Steenweg, M.E., Ghezzi, D., Haack, T., Abbink, T.E., Martinelli, D., van Berkel, C.G., Bley, A., Diogo, L., Grillo, E., Te Water Naudé, J.*, et al.* (2012). Leukoencephalopathy with thalamus and brainstem involvement and high lactate 'LTBL' caused by EARS2 mutations. Brain 135, 1387-1394.

Steriade, C., Andrade, D.M., Faghfoury, H., Tarnopolsky, M.A., and Tai, P. (2014). Mitochondrial encephalopathy with lactic acidosis and stroke-like episodes (MELAS) may respond to adjunctive ketogenic diet. Pediatr Neurol 50, 498-502.

Supnet, C., and Bezprozvanny, I. (2010). Neuronal calcium signaling, mitochondrial dysfunction, and Alzheimer's disease. J Alzheimers Dis 20 Suppl 2, S487-498.

Swanson, R.A., Morton, M.M., Sagar, S.M., and Sharp, F.R. (1992). Sensory stimulation induces local cerebral glycogenolysis: demonstration by autoradiography. Neuroscience 51, 451-461.

Szczepanowska, K., Maiti, P., Kukat, A., Hofsetz, E., Nolte, H., Senft, K., Becker, C., Ruzzenente, B., Hornig-Do, H.T., Wibom, R.*, et al.* (2016). CLPP coordinates mitoribosomal assembly through the regulation of ERAL1 levels. EMBO J 35, 2566-2583.

Szczepanowska, K., Senft, K., Heidler, J., Herholz, M., Kukat, A., Höhne, M.N., Hofsetz, E., Becker, C., Kaspar, S., Giese, H.*, et al.* (2020). A salvage pathway maintains highly functional respiratory complex I. Nat Commun 11, 1643.

Taivassalo, T., Gardner, J.L., Taylor, R.W., Schaefer, A.M., Newman, J., Barron, M.J., Haller, R.G., and Turnbull, D.M. (2006). Endurance training and detraining in mitochondrial myopathies due to single large-scale mtDNA deletions. Brain 129, 3391-3401.

Taivassalo, T., Shoubridge, E.A., Chen, J., Kennaway, N.G., DiMauro, S., Arnold, D.L., and Haller, R.G. (2001). Aerobic conditioning in patients with mitochondrial myopathies: physiological, biochemical, and genetic effects. Ann Neurol 50, 133-141.

TERRY, R.D., GONATAS, N.K., and WEISS, M. (1964). ULTRASTRUCTURAL STUDIES IN ALZHEIMER'S PRESENILE DEMENTIA. Am J Pathol 44, 269-297.

Theisen, B.E., Rumyantseva, A., Cohen, J.S., Alcaraz, W.A., Shinde, D.N., Tang, S., Srivastava, S., Pevsner, J., Trifunovic, A., and Fatemi, A. (2017). Deficiency of WARS2, encoding mitochondrial tryptophanyl tRNA synthetase, causes severe infantile onset leukoencephalopathy. Am J Med Genet A 173, 2505-2510.

Timmann, D., Dimitrova, A., Hein-Kropp, C., Wilhelm, H., and Dörfler, A. (2003). Cerebellar agenesis: clinical, neuropsychological and MR findings. Neurocase 9, 402-413.

Tolar, M., Keller, J.N., Chan, S., Mattson, M.P., Marques, M.A., and Crutcher, K.A. (1999). Truncated apolipoprotein E (ApoE) causes increased intracellular calcium and may mediate ApoE neurotoxicity. J Neurosci 19, 7100-7110.

Tyynismaa, H., Carroll, C.J., Raimundo, N., Ahola-Erkkilä, S., Wenz, T., Ruhanen, H., Guse, K., Hemminki, A., Peltola-Mjøsund, K.E., Tulkki, V.*, et al.*

(2010). Mitochondrial myopathy induces a starvation-like response. Hum Mol Genet 19, 3948-3958.

Uddin, M., Wildman, D.E., Liu, G., Xu, W., Johnson, R.M., Hof, P.R., Kapatos, G., Grossman, L.I., and Goodman, M. (2004). Sister grouping of chimpanzees and humans as revealed by genome-wide phylogenetic analysis of brain gene expression profiles. Proc Natl Acad Sci U S A 101, 2957-2962.

Vaccaro, V., Devine, M.J., Higgs, N.F., and Kittler, J.T. (2017). Miro1-dependent mitochondrial positioning drives the rescaling of presynaptic Ca2+ signals during homeostatic plasticity. EMBO Rep 18, 231-240.

Valente, E.M., Abou-Sleiman, P.M., Caputo, V., Muqit, M.M., Harvey, K., Gispert, S., Ali, Z., Del Turco, D., Bentivoglio, A.R., Healy, D.G.*, et al.* (2004). Hereditary early-onset Parkinson's disease caused by mutations in PINK1. Science 304, 1158-1160.

van Berge, L., Dooves, S., van Berkel, C.G., Polder, E., van der Knaap, M.S., and Scheper, G.C. (2012). Leukoencephalopathy with brain stem and spinal cord involvement and lactate elevation is associated with cell-type-dependent splicing of mtAspRS mRNA. Biochem J 441, 955-962.

van Berge, L., Hamilton, E.M., Linnankivi, T., Uziel, G., Steenweg, M.E., Isohanni, P., Wolf, N.I., Krägeloh-Mann, I., Brautaset, N.J., Andrews, P.I.*, et al.* (2014). Leukoencephalopathy with brainstem and spinal cord involvement and lactate elevation: clinical and genetic characterization and target for therapy. Brain 137, 1019-1029.

van Berge, L., Kevenaar, J., Polder, E., Gaudry, A., Florentz, C., Sissler, M., van der Knaap, M.S., and Scheper, G.C. (2013). Pathogenic mutations causing LBSL affect mitochondrial aspartyl-tRNA synthetase in diverse ways. Biochem J 450, 345-350.

van Groen, T., and Wyss, J.M. (1990). Connections of the retrosplenial granular a cortex in the rat. J Comp Neurol 300, 593-606.

van Groen, T., and Wyss, J.M. (1992). Connections of the retrosplenial dysgranular cortex in the rat. J Comp Neurol 315, 200-216.

Van Maele-Fabry, G., Hoet, P., Vilain, F., and Lison, D. (2012). Occupational exposure to pesticides and Parkinson's disease: a systematic review and meta-analysis of cohort studies. Environ Int 46, 30-43.

Vanlander, A.V., Menten, B., Smet, J., De Meirleir, L., Sante, T., De Paepe, B., Seneca, S., Pearce, S.F., Powell, C.A., Vergult, S.*, et al.* (2015). Two siblings

with homozygous pathogenic splice-site variant in mitochondrial asparaginyl-tRNA synthetase (NARS2). Hum Mutat 36, 222-231.

Verhage, M., Maia, A.S., Plomp, J.J., Brussaard, A.B., Heeroma, J.H., Vermeer, H., Toonen, R.F., Hammer, R.E., van den Berg, T.K., Missler, M.*, et al.* (2000). Synaptic assembly of the brain in the absence of neurotransmitter secretion. Science 287, 864-869.

Vilalta, A., and Brown, G.C. (2018). Neurophagy, the phagocytosis of live neurons and synapses by glia, contributes to brain development and disease. FEBS J 285, 3566-3575.

Vilchez, D., Ros, S., Cifuentes, D., Pujadas, L., Vallès, J., García-Fojeda, B., Criado-García, O., Fernández-Sánchez, E., Medraño-Fernández, I., Domínguez, J.*, et al.* (2007). Mechanism suppressing glycogen synthesis in neurons and its demise in progressive myoclonus epilepsy. Nat Neurosci 10, 1407-1413.

Viscomi, C., Bottani, E., and Zeviani, M. (2015). Emerging concepts in the therapy of mitochondrial disease. Biochim Biophys Acta 1847, 544-557.

Waagepetersen, H.S., Sonnewald, U., Gegelashvili, G., Larsson, O.M., and Schousboe, A. (2001). Metabolic distinction between vesicular and cytosolic GABA in cultured GABAergic neurons using 13C magnetic resonance spectroscopy. J Neurosci Res 63, 347-355.

Wallace, D.C., Singh, G., Lott, M.T., Hodge, J.A., Schurr, T.G., Lezza, A.M., Elsas, L.J., and Nikoskelainen, E.K. (1988). Mitochondrial DNA mutation associated with Leber's hereditary optic neuropathy. Science 242, 1427-1430.

Webb, B.D., Wheeler, P.G., Hagen, J.J., Cohen, N., Linderman, M.D., Diaz, G.A., Naidich, T.P., Rodenburg, R.J., Houten, S.M., and Schadt, E.E. (2015). Novel, compound heterozygous, single-nucleotide variants in MARS2 associated with developmental delay, poor growth, and sensorineural hearing loss. Hum Mutat 36, 587-592.

Weissig, V. (2020). Drug Development for the Therapy of Mitochondrial Diseases. Trends Mol Med 26, 40-57.

Wijburg, F.A., Barth, P.G., Bindoff, L.A., Birch-Machin, M.A., van der Blij, J.F., Ruitenbeek, W., Turnbull, D.M., and Schutgens, R.B. (1992). Leigh syndrome associated with a deficiency of the pyruvate dehydrogenase complex: results of treatment with a ketogenic diet. Neuropediatrics 23, 147-152.

Yamashita, S., Miyake, N., Matsumoto, N., Osaka, H., Iai, M., Aida, N., and Tanaka, Y. (2013). Neuropathology of leukoencephalopathy with brainstem and

spinal cord involvement and high lactate caused by a homozygous mutation of DARS2. Brain Dev 35, 312-316.

Yan, L.J., Christians, E.S., Liu, L., Xiao, X., Sohal, R.S., and Benjamin, I.J. (2002). Mouse heat shock transcription factor 1 deficiency alters cardiac redox homeostasis and increases mitochondrial oxidative damage. EMBO J 21, 5164-5172.

Yang, Y., Liu, W., Fang, Z., Shi, J., Che, F., He, C., Yao, L., Wang, E., and Wu, Y. (2016). A Newly Identified Missense Mutation in FARS2 Causes Autosomal-Recessive Spastic Paraplegia. Hum Mutat 37, 165-169.

Yao, P., and Fox, P.L. (2013). Aminoacyl-tRNA synthetases in medicine and disease. EMBO Mol Med 5, 332-343.

Yu, H., Porciatti, V., Lewin, A., Hauswirth, W., and Guy, J. (2018). Longterm Reversal of Severe Visual Loss by Mitochondrial Gene Transfer in a Mouse Model of Leber Hereditary Optic Neuropathy. Sci Rep 8, 5587.

Yu-Wai-Man, P., Turnbull, D.M., and Chinnery, P.F. (2002). Leber hereditary optic neuropathy. J Med Genet 39, 162-169.

Yubero, D., Montero, R., Santos-Ocaña, C., Salviati, L., Navas, P., and Artuch, R. (2018). Molecular diagnosis of coenzyme Q. Expert Rev Mol Diagn 18, 491-498.

Zhang, J., Liu, H., Luo, S., Lu, Z., Chávez-Badiola, A., Liu, Z., Yang, M., Merhi, Z., Silber, S.J., Munné, S.*, et al.* (2017). Live birth derived from oocyte spindle transfer to prevent mitochondrial disease. Reprod Biomed Online 34, 361-368.

Zheng, X., Boyer, L., Jin, M., Mertens, J., Kim, Y., Ma, L., Hamm, M., Gage, F.H., and Hunter, T. (2016). Metabolic reprogramming during neuronal differentiation from aerobic glycolysis to neuronal oxidative phosphorylation. Elife 5.

Acknowledgements

I am immensely grateful to **Prof. Dr. Aleksandra Trifunovic**. I joined your lab 5.5 years ago, as a master student and could not imagine that one day the small cell culture project I was given, would develop into a doctoral dissertation and a first author publication. Thank you for all opportunities I received. For the high level of independence, I have enjoyed it so much. For your mentorship, broad scientific knowledge and active contributions to my research. For your trust you have put in me and this project, especially in times, when I saw it to be a dead end. For your ability to listen. For all social gatherings in our lab that gave me a sense of belonging. For remaining a pillar of stability and common sense in 2020. But above all, thank you for letting me grow and evolve as a scientist.

Thank you, **Dr. David Vilchez** and **Prof. Dr. Guenter Schwarz**, for your time and being in my defence committee.

Also, I want to thank **Prof. Dr. Elena Rugarli** and **Prof. Dr. Natalia Kononenko**, who were my thesis advisors and were always keen to help me with advice, ideas and opinions.

I gratefully acknowledge **Dr. Elisa Motori** for being an excellent mentor. I found in you utmost scientific enthusiasm, willingness to help and to share with me your knowledge and expertise.

Additionally, I want to express my immense gratitude to **Dr. Katerina Vlantis**, scientific manager of CRC 1218 for professional and personal advice, and always being there for me when I had questions.

During these 5.5 years I came to know numerous members of Trifunovic lab. Huge thanks to all of you: former and current members. You made my experience unforgettable and amazing. All chats, getting-togethers, retreats, lunches, Christmas parties, coffees and cakes I shall keep in

memory. Special thanks to **Dr. Sarah Maciej** and **Milica Popovic**, the lab days would not have been the same without you. Additionally, thank you Milica, for your invaluable help with BN-PAGE.

Dr. Alexandra Kukat, our lab manager, thank you very much, for all the help with mouse experiments approvals and announcements. My project involved mostly animal experiments, and all the work you have put in writing, rewriting and answering LANUV questions was indispensable. Also, thank you very much for your scientific input and readiness to help in everyday lab-life.

Dr. Marija Herholz and **Dr. Karolina Szczepanowska**, thank you lots for your commitment to science and research, all advice, troubleshooting, clear and frank opinions, for creating the atmosphere for fruitful scientific exchange and discussions in the lab.

I would like to thank our excellent lab assistants **Katharina Senft** and **Linda Baumann** for ensuring lab running, taking care of numerous orders, and equipment.

My odyssey to PhD title is a defining, refulgent and remarkable time of my life. In ups and downs, in torturing moments of impostor syndrome, failures and self-doubt, I found strength and inspiration in people, whose support (sometimes unnoticed for them) was guiding, motivating, and empowering.

В моменты взлетов и падений, сомнения в собственных силах и изнуряющей полосе неудач, я черпала вдхновение в людях, чья поддержка (иногда незаметная для них самих) направляла, мотивировала и придавала мне сил.

JL, thank you very much for the best Spotify playlist, for the jokes and chilling vibes, for the voice that accompanied me during the most intense, isolating, inclement days. Eight hours of tissue cutting sessions would have been much less endurable without you.

Matthijs, thank you very much for the companionship, for all the help and advice stretching beyond just experiments. For coffee, chocolate, wine and cheese we have shared. For being there to listen to my complaints. And especially, for all experiments we have done together that made me cherish and see benefits of teamwork.

Toni, thank you very much for rekindling my passion for science. All the time I have struggled to find the most logical arguments to prove to you that this research, *my* research is worthy of EU taxpayers' money, reminded me how much I enjoy discussing, enjoy building logical arguments and enjoy finding fallacies. Thank you very much for staying with me in Germany during the most difficult for me weeks of the year. The final phase of writing of this dissertation would not have been the same without you being here with me. All inspiration and motivation you gave me, were precisely what I needed the most.

Simon, you have been my best friend 8 out of 9 years I have been living in Germany. You, like no one else, know all my struggles, the hardship, my constant inner conflict, and all sacrifices I have made. I was so totally not prepared in 2016 when I started my PhD, but you have always been there for me. I guess only you know what this dissertation and title mean to me. I have reached the finish line of this marathon, thanks to you. And I will not ever forget that.

Мама и папа, все мои достижения, включая эту диссертацию, стали возможными, только благодаря вам. Спасибо вам за то, что никогда не ограничивали мою свободу, позволяя мне самой принимать решения. Спасибо за то, что так много вложили в мое образование. Спасибо за то, что во всем поддерживали меня. Спасибо за то, что вы гордитесь мной. Спасибо за то, что вдохновляли и говорили мне, что возможно все, нужно просто больше стараться. Спасибо вам за то, что научили меня так многому.

Время – моменты и события, которыми мы так охотно пытаемся его измерять. [….] в любом моменте, в любом мгновении, в любом событии содержатся прошлое, настоящее и будущее. В любом мгновении сокрыта вечность. […] Все одновременно суть и начало, и конец.

Анджей Сапковский, Владычица озера

Erklärung

Hiermit versichere ich an Eides statt, dass ich die vorliegende Dissertation selbstständig und ohne die Benutzung anderer als der angegebenen Hilfsmittel und Literatur angefertigt habe. Alle Stellen, die wörtlich oder sinngemäß aus veröffentlichten und nicht veröffentlichten Werken dem Wortlaut oder dem Sinn nach entnommen wurden, sind als solche kenntlich gemacht. Ich versichere an Eides statt, dass diese Dissertation noch keiner anderen Fakultät oder Universität zur Prüfung vorgelegen hat; dass sie - abgesehen von unten angegebenen Teilpublikationen und eingebundenen Artikeln und Manuskripten - noch nicht veröffentlicht worden ist sowie, dass ich eine Veröffentlichung der Dissertation vor Abschluss der Promotion nicht ohne Genehmigung des Promotionsausschusses vornehmen werde. Die Bestimmungen dieser Ordnung sind mir bekannt. Darüber hinaus erkläre ich hiermit, dass ich die Ordnung zur Sicherung guter wissenschaftlicher Praxis und zum Umgang mit wissenschaftlichem Fehlverhalten der Universität zu Köln gelesen und sie bei der Durchführung der Dissertation zugrundeliegenden Arbeiten und der schriftlich verfassten Dissertation beachtet habe und verpflichte mich hiermit, die dort genannten Vorgaben bei allen wissenschaftlichen Tätigkeiten zu beachten und umzusetzen. Ich versichere, dass die eingereichte elektronische Fassung der eingereichten Druckfassung vollständig entspricht.

Teilpublikationen:

Anastasia Rumyantseva, Elisa Motori, Aleksandra Trifunovic, DARS2 is indispensable for Purkinje cell survival and protects against cerebellar ataxia, *Human Molecular Genetics*, Volume 29, Issue 17, 1 September 2020, Pages2845-2854, https://doi.org/10.1093/hmg/ddaa176

Anastasia Rumyantseva

Curriculum vitae

Anastasia Rumyantseva, M.Sc

Personal data

Date of birth:	15.12.1989
Place of birth:	Leningrad (curr. St.Petersburg), USSR (curr. Russia)
Address:	Mühlenstr.30, 53879, Euskirchen
Email:	anastasia.rumyantseva@uk-koeln.de
Nationality:	Russian

Education

12/2016-02/2021	**PhD Candidate** at Prof. Aleksandra Trifunovic lab, University of Cologne
10/2014-10/2016	**Master of Science** in Biological Sciences, University of Cologne
09/2011-09/2014	**Bachelor of Science** in Applied biology, Bonn-Rhein-Sieg University of Applied Sciences, Rheinbach
09/2007-06/2011	**Bachelor of Science** in Ecology and Nature Management (with distinction), Russian State Hydrometeorological University, St.Petersburg
06/2007	**University entrance qualification** (with distinction), State secondary school Nr.26 in Nevskii district of St. Petersburg

Publications

Rumyantseva A, Motori E, Trifunovic A, DARS2 is indispensable for Purkinje cell survival and protects against cerebellar ataxia, Hum Mol Genet., Volume 29, Issue 17, 1 September 2020, Pages 2845–2854,

Szczepanowska K, Senft K, Heidler J, Herholz M, Kukat A, Höhne MN, Hofsetz E, Becker C, Kaspar S, Giese H, Zwicker K, Guerrero-Castillo S, Baumann L, Kauppila J**, Rumyantseva A,** Müller S, Frese CK, Brandt U, Riemer J, Wittig I, Trifunovic A. A salvage pathway maintains highly functional respiratory complex I. Nat Commun. 2020 Apr 2;11(1):1643.

Theisen BE, **Rumyantseva A**, Cohen JS, Alcaraz WA, Shinde DN, Tang S, Srivastava S, Pevsner J, Trifunovic A, Fatemi Al. Deficiency of WARS2, encoding mitochondrial tryptophanyl tRNA synthetase, causes severe infantile onset leukoencephalopathy. Am J Med Genet Part A.2017;173A:2505–2510.

Orfanos Z, Gödderz MP, Soroka E, Gödderz T, **Rumyantseva A**, van der Ven PF, Hawke TJ, Fürst DO. Breaking sarcomers by in vitro exercise. Sci Rep. 2016 Jan 25;6:19614

Conference attendance

EMBO workshop Molecular Biology of mitochondrial gene expression 20-24 May 2018 Svartsjö, Sweden

Euromit 2017, 11-15 June, 2017 Cologne, Germany

Anastasia Rumyantseva

Human Molecular Genetics, 2020, Vol. 29, No. 17 2845–2854

doi: 10.1093/hmg/ddaa176
Advance Access Publication Date: 7 August 2020
General Article

GENERAL ARTICLE

DARS2 is indispensable for Purkinje cell survival and protects against cerebellar ataxia

Anastasia Rumyantseva[1,†], Elisa Motori[2] and Aleksandra Trifunovic[1,*,‡]

[1]Institute for Mitochondrial Diseases and Aging, Medical Faculty, Cologne Excellence Cluster on Cellular Stress Responses in Aging-Associated Diseases (CECAD) and Centre for Molecular Medicine (CMMC), University of Cologne, Cologne D-50931 , Germany and [2]Department of Mitochondrial Biology, Max Planck Institute for Biology of Ageing, Cologne D-50931, Germany

*To whom correspondence should be addressed at: CECAD Research Center, University of Cologne, Joseph-Stelzmann-Str. 26, Cologne 50931, Germany. Tel: +49 22147884291; Fax: +49 22147884261; Email: aleksandra.trifunovic@uk-koeln.de

Abstract

Leukoencephalopathy with brain stem and spinal cord involvement and lactate elevation disorder (LBSL) arises from mutations in mitochondrial aspartyl-tRNA synthetase (DARS2) gene. The disease has a childhood or juvenile-onset and is clinically characterized by cerebellar ataxia, cognitive decline and distinct morphological abnormalities upon magnetic resonance imaging. We previously demonstrated that neurons and not adult myelin-producing cells are specifically sensitive to DARS2 loss, hence likely the primary culprit in LBSL disorder. We used conditional Purkinje cell (PCs)-specific *Dars2* deletion to elucidate further the cell-type-specific contribution of this class of neurons to the cerebellar impairment observed in LBSL. We show that DARS2 depletion causes a severe mitochondrial dysfunction concomitant with a massive loss of PCs by the age of 15 weeks, thereby rapidly deteriorating motor skills. Our findings conclusively show that DARS2 is indispensable for PC survival and highlights the central role of neuroinflammation in DARS2-related PC degeneration.

Introduction

Mitochondrial dysfunction plays a critical role in neurodegeneration, likely due to the central nervous system's high-energy demand and its reliance on oxidative metabolism for adenosine triphosphate (ATP) production. Neurological syndromes are indeed the most frequent clinical presentation of mitochondrial diseases, a large group of genetically heterogeneous disorders caused by primary defects in mitochondrial oxidative phosphorylation (1). Autosomal recessive leukoencephalopathy with brainstem and spinal cord involvement and lactacidosis syndrome (LBSL, Online Mendelian Inheritance in Man® (OMIM) #611105) is a recently described mitochondrial disorder. It is caused by mutations in the *DARS2* gene, which encodes for the mitochondrial aspartyl-tRNA synthetase.

Mitochondrial aminoacyl-tRNA synthetases (Mt-aaRS2) are crucial components of mitochondrial protein synthesis, as they catalyze the attachment of an amino acid to its cognate tRNA at the first step of mitochondrial translation (2). To date, pathological mutations in each of the 19 mt-aaRS genes have been reported (3). Although mt-aaRSs pathological phenotypes are variable and might affect different organ systems, mitochondrial aspartyl-tRNA synthetase gene (*DARS2*) seems to be an exception. All reported *DARS2* patients, following the first described case, were diagnosed with LBSL (4,5). A distinctive magnetic resonance imaging pattern shows differences from the other defined leukoencephalopathies, thus giving a diagnostic tool for the disease (6). LBSL is a childhood or juvenile-onset disorder clinically characterized by cerebellar ataxia and spasticity (6).

[†]Anastasia Rumyantseva, http://orcid.org/0000-0002-7847-6178
[‡]Aleksandra Trifunovic, http://orcid.org/0000-0002-5472-3517
Received: June 14, 2020. **Revised:** July 25, 2020. **Accepted:** July 27, 2020

Deterioration of motor skills usually starts in childhood or adolescence, including dysarthria that develops over time. Occasional findings include epilepsy, learning problems, cognitive decline and neurologic deterioration (6).

Owning to the fact that LBSL is associated foremost with white matter abnormalities, we have previously generated and characterized oligodendrocyte-specific *Dars2* knockout (*Dars2*^{MYKO}—*Dars2*$^{fl/fl;}$ *Plp-CreERT*) mice (7). Remarkably, despite displaying a strong mitochondrial dysfunction, those mice neither showed demyelination, nor secondary neurodegeneration and neuroinflammation (7). In contrast, DARS2 specific depletion in forebrain cortical, hippocampal and striatal neurons, driven by *CamKIIα-Cre* (*Dars2*^{NEKO}—*Dars2*$^{fl/fl;}$ *CaMKIIα-Cre*), led to marked cerebral atrophy within 25 weeks, arising from dramatic neuronal death and accompanied by severe neuroinflammation (7). In line with this, a different study using the same model reported cell-stress response signaling, activation of inflammatory pathways, and concurrent cerebral atrophy (8). These studies suggest that neurons and not adult myelin-producing cells are the primary culprit in LBSL disorder.

Intriguingly, cerebellar ataxia is a primary clinical manifestation of LBSL syndrome, and loss of Purkinje cells (PCs) has been reported in patients, highlighting a potential role of DARS2 for PCs function and survival (9). However, very little is known about the specific PC contribution to LBSL phenotypes upon DARS2 loss.

Here, we explored the consequences of DARS2 depletion, specifically in PC. We show that loss of DARS2 results in severe mitochondrial dysfunction culminating in the massive PC loss accompanied by the upregulation of one-carbon metabolism, neuroinflammation and rapidly deteriorating motor skills.

Results and Discussion

To understand the role of DARS2 in the cerebellum, and unravel possible causes of cerebellar ataxia in LBSL patients, we generated a PC specific knockout mouse model (*Dars2_KO*^{PC}) by breeding *Dars2*$^{loxP/loxP}$ mice to mice expressing *Cre* recombinase under the PC protein 2 promoter (*L7-Cre*), resulting in *Dars2*$^{fl/fl}$*; L7-cre* mice (referred to as *Dars2_KO*^{PC} mice) (Fig. 1A). Using this strategy, we were able to observe changes in already developed Purkinje neurons as the *cre*-mediated recombination under control of L7 promoter starts at postnatal Day 5–7, and is fully active between 2–3 weeks of age (10).

As expected, *Dars2_KO*^{PC} animals were born at Mendelian ratio, and mice of both sexes were viable and indistinguishable from wild-type (WT) littermates. An evident motor impairment was observed at around 15 weeks in *Dars2_KO*^{PC} mice. Mutant animals lived up to 25 weeks of age, at which time they had to be sacrificed due to the severity of the observed phenotype. To enable unveiling of dynamic changes imposed by DARS2 deficiency in PCs, we thus set a time-course analysis of PC morphology starting from 6 weeks, at which mice showed no overt phenotype and up to 15 weeks, at which mice exhibited a motor phenotype.

Analysis of the PC layer by hematoxylin–eosin (H&E) staining in *Dars2_KO*^{PC} mice disclosed no overt changes at 6 and 8 weeks of age (Fig. 1B). In contrast, we observed a significant loss of Purkinje neurons, which resulted in the disruption of the PC layer in *Dars2_KO*^{PC} mice at 15 weeks (Fig. 1B). The brain mass and the bodyweight of *Dars2_KO*^{PC} mice were not affected at any of the analyzed time-points (Figs 1C and D). Importantly, despite the visible loss of Purkinje neurons in *Dars2_KO*^{PC} mice at 15 weeks of age, the cerebellar size was not different, indicating that DARS2 deficiency in PCs did not affect cerebellar growth or induced massive degeneration (Fig. 1E). This is in sharp contrast to mice with DARS2 loss of forebrain and hippocampal neurons, which showed a robust decrease in brain mass and body weight, preceding the strong overall phenotypes (7).

Massive PC loss leads to motor skills deterioration

To analyze cytoarchitecture of cerebella, we performed immunofluorescent staining on midsagittal cerebellar sections against the PC specific marker Calbindin, which is expressed abundantly in the PC somata and dendrites (Fig. 2A). In agreement with the previous data on general morphology, neither PC loss, nor structural changes in the PC layer and their dendritic network were present in *Dars2_KO*^{PC} mice at 8 weeks of age (Fig. 2A and C). Strikingly, *Dars2_KO*^{PC} mice displayed a 50% decrease in PC numbers at 15 weeks of age, indicating that disrupted mitochondrial protein synthesis and ample oxidative phosphorylation (OXPHOS) dysfunction, caused by the loss of DARS2 ultimately led to a massive loss of Purkinje neurons. Moreover, the remaining PC in 15 weeks old *Dars2_KO*^{PC} mice displayed a highly fragmented and disorganized dendritic network, suggesting impaired cerebellar connectivity (Fig. 2B). The most prominent PC loss was observed in the anterior (lobules I–V) and central zone (lobules VI–VII), whereas lobules IX and X had more Purkinje neurons preserved (Supplementary Material, Fig. S1).

Predictably, this dramatic loss of PC led to motor skill impairment, as evidenced by the altered performances on the ledge test, hind limb clasping, gait analysis and the occurrence of kyphosis (11). At 15 weeks of age, *Dars2_KO*^{PC} mice showed unsteady gait and were unable to keep their balance when walking on the ledge, receiving significantly higher scores than the control mice at this age (Fig. 2C). However, the 15-week-old *Dars2_KO*^{PC} mice did not show any difference in the hindlimb clasping, signifying a higher severity of motor dysfunction (Fig. 2C). Similarly, we observed kyphosis only in some animals of this age (Fig. 2C). In agreement with previous studies showing that despite progressively escalating ataxia, cerebellar defects alone do not cause premature death (Timmannn *et al.*, 2003; Quintana *et al.* 2010), *Dars2_KO*^{PC} mice live to post 15 weeks, albeit with severely deteriorated motor skills, confirmed by significantly higher phenotype scores at 22 weeks of age (Fig. 2D). Together these results demonstrate that DARS2 deficiency leads to PC loss after 8 weeks of age, leading to substantial impairment of motor skills in *Dars2_KO*^{PC} mice.

Strong respiratory chain dysfunction coincides with massive PC loss in *Dars2_KO*^{PC} mice

Loss of DARS2 affects mitochondrial protein synthesis, leading to impaired respiratory chain (RC) function (Dogan *et al.*, 2014). To assess the RC function, we used cytochrome c oxidase/succinate dehydrogenase (COX/SDH) staining, a histochemical technique that allows sequential analysis of enzymatic activities of Complex IV (COX) and Complex II (SDH), *in situ*. Although COX activity is highly dependent on the mitochondrial gene expression as its core subunits are encoded by mtDNA, SDH is entirely encoded by nuclear DNA, and its activity is typically unaltered, or even upregulated, by impaired mitochondrial gene expression (12). As expected, PCs in control mice displayed saturated brown staining at chosen time points, indicating functioning COX (Fig. 3A). In contrast, the presence of individual blue-stained PCs indicating sharply diminished COX activity, and increased SDH activity in individual cells already in 6 weeks old *Dars2_KO*^{PC} mice (Fig. 3A).

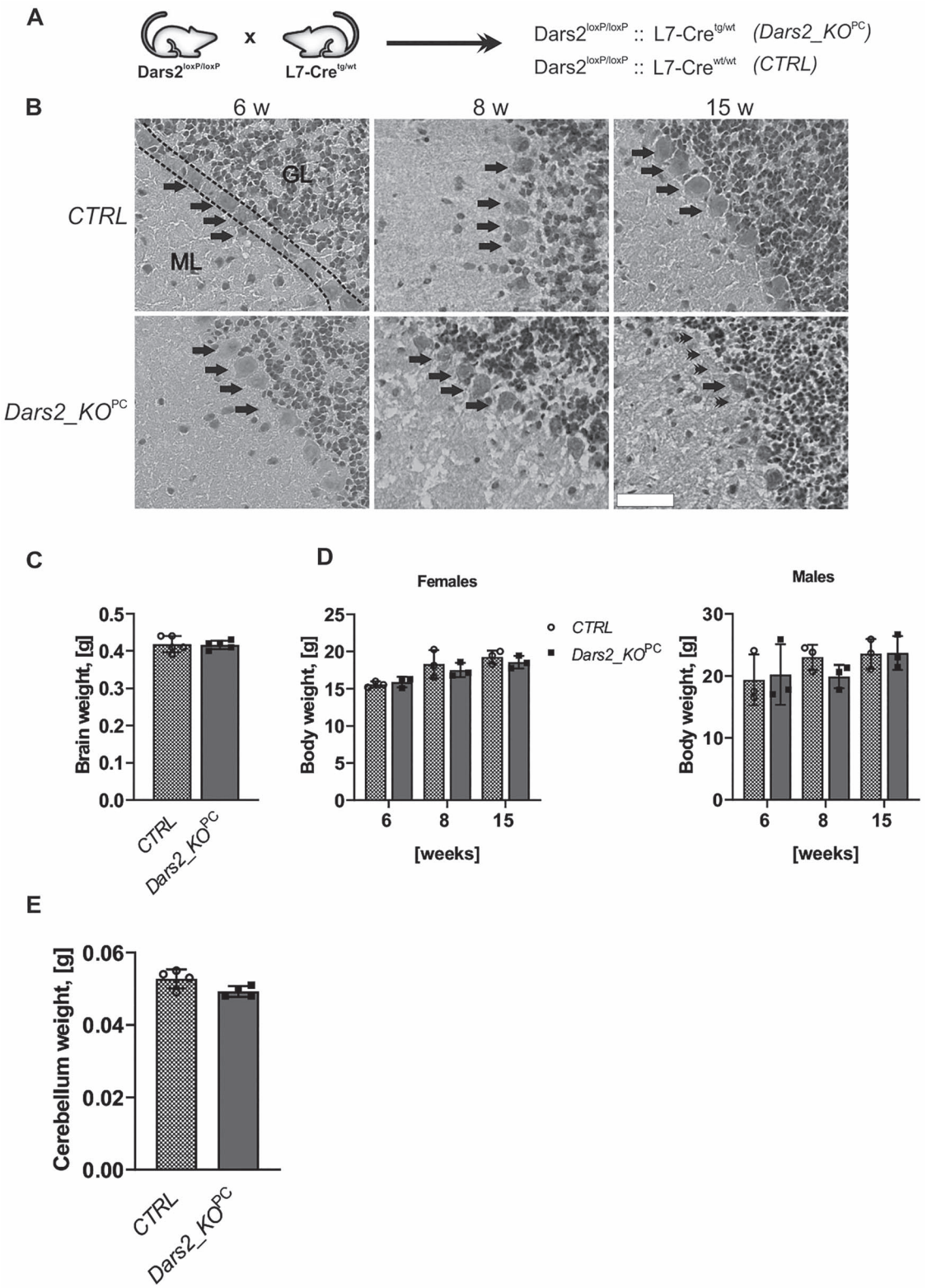

Figure 1. Generation of PC-specific Dars2 knock out mice (*Dars2_KO*^{PC}). (**A**) Breeding scheme to generate *Dars2_KO*^{PC}. (**B**) Representative images of H&E staining at the indicated time points, arrowheads indicate PC; GL: granular cell layer; ML: molecular cell layer; scale bar = 100 µm. (**C**) Brain weight of *CTRL* and *Dars2_KO*^{PC} at 15 weeks of age data presented as mean ± standard deviation (SD). (**D**) Bodyweight gain from 6- to 15-week-old female and male mice CTRL vs. *Dars2_KO*^{PC} data presented as mean ± SD ($n = 3$–5 mice per genotype per time point). (**E**) Cerebellum weight in CTRL vs. *Dars2_KO*^{PC} at 15 weeks of age data presented as mean ± SD ($n = 4$ mice per genotype).

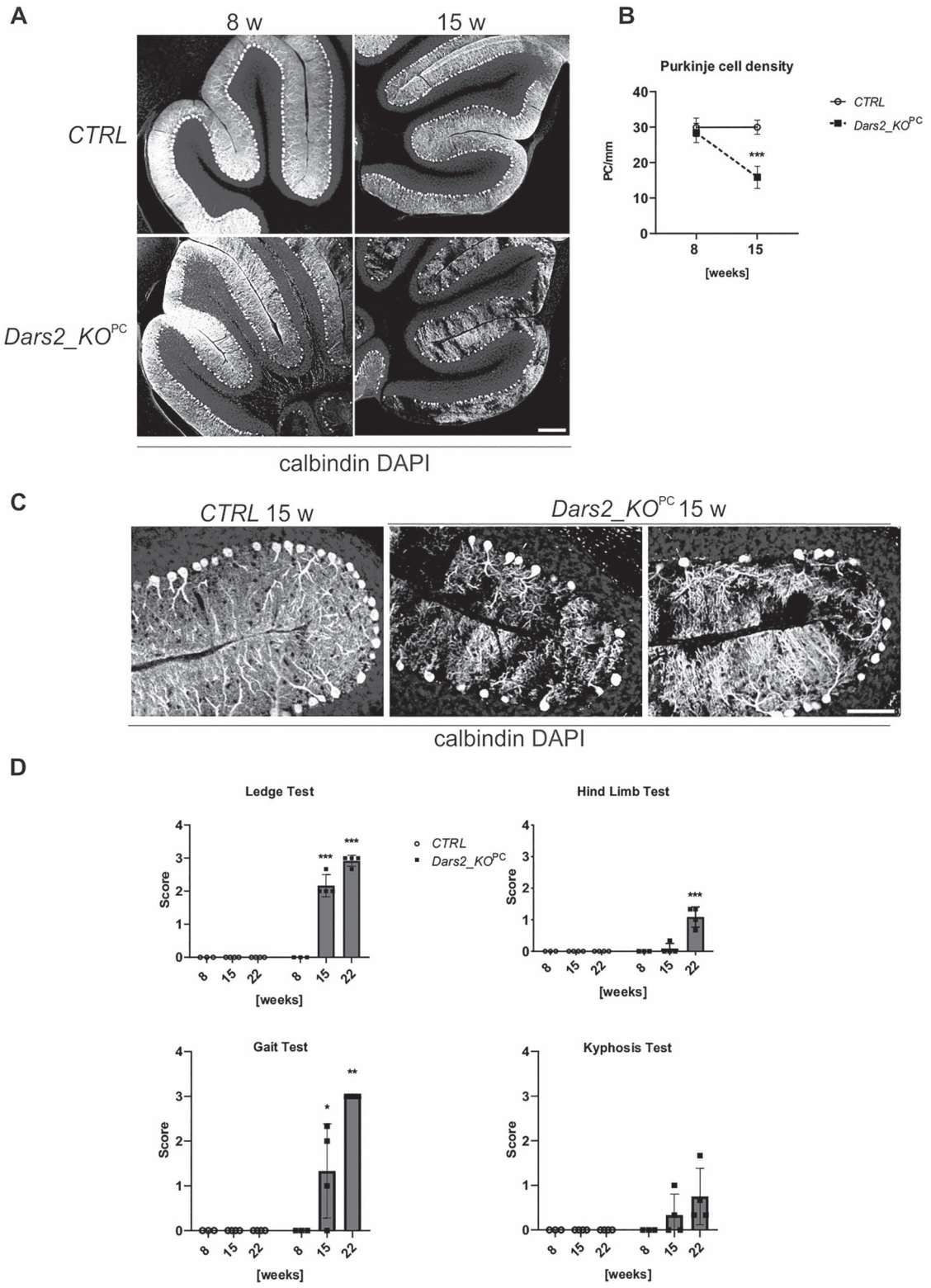

Figure 2. Massive PC loss leads to motor skills deterioration. (**A**) Representative confocal images of midsagittal sections of cerebellar vermis lobules II-III of *CTRL* and *Dars2_KO*^{PC} at the indicated time points labeled with antibodies against Calbindin (grey, Purkinje-specific marker) and DAPI (dark gray, nuclei) scale bar = 200 µm. (**B**) Quantification of PC density from (A), data presented as mean ± SD (One-way analysis of variance (ANOVA), $^{***}P < 0.001$, $n = 5$–7 lobules from three mice, per genotype and time-point). (**C**) Close-ups of PC layer in 15 weeks of age old *CTRL* and *Dars2_KO*^{PC} mice (lobules VI–VII and VIII) labeled with antibodies against Calbindin (grey, Purkinje-specific marker) and DAPI (blue, nuclei) scale bar = 100 µm. (**D**) Simple composite phenotype scoring, consisting of Ledge test, Hind Limb test, Gait test and Kyphosis test of *CTRL* and *Dars2_KO*^{PC} at the indicated time points, data presented as mean ± SD (one way ANOVA,$^{*}P < 0.05$; $^{**}P < 0.01$; $^{***}P < 0.001$).

The number of COX deficient PC increased over time, and at 15 weeks of age, all PC still present in *the Dars2_KO*^{PC} cerebellum were COX deficient (Fig. 3A). Remarkably, not only somata of PC displayed COX deficiency but also arborized PC dendrites, which are almost entirely occupied by mitochondria (Chen *et al.*, 2007), occasionally displayed characteristic blue color, denoting OXPHOS dysfunction (Fig. 3B).

To further probe the mitochondrial function, we analyzed the levels of ATP synthetase beta subunit (ATPB). No apparent difference in immunoreactivity was observed in *Dars2_KO*^{PC} mice at 8 weeks of age when compared with age-matched controls (Fig. 3C). However, when we performed immunohistochemistry (IHC) at a 15-week-old, not only we observed a decreased number of Purkinje neurons in *Dars2_KO*^{PC} mice, but the surviving PCs presented diminished ATPB levels and a fragmented mitochondrial network (Fig. 3C). These results highlight the importance of DARS2 for maintaining OXPHOS function in Purkinje neurons, which otherwise leads to the massive loss of these cells. However, the severe mitochondrial dysfunction and the loss of PCs were observed only when DARS2 was depleted entirely from these cells, as haploinsufficiency in *Dars2*$^{+/fl}$*; L7-Cre* mice were indistinguishable from WT littermates up to 38 weeks of age (Supplementary Material, Fig. S2A–C).

Surprisingly, although cerebellar atrophy is a common central nervous system (CNS) manifestation repeatedly reported in a large number of mitochondrial disorders (13), so far, no mouse models with specific ablation of RC components have been developed. To date, mouse models with PC-specific loss of function of mitochondrial proteins include a model with specific loss of AFG3L2, a mitochondrial inner membrane protease, or MFN1 and MNF2, outer mitochondrial membrane proteins that control mitochondrial fusion (14,15). Although these models also display a reduction in RC activity, it is not clear whether the OXPHOS defect in these mice is the primary cause of the Purkinje neuron dysfunction, or the other functions of these proteins might be more prevalent in this case (14,15). In this regard, a loss of the mitochondrial fatty acid synthesis in PCs using the same strategy (L7-Cre mediated deletion of mitochondrial enoyl-CoA/ACP reductase) led to a much slower progression of the phenotype (16). Remarkably, even proteins unrelated to mitochondria that cause primary cerebellar ataxia, like ataxin-1 (SCA1), were shown to cause COX deficiency and mtDNA depletion in PC, which ultimately led to the cell loss (17).

Despite the number of reports suggesting a temporal lag between the onset of a strong mitochondrial OXPHOS dysfunction and neurodegeneration (18,19), it seems that PC might be more vulnerable to OXPHOS dysfunction than other neural cell types. It is not unreasonable to speculate that given their unique, highly arborized, mitochondria-rich dendritic network, and having a central role in the cerebellar function, PC cannot tolerate OXPHOS dysfunction for a prolonged time. However, we cannot exclude that PCs are specifically sensitive to loss of DARS2, contrary to the enzymes involved in mtDNA maintenance (7,18,19) or that mitochondrial protein synthesis resulting from DARS2-depletion cannot be compensated for prolonged periods.

PC loss evokes neuroinflammation and is preceded by 1C metabolism upregulation

We anticipated that impaired cerebellar homeostasis following OXPHOS dysfunction in PC, and their consecutive decline, would result in the activation of astrocytes and glial cells, culminating in neuroinflammation. Interestingly, immunoreactivities of glial fibrillary acidic protein (GFAP) (a marker for activated astrocytes) and the microglia marker IBA-1 were mostly unaltered despite commenced mitochondrial dysfunction in *Dars2_KO*^{PC} mice at 8 weeks of age, indicating that early events of OXPHOS dysfunction in PCs are not sufficient to trigger the immune response, and induce hypertrophy of Bergmann glia (Figs 4A and 5A). To evaluate if PC loss triggers neuroinflammation, we turned to 15 weeks old *Dars2_KO*^{PC} mice. Predictably, a dramatic increase of activated microglia (Fig. 4A) and hypertrophic Bergmann glia (Fig. 5A) was notable in *Dars2_KO*^{PC} mice at 15 weeks. Consistently, we detected a significant increase in protein levels of these markers at 15 weeks old *Dars2_KO*^{PC} mice, but not at 6 weeks of age (Figs 4B–5B). The increase in neuroinflammation occurred gradually, as we detected changes in the amount of Bergmann glia at 9 and 13 weeks of age, but no significant changes in the amount of microglia (Supplementary Material, Fig. S3). These results could be explained by the different response of the two types of glial cells in the cerebellum when activated: although Bergmann glia activation results in high cell proliferation, the microglia instead changes morphology upon activation (20).

A dramatic increase of neuroinflammation markers coupled with a significant PC loss was described in previous studies in mouse models for PC-specific dysfunction (14,21). The potential release of damage-associated molecular patterns, which is known to be stimulated by mitochondrial dysfunction, might promote migration and activation of microglia, thereby amplifying neuroinflammation. Remarkably, previous studies have demonstrated that activated microglia are capable of phagocytosing dendrites and axons of living neurons, further amplifying neurodegeneration (22,23). In this study we observed PC somata with shrunken or almost disappeared dendritic network, while in the same time, the molecular layer where these dendrites were projected was strongly infiltrated by microglia, further supporting the notion that active phagocytosis of dendrites by microglia might play a role in the cerebellar pathology observed in *Dars2_KO*^{PC} mice.

A growing body of evidence identifies the remodeling of one-carbon metabolism as an immediate effect of mitochondrial dysfunction (24,25). One-carbon metabolism spans a vast range of biosynthetic reactions, occurring in cytoplasm and mitochondria, resulting in one-carbon (methyl) units further utilized in various cellular processes. Intriguingly, enzymes belonging exclusively to the mitochondrial branch of one-carbon flux have been demonstrated to be upregulated in cell models and the heart and skeletal muscles of mouse models with mitochondrial dysfunction (24,25). In line with this, *Dars2_KO*^{PC} mice displayed strong immunoreactivity for serine hydroxymethyltransferase 2 (SHMT2), which catalyzes the first step in mitochondrial one-carbon metabolism that produces tetrahydrofolate-conjugated one-carbon units further used in cytoplasmic reactions (26) (Fig. 5C). Higher levels of SHMT2 were already visible at 8 weeks and persisted in the remaining PCs of old *Dars2-KO*^{PC} mice at 15 weeks of age (Fig. 5C and D).

Recent studies in mice and *Drosophila melanogaster* have shown that the upregulation of one-carbon metabolism occurs at the early phase of a broad, integrated stress response (ISR) in ATF4-dependent manner (Celardo *et al.*, 2018; Forrström *et al.*, 2019). Interestingly, we previously demonstrated a strong upregulation of *Atf4* levels in DARS2-deficient hearts (27). Here, we provide evidence that the SHMT2 upregulation preceded PC loss and massive inflammation, and instead coincides with initial signs of OXPHOS dysfunction. This result supports the notion that remodeling of one-carbon metabolism occurs early during mitochondrial dysfunction and that this process is

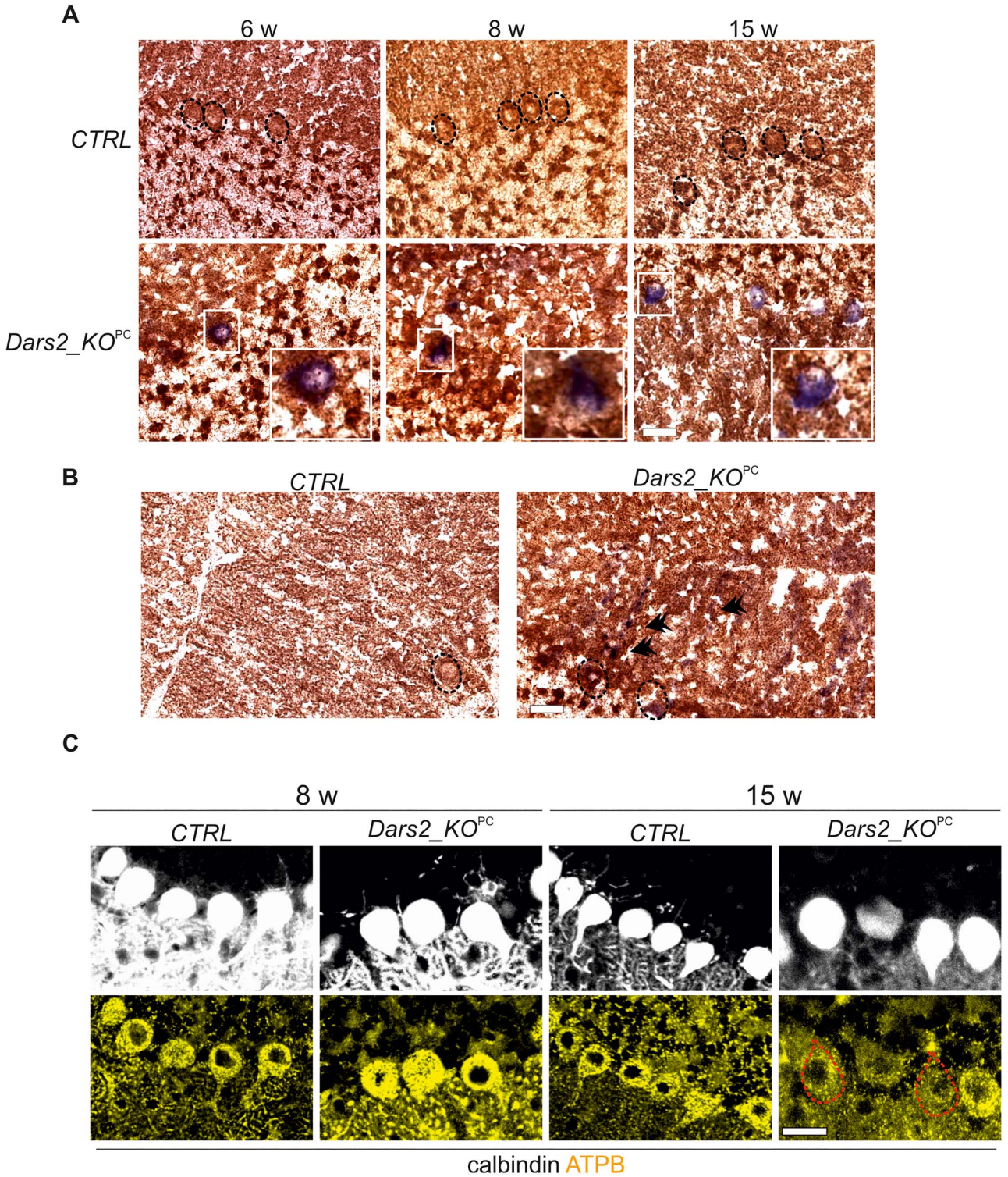

Figure 3. Strong RC dysfunction coincides with massive PC loss in *Dars2_KO*^{PC} mice. (**A**) Representative images of midsagittal sections of cerebellar vermis stained for COX/SDH activity at the time points, PCs are marked by a dashed circle scale bar = 100 µm. (**B**) Representative images of midsagittal sections of cerebellar vermis stained for COX/SDH activity showing PC (dashed circles), cerebellar molecular layer, and PC dendrites (double arrowheads), scale bar = 100 µm. (**C**) Representative confocal images of midsagittal sections of cerebellar vermis lobule VI-VII of *CTRL* and *Dars2_KO*^{PC} at the indicated time points labeled with antibodies against Calbindin (grey, Purkinje-specific marker) and ATPB (yellow, mitochondria) scale bar = 25 µm.

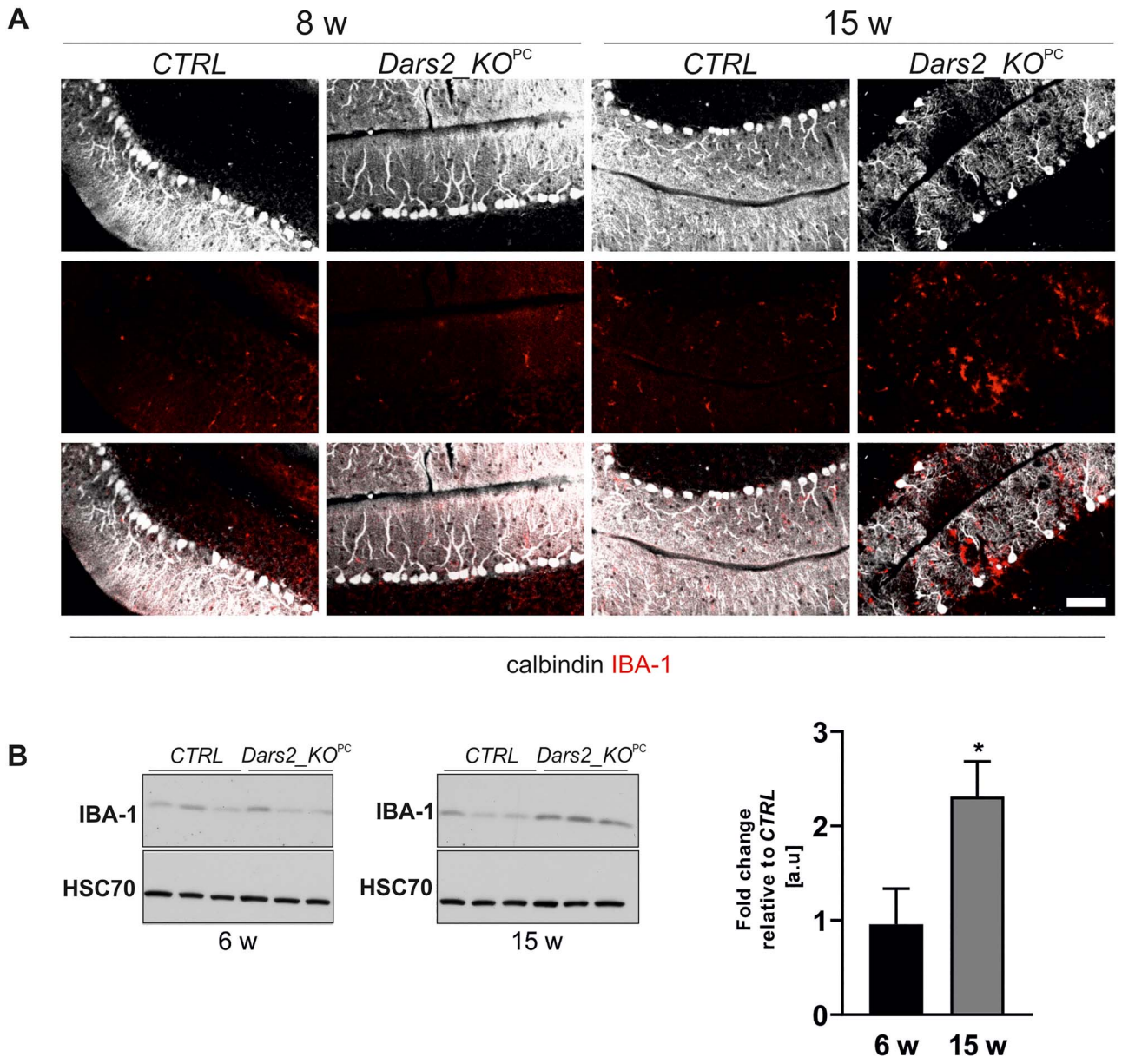

Figure 4. PC death leads to neuroinflammation. (**A**) Representative confocal images of midsagittal sections of cerebellar vermis of *CTRL* and *Dars2_KO*^{PC} at the indicated time points (lobule IV–V at 8 w; lobule VI–VII at 15 w) labeled with antibodies against Calbindin (grey, Purkinje-specific marker) and IBA-1 (red, microglia) scale bar = 100 µm. (**B**) Immunoblots of whole cerebellar lysates *CTRL* vs. *Dars2_KO*^{PC} at 6 and 15 weeks of age for a microglia marker (IBA-1), quantification presented as mean ± SEM, Student's t-test, $^{*}P < 0.05$.

also conserved in CNS. Further studies are required to unravel whether ISR cascade in CNS is similar to changes observed in cardiac and skeletal muscles (24,27), and what are the metabolic consequences for affected neurons.

In summary, we demonstrated that DARS2 is essential for the PC function, as its absence leads to mitochondrial RC deficiency resulting in early loss of Purkinje neurons likely contributing to LBSL cerebellar pathologies observed in patients. Substantial neuroinflammation that accompanies DARS2 deficiency in different brain regions, via the phagocytotic function of microglia, likely contributes to the loss of myelinated axons. We further show that in neurons, similar to other cell types, mitochondrial dysfunction leads to strong upregulation of one-carbon metabolism, which coincides with early signs of RC deficiency. It is still not clear if these stress responses are overall beneficial or detrimental for the course of diseases and if they might be potential, yet unexplored targets of therapeutic interventions in LBSL and other mitochondrial diseases.

Materials and Methods

Mouse lines

Dars2$^{fl/fl}$ mice described previously (27) were crossed to *L7-cre* mice (10). The resulting double heterozygous animals (*Dars2*$^{+/fl}$; *L7-Cre*$^{+/tg}$) were crossed to *Dars2*$^{fl/fl}$ mice to generate PC-specific knockouts (*Dars2_KO*^{PC}—*Dars2*$^{fl/fl}$; *L7-Cre*$^{+/tg}$). All animal experiments were approved by the Landesamt für Natur, Umwelt,

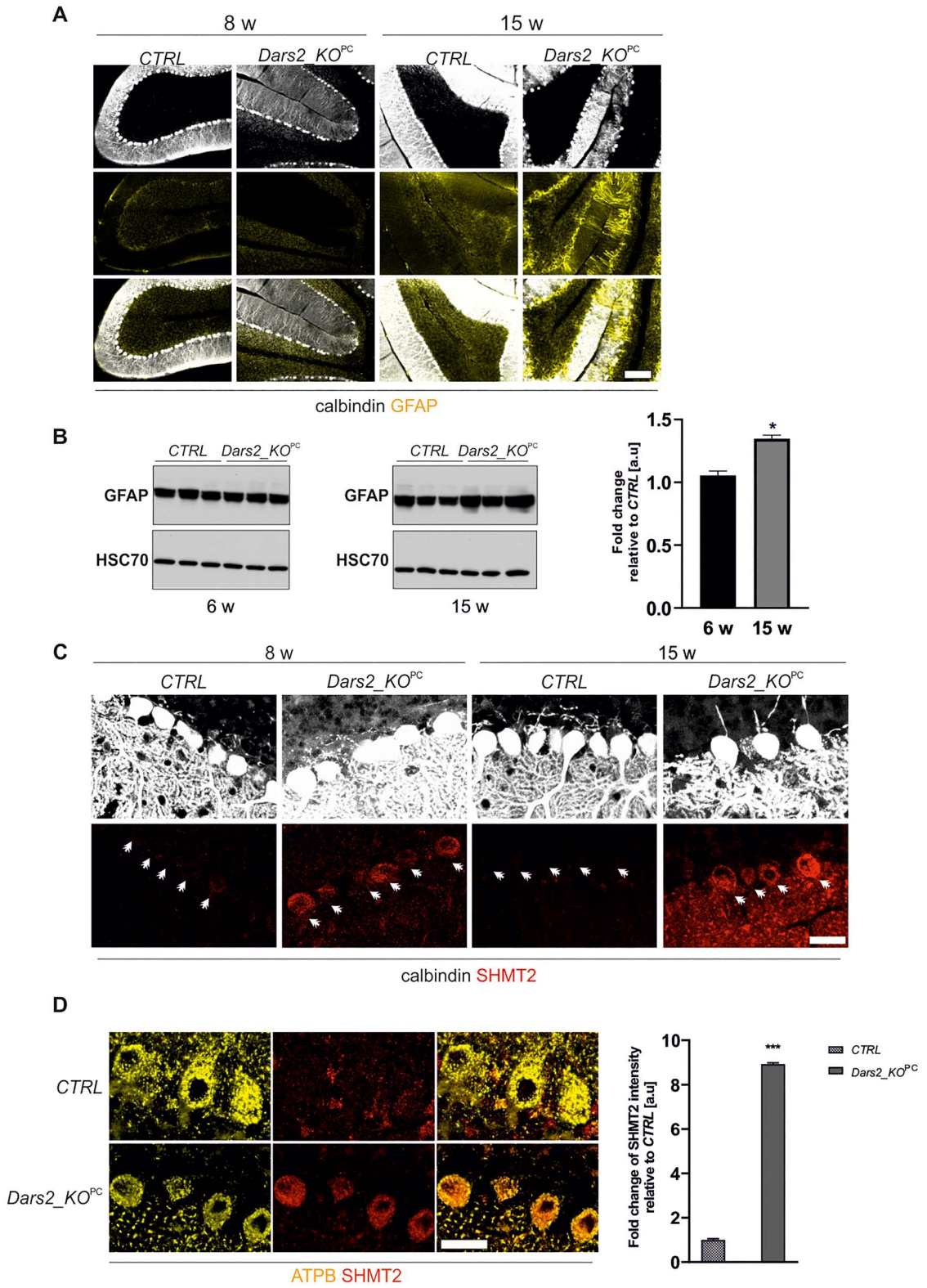

Figure 5. PC death causes astrogliosis and is preceded by SHMT2 upregulation. (**A**) Representative confocal images of midsagittal sections of cerebellar vermis of *CTRL* and *Dars2_KO*^{PC} at the indicated time points (lobule IV–V at 8 w; lobule VI–VII at 15 w) labeled with antibodies against Calbindin (grey, Purkinje-specific marker) and GFAP (yellow, astrocytes) scale bar = 100 µm. (**B**) Immunoblot of whole cerebellar lysates of *CTRL* vs. *Dars2_KO*^{PC} mice at 6 and 15 weeks for an astrocytes marker (GFAP), quantification presented as mean ± SEM, Student's *t*-test, $^{*}P < 0.05$. (**C**) Representative confocal images of midsagittal sections of cerebellar vermis lobule IV-V of *CTRL* and *Dars2_KO*^{PC} at the indicated time points labeled with antibodies against Calbindin (grey, Purkinje-specific marker) and SHMT2 (red) scale bar = 25 µm. (**D**) Representative confocal images of sections of cerebellar vermis lobule III of *CTRL* and *Dars2_KO*^{PC} at 8 weeks of age labeled with antibodies against ATPB (yellow, mitochondria) and SHMT2 (red) scale bar = 25 µm. The fraction of mitochondria displaying SHMT2 expression was quantified and normalized over ATPB (Student's *t*-test; $n = 20$ cells from 2 mice per genotype).

Verbraucherschutz, Nordrhein-Westfalen, Germany. All procedures were conducted in accordance with institutional, national, European recommendations and followed the guidelines of the Federation of European Laboratory Animals Associations.

Phenotype scoring system

The simple composite scoring system was done following the previously published protocol (11). Measures include hind limb clasping, ledge test, gait analysis and kyphosis. Each measure is recorded on a scale of 0–3 and presented individually.

Histology and IHC

For histological analysis, fresh-frozen cerebella were sectioned (10 µm) and stained either with hematoxylin and eosin (Sigma Aldrich) according to standard protocol, or for COX and SDH activity as described previously (7). Briefly, cryosections were first incubated 45 min at 37°C with COX solution (0.8 ml 3, 3 diaminobenzidine tetrahydrochloride, 0.2 ml 500 µM cytochrome c, a few grains of catalase). Next, cryosections were washed briefly in ddH_2O and incubated 90 min at 37°C with SDH solution (0.8 ml 1.875 mM nitroblue tetrazolium, 0.1 ml 1.3 M sodium succinate, 0.1 ml 2 mM phenazine methosulphate, 0.01 ml 100 mM sodium azide). Cryosections were briefly washed in ddH_2O, dehydrated through graded alcohols, cleared in xylol and mounted with Entellan (Merck Millipore).

For IHC, animals were anesthetized *i.p* with ketamine (100 mg/kg) and xylazine (10 mg/kg) and perfused transcardially with 0.1 M phosphate buffer saline (PBS) followed by 4% paraformaldehyde (PFA) in PBS. Cerebella were dissected, post-fixed overnight at +4°C in 4% PFA, and stored until use in 0.1 M PBS. Free-floating midsagittal sections (50 µm) were prepared using a vibratome (Leica Microsystems). The staining of free-floating sections was performed as described previously (28). The sections were first permeabilized with 0.5% Triton-X/PBS for 15 min at room temperature (RT). For SHMT2, this step was exchanged for heat-induced antigen retrieval in Tris-EDTA pH = 9 buffer for 25 min at 80°C. Next, sections were incubated overnight at +4°C under agitation with primary antibodies in 3% bovine serum albumine (BSA)/PBS. Primary antibodies used for IHC: anti-Calbindin D-28 K (1:1000, cat. no. 300, SWANT), Calbindin D1I4Q (1:1000, cat. no. 13176, Cell Signaling), IBA-1 (1:2000, cat. no 019–19741, Fujifilm Wako Chemicals), GFAP GA5 (1:2000, cat. no. 3670, Cell Signaling), ATPB (1:500, cat.no. ab5432, Abcam), SHMT2 (1:100, cat. no. HPA020543). The next day, sections were washed three times 10 min under agitation in 3% BSA/PBS and incubated 2 h, RT under agitation with secondary fluorophore-conjugated antibodies in PBS. Secondary antibodies used for IHC: goat anti-rabbit IgG (H + L)-Alexa fluor 546 (1:2000, cat. no. A-11035, Invitrogen), goat anti-mouse IgG (H + L)-Alexa fluor 488 (1:200, cat. no. A-11001, Invitrogen). Next, sections were washed in PBS, counterstained with 4′,6-diamidino-2-phenylindole (DAPI) and mounted with AquaPolymount (Polysciences, Inc.).

Image capture, analysis, and processing

Brightfield images of H&E and COX/SDH stained sections were taken with slide scanner (Leica SCN400).

IHC stained sections were imaged with a confocal laser-scanning microscope (TCS SP8 Leica Microsystems). Z-stack images were acquired following the Nyquist sampling in sequential mode. LAS X software (Leica Microsystems), Image J and CorelDRAW 2018 were used further to set up uniformly contrast and brightness. Figure preparation was done with CorelDRAW 2018.

PC density was assessed by counting the number of PC and dividing it by the length of the cerebellar loop occupied by the counted cells.

Western blot

Western blot analysis was performed on protein lysates of homogenized cerebella, as described previously (7). Following primary antibodies used: anti-Calbindin D-28 K (1:1000, cat. no. 300, SWANT), IBA-1 (1:2000, cat. no 019–19741, Fujifilm Wako Chemicals), GFAP GA5 (1:20 000, cat. no. 3670, Cell Signaling) and HSC70 B-6 (1:4000, cat no. sc-7298, Santa Cruz Biotechnology, Inc.). Secondary anti-mouse and anti-rabbit antibodies conjugated to horseradish peroxidase were purchased from Sigma Aldrich and used in 1:2000 dilution.

Statistical analysis

All statistical analyses were performed using Graph Pad Prism 8.0.2 software. Details of statistical tests can be found at corresponding figure legends. Unless stated otherwise, all data are present as mean ± SD.

Supplementary Material

Supplementary Material is available at *HMG* online.

Acknowledgements

The authors wish to thank the CECAD Imaging Facility for their excellent support in acquiring microscopic images.

Conflict of Interest statement. None declared.

Funding

A. Trifunovic's grants of the Deutsche Forschungsgemeinschaft (German Research Foundation – SFB 1218-Projektnummer 269925409 and TR 1018/3-1) and Centre for Molecular Medicine Cologne, University of Cologne.

References

1. Lightowlers, R.N., Taylor, R.W. and Turnbull, D.M. (2015) Mutations causing mitochondrial disease: What is new and what challenges remain? *Science*, **349**, 1494–1499.
2. Schimmel, P. (1987) Aminoacyl tRNA synthetases: general scheme of structure-function relationships in the polypeptides and recognition of transfer RNAs. *Annu. Rev. Biochem.*, **56**, 125–158.
3. Sissler, M., Gonzalez-Serrano, L.E. and Westhof, E. (2017) Recent advances in mitochondrial aminoacyl-tRNA synthetases and disease. *Trends Mol. Med.*, **23**, 693–708.
4. Scheper, G.C., van der Klok, T., van Andel, R.J., van Berkel, C.G., Sissler, M., Smet, J., Muravina, T.I., Serkov, S.V., Uziel, G., Bugiani, M. *et al.* (2007) Mitochondrial aspartyl-tRNA synthetase deficiency causes leukoencephalopathy with brain stem and spinal cord involvement and lactate elevation. *Nat. Genet.*, **39**, 534–539.

5. Fine, A.S., Nemeth, C.L., Kaufman, M.L. and Fatemi, A. (2019) Mitochondrial aminoacyl-tRNA synthetase disorders: an emerging group of developmental disorders of myelination. *J. Neurodev. Disord.*, **11**, 29.
6. van Berge, L., Hamilton, E.M., Linnankivi, T., Uziel, G., Steenweg, M.E., Isohanni, P., Wolf, N.I., Krageloh-Mann, I., Brautaset, N.J., Andrews, P.I. *et al.* (2014) Leukoencephalopathy with brainstem and spinal cord involvement and lactate elevation: clinical and genetic characterization and target for therapy. *Brain*, **137**, 1019–1029.
7. Aradjanski, M., Dogan, S.A., Lotter, S., Wang, S., Hermans, S., Wibom, R., Rugarli, E. and Trifunovic, A. (2017) DARS2 protects against neuroinflammation and apoptotic neuronal loss, but is dispensable for myelin producing cells. *Hum. Mol. Genet.*, **26**, 4181–4189.
8. Nemeth, C.L., Tomlinson, S.N., Rosen, M., O'Brien, B.M., Larraza, O., Jain, M., Murray, C.F., Marx, J.S., Delannoy, M., Fine, A.S. *et al.* (2020) Neuronal ablation of mt-AspRS in mice induces immune pathway activation prior to severe and progressive cortical and behavioral disruption. *Exp. Neurol.*, **326**, 113164.
9. Yamashita, S., Miyake, N., Matsumoto, N., Osaka, H., Iai, M., Aida, N. and Tanaka, Y. (2013) Neuropathology of leukoencephalopathy with brainstem and spinal cord involvement and high lactate caused by a homozygous mutation of DARS2. *Brain Dev.*, **35**, 312–316.
10. Barski, J.J., Dethleffsen, K. and Meyer, M. (2000) Cre recombinase expression in cerebellar Purkinje cells. *Genesis*, **28**, 93–98.
11. Guyenet, S.J., Furrer, S.A., Damian, V.M., Baughan, T.D., La Spada, A.R. and Garden, G.A. (2010) A simple composite phenotype scoring system for evaluating mouse models of cerebellar ataxia. *J. Vis. Exp.*, **39**, e1787.
12. Sciacco, M. and Bonilla, E. (1996) Cytochemistry and immunocytochemistry of mitochondria in tissue sections. *Methods Enzymol.*, **264**, 509–521.
13. Finsterer, J. and Zarrouk-Mahjoub, S. (2018) Cerebellar atrophy is common among mitochondrial disorders. *Metab. Brain Dis.*, **33**, 987–988.
14. Almajan, E.R., Richter, R., Paeger, L., Martinelli, P., Barth, E., Decker, T., Larsson, N.G., Kloppenburg, P., Langer, T. and Rugarli, E.I. (2012) AFG3L2 supports mitochondrial protein synthesis and Purkinje cell survival. *J. Clin. Invest.*, **122**, 4048–4058.
15. Chen, H., McCaffery, J.M. and Chan, D.C. (2007) Mitochondrial fusion protects against neurodegeneration in the cerebellum. *Cell*, **130**, 548–562.
16. Nair, R.R., Koivisto, H., Jokivarsi, K., Miinalainen, I.J., Autio, K.J., Manninen, A., Poutiainen, P., Tanila, H., Hiltunen, J.K. and Kastaniotis, A.J. (2018) Impaired mitochondrial fatty acid synthesis leads to Neurodegeneration in mice. *J. Neurosci.*, **38**, 9781–9800.
17. Ripolone, M., Lucchini, V., Ronchi, D., Fagiolari, G., Bordoni, A., Fortunato, F., Mondello, S., Bonato, S., Meregalli, M., Torrente, Y. *et al.* (2018) Purkinje cell COX deficiency and mtDNA depletion in an animal model of spinocerebellar ataxia type 1. *J. Neurosci. Res.*, **96**, 1576–1585.
18. Sorensen, L., Ekstrand, M., Silva, J.P., Lindqvist, E., Xu, B., Rustin, P., Olson, L. and Larsson, N.G. (2001) Late-onset corticohippocampal neurodepletion attributable to catastrophic failure of oxidative phosphorylation in MILON mice. *J. Neurosci.*, **21**, 8082–8090.
19. Ignatenko, O., Chilov, D., Paetau, I., de Miguel, E., Jackson, C.B., Capin, G., Paetau, A., Terzioglu, M., Euro, L. and Suomalainen, A. (2018) Loss of mtDNA activates astrocytes and leads to spongiotic encephalopathy. *Nat. Commun.*, **9**, 70.
20. Kriegstein, A.R. and Gotz, M. (2003) Radial glia diversity: a matter of cell fate. *Glia*, **43**, 37–43.
21. Kavetsky, L., Green, K.K., Boyle, B.R., Yousufzai, F.A.K., Padron, Z.M., Melli, S.E., Kuhnel, V.L., Jackson, H.M., Blanco, R.E., Howell, G.R. and Soto, I. (2019) Increased interactions and engulfment of dendrites by microglia precede Purkinje cell degeneration in a mouse model of Niemann pick type-C. *Sci. Rep.*, **9**, 14722.
22. Vilalta, A. and Brown, G.C. (2018) Neurophagy, the phagocytosis of live neurons and synapses by glia, contributes to brain development and disease. *FEBS J.*, **285**, 3566–3575.
23. Garber, C., Soung, A., Vollmer, L.L., Kanmogne, M., Last, A., Brown, J. and Klein, R.S. (2019) T cells promote microglia-mediated synaptic elimination and cognitive dysfunction during recovery from neuropathogenic flaviviruses. *Nat. Neurosci.*, **22**, 1276–1288.
24. Nikkanen, J., Forsstrom, S., Euro, L., Paetau, I., Kohnz, R.A., Wang, L., Chilov, D., Viinamaki, J., Roivainen, A., Marjamaki, P. *et al.* (2016) Mitochondrial DNA replication defects disturb cellular dNTP pools and remodel one-carbon metabolism. *Cell Metab.*, **23**, 635–648.
25. Bao, X.R., Ong, S.E., Goldberger, O., Peng, J., Sharma, R., Thompson, D.A., Vafai, S.B., Cox, A.G., Marutani, E., Ichinose, F. *et al.* (2016) Mitochondrial dysfunction remodels one-carbon metabolism in human cells. *elife*, **5**, e10575.
26. Ducker, G.S. and Rabinowitz, J.D. (2017) One-carbon metabolism in health and disease. *Cell Metab.*, **25**, 27–42.
27. Dogan, S.A., Pujol, C., Maiti, P., Kukat, A., Wang, S., Hermans, S., Senft, K., Wibom, R., Rugarli, E.I. and Trifunovic, A. (2014) Tissue-specific loss of DARS2 activates stress responses independently of respiratory chain deficiency in the heart. *Cell Metab.*, **19**, 458–469.
28. Motori, E., Puyal, J., Toni, N., Ghanem, A., Angeloni, C., Malaguti, M., Cantelli-Forti, G., Berninger, B., Conzelmann, K.K., Gotz, M. *et al.* (2013) Inflammation-induced alteration of astrocyte mitochondrial dynamics requires autophagy for mitochondrial network maintenance. *Cell Metab.*, **18**, 844–859.

Supplementary Material

Figure S1: PC loss in 15 w old *Dars2_KO*^{PC}

PC loss was the most prominent in lobules I-VIII, lobule X was less affected. Representative confocal images of lobules III, IV-V, VI-VII and X are shown. Scale bar=200 µm.

Figure S2: PC-specific Dars2 heterozygous mice (*Dars2_Hz*^{PC}) are not different from WT control littermates (*CTRL)*

(A) Representative images of midsagittal sections of cerebellar vermis of H&E staining at the indicated time points, arrowheads indicate PC; scale bar=100 µm. **(B)** Representative images of midsagittal sections of cerebellar vermis COX/SDH staining at the time points, PCs are marked by a dashed circle scale bar=100 µm **(C)** Body weight and brain weight of *CTRL* and *Dars2_KO*^{PC} at indicated time points data presented as mean ± SD (n=2 mice per genotype per time point).

Figure S3 Western blot analysis of the neuroinflammation markers at 9 and 13 weeks-of-age

Immunoblots of whole cerebellar lysates *CTRL* vs. *Dars2_KO*^{PC} mice at 9 and 13 weeks for a microglia marker (IBA-1), astrocytes marker (GFAP), and PC marker (Calbindin) quantification presented as mean ± SEM, Student's t-test, *$p < 0.05$

Supplementary figure 1

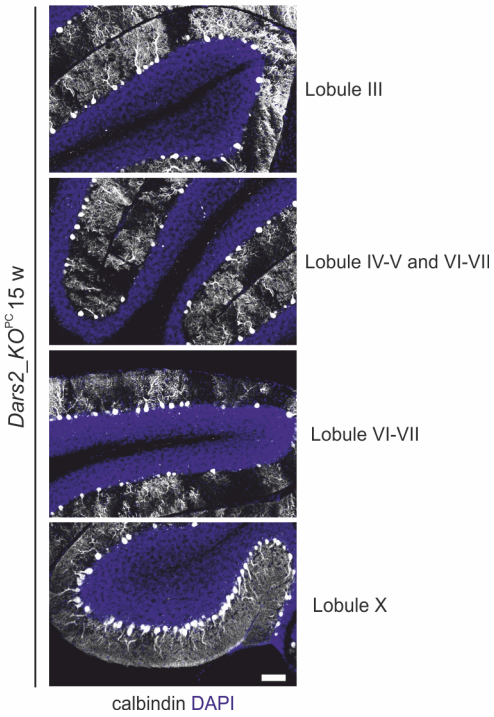

Supplementary figure 2

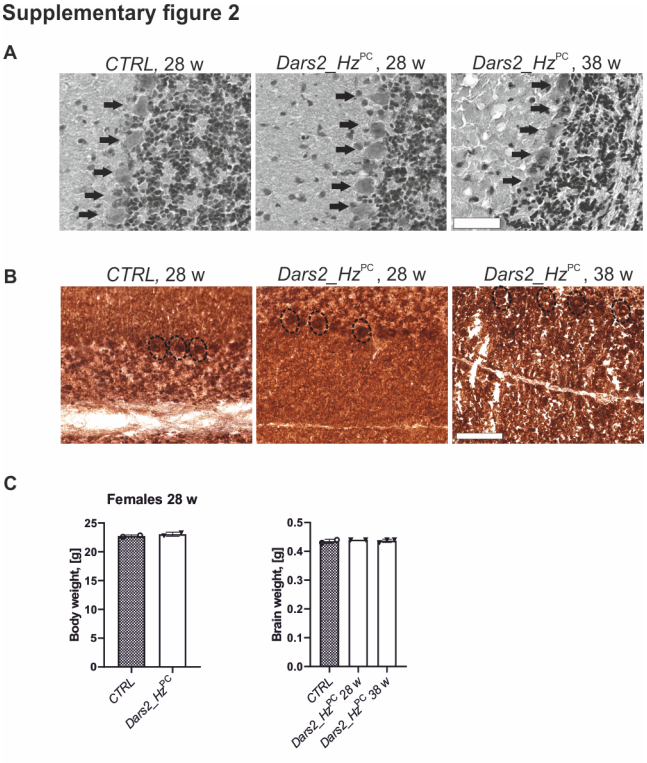

Supplementary figure 3